2017

Development of Heterogeneous Catalysts for Upgrading Biomass Pyrolysis Bio-Oils into Advanced Biofuels

Shouyun Cheng
South Dakota State University

DEVELOPMENT OF HETEROGENEOUS CATALYSTS FOR UPGRADING BIOMASS PYROLYSIS BIO-OILS INTO ADVANCED BIOFUELS

BY

SHOUYUN CHENG

A dissertation submitted in partial fulfillment of the requirements for the

Doctor of Philosophy

Major in Agricultural, Biosystems, and Mechanical Engineering

South Dakota State University

2017

DEVELOPMENT OF HETEROGENEOUS CATALYSTS FOR UPGRADING BIOMASS PYROLYSIS BIO-OILS INTO ADVANCED BIOFUELS

This dissertation is approved as a creditable and independent investigation by a candidate for the Doctor of Philosophy in Agricultural, Biosystems, and Mechanical Engineering degree as is acceptable for meeting the dissertation requirements for this degree. Acceptance of this dissertation does not imply that the conclusions reached by the candidate are necessarily the conclusions of the major department.

Lin Wei, Ph.D.

Major and Dissertation Advisor Date

Van C. Kelley, Ph.D.

Head, Department of Agricultural and Biosystems Engineering Date

Dean, Graduate School Date

ACKNOWLEDGEMENTS

I, hereby, acknowledge my great gratitude to my advisor Dr. Lin Wei for his esteemed guidance, constant encouragement, financial support of the project, kind help in daily life, critical and constructive evaluation of this dissertation. I am appreciated that he arranged many conferences for me to attend to communicate and learn from other researchers to further deeply understand my research projects.

I would like to thank my advisory committee members, Professor James Julson, Professor Kasiviswanathan Muthukumarappan, and Professor Rebecca Bott for their efficient guidance and suggestions. I would like to express my gratitude to them for their timely response and valuable time shared with me during my PhD study. I would like to thank Professor Joe Darrington, Professor Parashu Ram Kharel, Professor Zhengrong Gu, Professor Qiauan Qiao, Professor Gary Anderson, Professor Erin Cortus, Professor Van Kelley, Professor Douglas Raynie, Ms. Candy Rogess, Ms. Susan Goens, Mr. Scott Cortus, Mr. Jeff Vander Schaaf, Ms. Jasmine Greene, Ms. Kristina Lapsley for their kind help in my study here.

I would like to thank my former and current colleagues including Xianhui Zhao, Yinbing Huang, Yong Yu, Yang Gao, Ethan Kadis, Fletcher Corbin, Yu Shen, Mustafa Alsowij, Zeyad Ali Albahr, Yuhe Cao, Qinghui Cheng, Keliang Wang, Umesh Lohani, Bishnu Karki, Vijay Sundaram, Poonam Singha, Changling Qiu, Dan Liu, Jianyuan Sun and Ashish Dubey.

I would like to express my deep gratitude to my family members including my parents, wife, son, sister-in-law and relatives. I would like to thanks my friends including Chunyang Wang, Li Wang, Yaming Lu, Tong Wang, Hailong Jin, Tao Lin, Runxia Liu for their help and care in my life here.

The research is supported by U.S. Department of Energy (Award No. SA0900160) and Department of Transportation (Award No. SA0700149) through the North Central Sun Grant Initiative. This research is also partially supported by South Dakota Innovation Partner (Grant No. SA1600799).

TABLE OF CONTENTS

LIST OF TABLES

LIST OF FIGURES

ABSTRACT

DEVELOPMENT OF HETEROGOGENEOUS CATALYSTS FOR UPGRADING BIOMASS PYROLYSIS BIO-OILS INTO ADVANCED BIOFUELS

SHOUYUN CHENG

2017

The massive consumption of fossil fuels and associated environmental issues result in an increased interest in alternative resources such as biofuels. The renewable biofuels can be upgraded from bio-oils that are derived from biomass pyrolysis. Catalytic cracking and hydrodeoxygenation (HDO) are two most promising bio-oil upgrading techniques for biofuel production. Heterogeneous catalysts are essential for upgrading bio-oil into hydrocarbon biofuel. Although some progresses have been made, the cost and effectiveness of catalysts still remain challenges. The main objective of this study was to develop efficient heterogeneous catalysts for upgrading bio-oils into advanced hydrocarbon biofuel with low costs.

In catalytic cracking, Ni/HZSM-5 and Co-Mo/HZSM-5 were used for upgrading bio-oils derived from prairie cordgrass (PCG) and alkali lignin pyrolysis in a two-stage reactor system. 12%Ni/HZSM-5 catalyst yielded the highest amount of gasoline fraction hydrocarbons (32.45%) for PCG bio-oil upgrading. 4%Mo-2%Co/HZSM-5 catalyst showed a robust ability in the PCG catalytic cracking with highest yield of hydrocarbons at 41.08 %. 1.27% NiO/HZSM-5 catalyst generated

the highest biofuel yield at 27.5% and produced biofuel with the highest content of hydrocarbons at 69.4 % in alkali lignin bio-oil upgrading.

In hydrodeoxygenation (HDO), Ni based activated carbon catalysts including Ni/AC, Ni-Fe/AC, Ni-Mo/AC and Ni-Cu/AC, and Ni-Zn/Al_2O_3 catalysts with different Ni and/or Zn loading ratios were designed for HDO of PCG and pine sawdust (PSD) bio-oils. The Ni/AC catalysts produced the highest content of gasoline range hydrocarbons (C6-C12) at 32.63% in PCG biofuel product, while Ni-Mo/AC generated biofuel product with the highest content of gasoline blending alkyl-phenols at 38.41%. 15%Ni-5%Zn/Al_2O_3 catalyst generated the highest PSD biofuel yield at 44.64 wt.% and the highest hydrocarbon content at 50.12% in biofuel product.

However, the upgrading cost of HDO is still high due to the high consumption of external hydrogen. In this paper, the hydrogen generated from cheap water using zinc hydrolysis for in-situ bio-oil HDO was firstly reported. The effect of different temperatures (200 °C, 250 °C and 300 °C) on PSD bio-oil HDO over Pd/C catalyst was investigated. The results show that 250 °C yielded biofuel with the highest heating value at 30.17 MJ/kg and the highest hydrocarbons content at 24.09%. In bio-oil HDO using zinc metal only, 400°C bio-oil upgrading process produced biofuel product with highest hydrocarbons content at 68.95%.

CHAPTER 1

Introduction and Background

1.1 Introduction

More than 80% of global energy supplies come from fossil fuels including coal, petroleum, and natural gas [1]. However, environmental issues such as global warming and air pollution due to fossil fuel consumption, growing energy demand, and depletion of fossil fuels have stimulated the demand for renewable liquid fuels [2].

Biomass is a promising eco-friendly alternative source of renewable energy in the context of current energy scenarios [3]. Biomass is a form of carbon–neutral energy because the CO_2 released during its utilization is equal to the CO_2 absorbed from the atmosphere during its growth through photosynthesis. It also has lower contents of sulfur, nitrogen, and heavy metals than coal [4]. Therefore, utilization of biomass-derived fuels is crucial to reducing the carbon dioxide emission and air pollution problems caused by fossil fuels. Compared to fossil fuels, the production of biofuels is more environmentally friendly and sustainable since biomass is readily available, annually renewable, and inexpensive. The challenges of fossil fuel depletion, climate change, and other environmental concerns may be addressed if biomass can be efficiently converted into valuable biofuels and chemicals with a low carbon footprint.

Biomass can be converted to liquid biofuels through thermochemical processes. Within the last decades biomass fast pyrolysis has emerged as one of the most promising processes for thermochemical conversion of lignocellulosic

biomass to liquid bio-oils. During pyrolysis, biomass is heated up to 400–650 °C in the absence of air and thus broken down into three products: liquid bio-oil and a small amount of solid bio-char and non-condensable gas (also named syngas). Biomass fast pyrolysis is a simultaneous mix of dehydration, depolymerization, re-polymerization, fragmentation, and rearrangement. These reactions result in a bio-oil liquid that contains over 300 individual compounds including a large variety of oxygenates that cause many of the negative properties of bio-oil, such as low higher heating value(HHV), high corrosiveness, high viscosity, and instability [5]. These properties greatly limit the application of bio-oil, particularly as transportation liquid fuels. Therefore, crude bio-oil has to be upgraded before it can be used as liquid biofuel for fueling engines.

The purpose of bio-oil upgrading is to refine crude bio-oil into hydrocarbons or other intermediates that can be directly dropped into an existing petroleum refinery for production of "green" gasoline, diesel, or other industrial chemicals. This upgrading process is to remove oxygenated compounds from bio-oil via H_2O, CO, and CO_2 formation while at the same time reducing molecular weight and altering chemical structures. Generally, bio-oil upgrading may involve a one-pot reaction where simultaneous or tandem multiple reactions of catalytic cracking, hydrodeoxygenation, decarbonylation, decarboxylation, hydrocracking, or hydrogenation occur in one reactor. Different catalysts must be used to produce different targeted products. Each of the individual components in bio-oil may play a certain role in bio-oil upgrading one-pot reactions. A series of consecutive and parallel reactions competing against each other between liquid and gaseous products may occur in a one-pot bio-oil upgrading process. There are various intermediates and products generated simultaneously during bio-oil upgrading.

Many of them are reactive. The products from one component may react with products from other components while the mineral compounds like alkali and alkaline earth metals that come from biomass can also act as catalysts. This changes product distribution dramatically and can make one-pot reactions more perplexing. Such complex reaction networks make bio-oil upgrading, product separation or purification very difficult. The competitive reactions and impurities in bio-oil also deactivate the catalysts used in the one-pot reactions. This leads to low carbon conversion efficiency and high processing costs. The processing efficiency of bio-oil upgrading relies heavily upon the activity, selectivity, and energy efficiency of the catalysts used. Catalyst deactivation is one of biggest challenges to developing active stable catalysts.

Catalytic cracking and hydrodeoxygenation have proven to be the most promising for upgrade crude bio-oils into liquid hydrocarbon biofuels. These two methods can effectively reduce the contents of oxygenated compounds while producing high yields of hydrocarbons. Heterogeneous catalysts have achieved great success for petroleum refining and are promising for bio-oil upgrading. The objective of this study is to address the issues in the use of cheap and effective heterogeneous catalysts for bio-oil upgrading.

1.2 Bio-Oil Properties and Compositions

Among the different pyrolysis processes used for biomass conversion, slow pyrolysis is currently the most mature and commercially used pyrolysis technology [6]. During slow pyrolysis, biomass is heated to around 500 °C at a slow heating rate up to 20 °C/min and a long vapor residence time (5–30 min). This results in a lower yield of liquid bio-oil (around 30 wt%), higher yields of charcoal (around 35

wt%) and gas products (around 35 wt%) [7]. Slow pyrolysis has traditionally been used for the production of charcoal rather than bio-oil or gas [8]. Fast pyrolysis of biomass is a promising technology for converting biomass to liquid fuels [9]. Fast pyrolysis produces a high yield of liquid bio-oil (50–75 wt%) at moderate temperatures (400–650 °C), atmospheric pressure, high heating rates (>103 °C/s) and short vapor residence time (<2 s) [10]. Biomass fast pyrolysis is generally conducted in fluidized bed, rotating cones, vacuum or ablative pyrolysis reactors [11]. However, the biomass-derived bio-oil is not suitable for direct application as transportation fuels due to the lower heating value (17.4–32.46 MJ/kg) in comparison with heavy fuel oil (44.17 MJ/kg). The comparison of bio-oil and heavy fuel oil properties are listed in Table 1.1. The low heating value of bio-oil results from its high water content (12–30 wt%) and oxygen content (19.40–50.30 wt%). Also bio-oil has high viscosity and acidity. Bio-oil is also unstable, and reactions of oxygen-derived compounds during storage, results in reduced bio-oil quality [12].

Pyrolysis bio-oils are complex mixtures containing more than 300 components derived from the depolymerization and fragmentation reactions of cellulose, hemicellulose, and lignin present in biomass. Depending on production conditions, and biomass feedstock type and quality, fast pyrolysis bio-oil composition can vary drastically [13]. The chemical compositions of bio-oils produced from several biomass feedstocks are listed in Table 1.2. There are many categories of oxygenated compounds present in bio-oil, which include phenols, ketones, aldehydes, acids, esters, furans, ethers, and alcohols.

1.3 Bio-oil upgrading

The oxygenated compounds in raw bio-oils have caused some undesirable properties of bio-oil including high viscosity, corrosiveness, instability, and low heating values for use in transportation fuels [11]. Acids contribute to the corrosiveness of bio-oil, and the presence of aldehydes and phenols results in storage instability [14]. Raw bio-oil requires considerable upgrading to be usable. Two widely investigated methods for upgrading bio-oil into hydrocarbon biofuels are: catalytic cracking and hydrodeoxygenation.

1.4 Catalytic Cracking

Catalytic cracking is an effective bio-oil upgrading method, and it is generally conducted in the presence of heterogeneous catalysts at atmospheric pressure and at temperatures ranging from 350 °C to 650 °C. Catalytic cracking removes oxygen in the form of CO, CO_2, and/or H_2O [15]. The oxygenated compounds in raw bio-oil can be transformed into light hydrocarbon biofuel containing high contents of aromatic hydrocarbons by catalytic cracking. Catalytic cracking can be classified into in-situ and ex-situ processes. In the in-situ process, the biomass and catalysts were mixed together in a single reactor, and this method reduces the capital and operating costs [16]. In the ex-situ process, bio-oil catalytic upgrading is completed in a secondary reactor separate from the biomass pyrolysis reactor. This process enables easier catalyst performance optimization and reduces catalyst to biomass ratio. Catalysts include zeolite and oxides.

1.4.1 Catalysts in Catalytic Cracking

1.4.1.1 Zeolite Catalysts

Zeolite catalysts have been shown to be effective in the deoxygenation of bio-oil, resulting in the formation of aromatics and effectively increasing the C/O ratio in upgraded bio-oil. Zeolite catalysts such as HZSM-5 (Zeolite Socony Mobil–5), β-zeolite, Y-type zeolite, ferrierite zeolite, mordenite zeolite, MCM-41(Mobil Composition of Matter No. 41), and SBA-15 (Santa Barbara Amorphous) have documented use for bio-oil catalytic cracking [17, 18]. Among these catalysts, HZSM-5 is most effective due to its high activity , strong acidity, and shape selectivity [19]. HZSM-5 zeolite bio-oil upgrading has effectively transformed bio-oil to liquid biofuel, abundant in aromatic hydrocarbons through deoxygenation, dehydration, decarboxylation, decarbonylation, cracking, oligomerization, alkylation, isomerization, cyclisation and aromatization reactions [20]. However, HZSM-5 is easily deactivated by coking, resulting in low yields and short life cycle times.

1.4.1.2 Oxides Catalysts

Inexpensive oxide catalysts have been widely used as mild catalysts to reduce the oxygen content in bio-oil. Alumina, nickel monoxide, zirconia/titania, tetragonal zirconia, titania, and silica alumina were investigated for use with catalytic pyrolysis of beech wood in a fixed bed reactor at 500 °C [21]. The results indicated that alumina showed the highest selectivity towards hydrocarbons and yielded low organic liquid products. In comparison, zirconia/titania exhibited good selectivity towards hydrocarbons and yielded higher organic liquid product than alumina. Natural derived basic magnesium oxide (MgO) catalyst effectively

reduced the oxygen content of the produced bio-oil and exhibited similar or even better catalytic performance in bio-oil upgrading compared to that of an industrial ZSM-5 catalyst, although the coke yield of MgO catalyst was a bit higher than that of ZSM-5 [22]. The reduction of acids and deoxygenation of bio-oils via ketonization and aldol condensation reactions occurred in the basic sites of MgO catalysts, and the preferred pathway for removing oxygen was mainly via CO_2 formation instead of CO and/or water. Zinc oxide (ZnO) catalyst was used for catalytic pyrolysis of rice husks to produce bio-oil in a fixed-bed reactor. ZnO catalyst decreased the amount of undesired oxygenated compounds in bio-oils [23]. Boric oxide (B_2O_3) selectively eliminated 50%–80% of the hydroxyl and methoxy groups in the bio-oil produced from empty palm oil fruit bunch and oil palm fronds in a fixed-bed reactor at 400 °C [24]. Boric oxide enhanced the cleavage of C–O bonds in the biomass polymers. This was due to the change of the boric oxide structure from a planar triangular BO_3 to a tetrahedral BO_4 using the oxygen generated from the oxygenated groups in the bio-oil. Nano metal oxides also exhibited good catalytic activity in bio-oil upgrading. For instance, nano MgO, CaO, TiO_2, Fe_2O_3, NiO, and ZnO were used in catalytic cracking of poplar wood pyrolysis vapors in a pyrolysis tube [25]. The results indicated that CaO was the most effective catalyst in increasing the formation of hydrocarbons, reducing the production of anhydrosugars and phenols, and eliminating acids.

1.5 Hydrodeoxygenation

Hydrodeoxygenation (HDO) is an effective bio-oil upgrading technique using a variety of heterogeneous catalysts at high hydrogen pressure (7.5–30 MPa) and temperatures (250–450 °C) [26]. HDO removes oxygen in bio-oil as H_2O, CO,

and/or CO_2 [27]. This results in the production of stable hydrocarbon biofuel with higher energy content. During the bio-oil HDO process, multiple reactions including hydrogenation, hydrogenolysis, hydrodeoxygenation, decarboxylation, decarbonylation, cracking/hydrocracking, and polymerization reactions occurred. An efficient HDO catalyst should effectively remove oxygen with low hydrogen consumption and suppress the coke formation that leads to catalyst deactivation. Various noble and transitional metal catalysts supported on carriers of alumina, silica, titania, zirconia, magnesium oxide, active carbon, and HZSM-5 have been tested on bio-oil and model HDO compounds.

1.5.1 Catalysts Used in Bio-Oil HDO

1.5.1.1 Sulfided Catalysts

Sulfided catalysts including mixed sulfides of (Co, Ni) and (Mo, W) dispersed on γ-Al_2O_3 or MgO have been used for bio-oil HDO due to the good catalytic performance [28]. Sulfided CoMo/γ-Al_2O_3 and NiMo/γ-Al_2O_3 catalysts were used for wood-derived bio-oil HDO upgrading [29]. The results indicated that CoMo/γ-Al_2O_3 showed higher selectivity to diesel-like products and higher activity for removal of gaseous intermediates (CO_x) by hydrogenation than NiMo/γ-Al_2O_3. The active sites that exhibited Lewis acid character on sulfided catalysts were sulphur anion vacancies (coordinately unsaturated sites), and located at the edges of MoS_2 nanoclusters [30]. Compared with NiMo/γ-Al_2O_3 catalyst, NiW/γ-Al_2O_3 catalyst presented a higher isomerization activity leading to higher phenol conversion in phenol HDO [30]. In sulfided NiW catalysts, WS_2 was the HDO active phase while Ni was used as the promoter. Phosphorus (P) doping has been used to improve the activity of sulfide catalysts, and CoMoP/MgO catalyst showed higher activity for

phenol HDO than CoMo/MgO [31]. The activity-promoting effects of P was due to the increase in Mo dispersion, stacking of MoS_2 crystallites and formation of new Lewis and Brönsted acid sites on the catalyst surface.

Sulfided catalysts are not very desirable for bio-oil HDO due to the addition of sulfur-containing compounds. They can result in the contamination of biofuel products and increase upgrading cost. Besides, alumina is unstable under hydrothermal conditions, and it can partially transform into boehmite in the presence of water vapor at reaction temperature (140–380 °C) [32]. Finally, Al_2O_3 support shows a high tendency for polymerization reactions due to the high acidity resulting in coke deposition [27].

1.5.1.2 Noble Metal Catalysts

Noble metal (Rh, Pt, Pd, and Ru) catalysts showed excellent bio-oil HDO catalytic performance. These catalysts do not require the consumption of environmentally unfriendly sulfur compounds. These metal catalysts are active at low temperatures, and this could possibly prevent thermal reactions leading to coke formation and deactivation. The effectiveness of noble metal catalysts was affected by the types of biomass and noble metals. During HDO of fast-pyrolysis bio-oils from several feedstocks (switchgrass, eucalyptus benthamii, and equine manure) using Pt/C, Ru/C, and Pd/C catalysts, switchgrass bio-oil over Pt/C showed the best hydrogen consumption and deoxygenation efficiency [13]. A variety of heterogeneous noble-metal catalysts (Ru/C, Ru/TiO_2, Ru/Al_2O_3, Pt/C, and Pd/C) were screened for the upgrading of beech wood fast pyrolysis oil [33]. Among the tested catalysts, Ru/C catalyst was found to be the most effective catalyst with respect to oil yield (up to 60 wt%) and deoxygenation level (up to 90 wt%). HDO

of pinewood derived bio-oil using monometallic and bimetallic noble metal (Rh, Pd, Pt) catalysts supported on ZrO_2 showed Pd/ZrO_2 produced the highest activity followed by Rh/ZrO_2 [34]. This was due to the higher sulfur (present in bio-oil) tolerance of Pd/ZrO_2 than other metal catalysts.

The support properties including pore sizes, acidity, and surface areas have a significant influence on noble metal catalyst activity. Pt/ZSM-5 showed much higher deoxygenation ability than Pt/Al_2O_3 during HDO of pyrolysis bio-oil [35]. This was attributed to the mesoporous structure and high acidity of Pt/ZSM-5. Pt catalysts supported over carriers such as HZSM-5, Mesoporous Beta, HBeta, MMZBeta, Al-MCM-48, and Si-MCM-48 were tested for HDO of guaiacol in a batch-type reactor at 4 MPa and 250 °C [36]. This study indicated that Pt/Mesoporous Beta and Pt/HBeta catalysts showed higher guaiacol conversions due to the large pores and strong acid sites of the catalysts. Five carbon materials including multi-walled carbon nanotubes (MWCNT), carbon aerogel (CARF), carbonblack (Vulcan carbon), activated carbon (AC), and graphite were used as supports for Ru catalysts for HDO of oak chips pyrolysis oil [37]. The results showed that Ru/MWCNT exhibited the highest deoxygenation activity as a result of the high Ru surface area and external surface area of the MWCNTs.

The availability and high cost of noble metals are the main challenges for the application of noble metal catalysts. Besides, noble metal catalysts show a rather low resistance towards poisoning by low levels of elements such as iron or sulfur in bio-oil when compared to sulfided catalysts [38].

1.5.1.3 Transition Metal Catalysts

Transition metal catalysts showed good catalytic performance for bio-oil upgrading. They can be used as a potential alternative for precious metal and sulfided catalysts due to the high activity and low cost. For instance, non-sulfided catalysts including MoNi/γ-Al_2O_3, NiCu/δ-Al_2O_3, and NiFe/γ-Al_2O_3 have attracted much attention because of their good catalytic activity for HDO of pyrolysis oil [39, 40]. MoNi/γ-Al_2O_3 considerably improved properties of pine sawdust bio-oil including hydrogen content and the acidity [41]. The addition of Mo as a promoter benefited nickel species uniformity and inhibited $NiAl_2O_4$ spinel formation in MoNi/γ-Al_2O_3 catalyst. Bimetallic Ni-Cu/δ-Al_2O_3 catalysts were more active and outperformed monometallic Ni/δ-Al_2O_3 or Cu/δ-Al_2O_3 for the HDO of fast pyrolysis oil [39]. This was due to the smaller size and increased number of active Ni_xCu_{1-x} clusters in the catalyst. NiFe/γ-Al_2O_3 improved the heating value of straw bio-oil from 37.8 MJ/kg to 43.9 MJ/kg after bio-oil HDO. This was due to the formation of NiFe alloy in the NiFe/γ-Al_2O_3 catalysts [40]. The major reaction pathway was the cleavage of C–O rather than C–C during the bio-oil HDO process. Fe/SiO_2 was an active and selective catalyst for HDO upgrading of guaiacol to produce aromatic hydrocarbons, and it exhibited a good selectivity for BT (benzene, toluene) production [42].

Bifunctional metal/acid catalysts including Ni/HBeta, Fe/HBeta, and NiFe/HBeta were used for HDO of a simulated phenolic bio-oil consisting of phenol, o-cresol, and guaiacol [43]. The results indicated that bimetallic NiFe/HBeta catalyst showed higher HDO activity when compared to monometallic Ni/HBeta and Fe/HBeta. This is due to the synergistic effect between the two metals. NiFe/HBeta catalysts converted phenolic compounds to oxygen-free products via hydrogenation and hydrogenolysis reactions.

1.6 Objectives

The main objective of this study was to develop effective heterogeneous catalysts for upgrading biomass pyrolysis bio-oil to advanced biofuels using catalytic cracking and hydrodeoxygenation methods. The designed catalysts will have lower coke formation and higher activity to improve biofuel yield and quality (pH/total acid number, water content, viscosity, higher heating values and chemical compositions). The specific objectives of this study include:

- Upgrade bio-oil to hydrocarbon biofuels using catalytic cracking and HDO approaches.
- Develop novel in-situ hydrogen generation method for bio-oil upgrading.
- Develop efficient catalysts for catalytic cracking and HDO of bio-oil to hydrocarbon biofuel.
- Optimize metal loading ratios of designed catalysts and operation conditions for bio-oil catalytic cracking and HDO upgrading.

1.7 Outline of dissertation

This dissertation provides the information of study background, upgrading bio-oil to advanced biofuel through catalytic cracking and HDO, and development of effective catalysts for bio-oil upgrading. The information including motivation of study, basic knowledge of biomass pyrolysis bio-oil, catalytic cracking and HDO, the used catalysts for bio-oil upgrading, and the problems of current used catalysts were introduced in Chapter 1. The developing of bifunctional Ni/HZSM-5 catalyst

for converting PCG pyrolysis bio-oil to hydrocarbon biofuel using a two-stage reactor system was described in Chapter 2. The study of upgrading PCG pyrolysis bio-oil to hydrocarbon biofuel over Co-Mo/HZSM-5 was narrated in Chapter 3. The HDO of PCG pyrolysis bio-oil over Ni based activated carbon synergistic catalysts combined with different metals was reported in Chapter 4. The in-situ HDO upgrading of PSD bio-oil to hydrocarbon biofuel using zinc assisted Pd/C catalyst was presented in Chapter 5. The HDO upgrading of PSD bio-oil using zinc metal with zero valency was reported in Chapter 6. The study of converting alkali lignin over NiO/HZSM-5 catalysts to hydrocarbon biofuel was reported in Chapter 7. Hydrocarbon bio-oil production from PSD pyrolysis bio-oil using non-sulfide Ni-Zn/Al2O3 catalyst was presented in Chapter 8. The general conclusions of the overall dissertation studies were summarized in Chapter 9. The recommendations for future study were presented in Chapter 10.

Table 1.1 Typical properties of bio-oil and heavy fuel oil

Physicochemical Properties	**Bio-Oil**	**Heavy Fuel Oil**
Water content (wt%)	12–30	0.10
Carbon (wt%)	41.70–69.50	85.60–86.68
Hydrogen (wt%)	5.70–9.40	10.30–12.04
Oxygen (wt%)	19.40–50.30	0.60–0.65
Nitrogen (wt%)	0–9.80	0.60
Sulfur (wt%)	0–0.77	2.50
Ash (wt%)	<0.25	0.04
pH	2.26–4.30	-*
Viscosity (Pa·s)	11.10–62.20@25 °C	0.23@30 °C
Density (g/mL)	0.98–1.19	0.94
Higher heating value (HHV, MJ/kg)	17.40–32.46	44.17
Reference	[10]	[10]

* Not available

Table 1.2 Typical chemical compositions of bio-oils produced from different feedstocks

Feedstock	Switchgrass (%[1])	Rice husk (%)	Palm Shells (%)	Pine Sawdust (%)	Algae (%)	Corn Stover (wt%[2])	Switch grass (wt%)	Algae (wt%)	Pine (wt%)	Hard wood (wt%)	Soft wood (wt%)
Temperature (°C)	510	450	490	500	500	500	500	360	520	460	510
Phenols	18.95	29.20	50.44	16.98	27.93	2.39	0.97	1.70	-	1.40–3.90	1.40–3.90
Ketones	9.86	2.80	-	-	3.16	0.20	1.39	1.50	5.36	0.08–0.96	0.02–0.73
Aldehydes	10.26	0.00	3.42	-	-	4.00	-	-	9.73	1.03–14.36	0.52–0.70
Acids	3.25	5.10	6.87	4.64	10.42	6.26	10.03	0.50	5.60	3.30–21.50	2.20–19.00
Esters	4.23	-	-	-	-	-		-	-	-	-
Furans	7.81	2.30	-	-	6.41	0.71	3.38	-	4.47	0.20–1.93	0.39–1.83
Ethers	9.22	-	4.51	-	-	-	-	-	-	-	-
Alcohols	5.66	9.40	1.01	-	0.36	7.12	0.64	-	2.9	6.41–7.82	1.78–3.17
Others	30.76	51.20	33.75	78.38	51.72	79.32	83.59	96.30	71.94	49.53–87.58	70.67–94.21
Reference	[44]	[44, 45]	[46]	[47]	[48]	[49]	[50]	[51]	[52]	[53]	[53]

[1] peak area; [2] mass percentage

CHAPTER 2

Develop bifunctional Ni/HZSM-5 catalyst for converting prairie cordgrass to hydrocarbon biofuel

2.1 Abstract

Ni/HZSM-5 catalysts were prepared using the impregnation method. The HZSM-5 and impregnated Ni/HZSM-5 catalysts were characterized by Brunauer-Emmett-Teller and X-ray diffraction. The HZSM-5 and Ni/HZSM-5 catalysts were used for prairie cordgrass thermal conversion in a two-stage catalytic pyrolysis system. The products contained gas, biofuel and bio-char. The gas and biofuel were analyzed by Gas chromatography and Gas chromatography–mass spectrometry separately. Higher heating values and elemental composition of bio-char were determined. The results indicated that 12% Ni/HZSM-5 treatment yielded the highest amount of gasoline fraction hydrocarbons and showed a robust ability to upgrade bio-oil vapor.

2.2 Introduction

Energy demand is increasing due to the rapid growth of population and industrialization, and it is mainly fulfilled by fossil fuels. The massive utilization of fossil fuels leads to their reserve depletion and climate change. Alternative fuels such as biofuel can be utilized to alleviate dependence on fossil fuels and mitigate environmental problems [54]. Biofuel can be produced from different types of biomass, such as lignocellulosic biomass which includes forests wastes, agricultural

waste and energy crops [55]. One of the energy crops, prairie cordgrass (PCG) has high potential for biomass production. Pyrolysis is one of the most promising methods that can directly convert biomass into liquid biofuels (bio-oils).

However, the direct application of bio-oil produced from pyrolysis as fuels for engines is limited due to its high acidity, high viscosity and instability. Therefore, it requires further processing to become an acceptable fuel. Catalytic cracking is one promising bio-oil processing method, since it could be operated at atmospheric pressure without addition of hydrogen. HZSM-5 is the most effective for bio-oil catalytic cracking due to its shape-selectivity, ion exchange capacity and unique solid acid characteristics [56]. Nickel, a cheap transition metal, can be used to modify HZSM-5 because it can increase the yield of aromatic hydrocarbons and the hydrothermal stability of HZSM-5[57]. Ni/HZSM-5 is also a good catalyst for light olefin oligomerization [58].

2.3 Materials and Methods

PCG was harvested from South Dakota State University agriculture extension farm. HZSM-5 was promoted with Ni (1wt.%, 6wt.% and 12wt.%) using wet impregnation method with aqueous solutions of nickel(II) nitrate hexahydrate. The Ni/HZSM-5 and HZSM-5 were dried at 120□ for 3h and then calcined at 550□ for 3 h. The BET analysis of catalysts was determined by automatic Micromeritics ASAP 2020 apparatus. XRD measurements were conducted on Rigaku Smartlab.

Experiments were conducted in a two stage reactor system which included a pyrolysis reactor (ID 5.08 cm, height 45.72 cm), a catalytic reactor (ID 2.54 cm, height 40.64 cm and a condenser (cooling temperature -10±2□). PCG（100 g）and catalysts (10 g) were used. Pyrolysis reaction was set at 500℃. A series of treatments were conducted on in catalytic reactor, which included non-catalytic reaction at 500℃, catalytic reaction at 500℃ using HZSM-5, catalytic reaction at 500℃ using 1%Ni/HZSM-5, catalytic reaction at 500℃ using 6%Ni/HZSM-5 and catalytic reaction at 500℃ using 12%Ni/HZSM-5. Gas and biofuel were collected and analyzed by Agilent GC-7890A and Agilent GC–MS separately.

2.4 Results and discussions

2.4.1 Feedstock and catalyst characterizations

The carbon, hydrogen, nitrogen content of PCG were 44.27 wt.%, 5.82 wt.% and 4.13 wt.% respectively. The moisture content was 7.14 wt.%, and the higher heating value was 17.42MJ/kg. Table 2.1 listed BET surface areas and pore volumes of catalysts. The surface area and total pore volume of HZSM-5 decreased when NiO was added to the HZSM-5 supports. This reduction was due to pore blocking by metal species dispersed in the channels or by the presence of metal oxide aggregates [59]. The XRD patterns of fresh catalysts in the angle region (5–50°) are presented in Figure 2.1. The similarity of the XRD patterns indicates that the framework of HZSM-5 was still kept after loading nickel. The XRD peaks of NiO

（37.2°, 43.3°）were detected in 6%Ni/HZSM-5 and 12%Ni/HZSM-5, which means crystallinity of NiO was generated on the surface of the catalyst [60].

2.4.2 Product yields and analysis

Three main products: biofuel, gas and bio-char are formed from biomass decomposition. As shown in Table 2.2, bio-char yields of all treatments show no significant difference due to the same pyrolysis condition. There is no significant difference in yields of biofuel and gas among all treatments except 6%Ni/HZSM-5 treatment. 6%Ni/HZSM-5 generated the lowest biofuel yield and highest gas yield, which is probably due to the minimal catalyst deactivation that results from the least coke deposition [61].

Composition of biofuels is presented in Table 2.3. Biofuel produced by non-catalytic treatment mainly contained furans, phenols, aldehydes and ketones. In contrast, the content of furans reduced to some degree in catalytic treatments. Especially the 6%Ni/HZSM-5 and 12%Ni/HZSM-5 treatments obtained biofuels without furans. Compared to non-catalytic treatment, HZSM-5 and 1%Ni/HZSM-5 treatments improved the total percentage of phenols. This indicated that part of pyrolytic lignin was converted into phenolic compounds on the HZSM-5 and 1%Ni/HZSM-5. However, no phenols were identified in biofuels generated by 6%Ni/HZSM-5 and 12%Ni/HZSM-5 treatment, which indicates that more Ni loading to HZSM-5 promotes transformation of phenols to other compounds such as aromatic hydrocarbons. This is probably due to decarbonylation and

oligomerization (Veses et al., 2015). The aldehydes can be even removed by catalytic treatment. This may be due to a series of transformations of acetalization, etherification and rearrangement, or by thermal degradation into carbonaceous deposits [62]. Secondary degradation reactions by the catalysts were beneficial for decreasing the ketone content in biofuels. Ni/HZSM-5 catalysts performed better at converting ketones compared to HZSM-5 catalysts.

Hydrocarbons in the biofuel are the principal compounds that most researchers focused on. The strong Brønsted acid sites in the HZSM-5 facilitate the formation of aromatics hydrocarbons through dehydration, cracking, decarbonylation, decarboxylation and aromatization. Formation of hydrocarbons increased for all catalytic treatments, with HZSM-5 having the most effect. However, the hydrocarbons in the biofuel obtained by HZSM-5 treatment mainly contained heavy compounds (≥C13). All Ni/HZSM-5 treatments seem to increase the formation of light hydrocarbons（C4-C12, mainly gasoline fraction）in the biofuel, especially12% Ni/HZSM-5 obtain the highest yield at 32.45%. When the NiO was loaded on HZSM-5, the framework of HZSM-5 interacted with NiO at channels decreased the Brønsted acid sites, which may lead to obtaining more light hydrocarbons.

Moreover, Ni/HZSM-5 is an efficient catalyst for ethylene, propene and butene oligomerization. C_2H_4, C_3H_6 and C_4H_8 were the three components in the bio-oil vapor from the pyrolysis reactor. Therefore, they can be converted into hydrocarbons over Ni/HZSM-5 catalysts, which is one possible reason for the increase of hydrocarbons.

Gas distribution is listed in Table 2.4. Compared to non-catalytic treatment, catalytic treatments increased total amount of carbon dioxide and carbon monoxide. This is due to the decarboxylation and decarbonylation reactions that occurred on zeolite catalysts respectively.

Bio-char is a solid material gained from the carbonization of biomass. Physical properties of bio-chars are presented in Table 2.5. Since all bio-chars were obtained in the same pyrolysis conditions in the pyrolysis reactor, there is no significant difference in their HHV and elemental analysis.

2.5 Conclusions

Catalytic effects of Ni/HZSM-5 and HZSM-5 catalysts on product yields and distribution were conducted in the two stage reactor system. 12%Ni/ HZSM-5 treatment yielded the highest amount of gasoline（C4-C12） hydrocarbons and exhibited an excellent ability to upgrade bio-oil vapor.

Table 2.1 BET parameters of different Catalysts

Catalyst	Surface area (m^2/g)	Pore volume (cm^3/g)		
	BET	Total[a]	Micropores	Mesopores
HZSM-5	473.33	0.46	0.09	0.25
1%Ni/HZSM-5	451.41	0.44	0.07	0.21
6%Ni/HZSM-5	442.71	0.42	0.06	0.24
12%Ni/HZSM-5	386.16	0.36	0.07	0.16

[a] Total pore volume, measured at P/P_0= 0.995

Table 2.2 Product yields of different Treatments

Treatments	Liquid (wt.%)	Solid(wt.%)		Gas(wt.%)
	Biofuel	Bio-char	Coke	
No catalyst	29.33±0.17	26.07±0.34	-*	44.60±0.34
HZSM-5	24.98±0.08	30.59±0.25	1.41±0.08	43.02±0.45
1%Ni/ HZSM-5	25.43±0.12	32.73±0.17	1.47±0.15	40.37±0.87
6%Ni/ HZSM-5	18.17±0.65	31.46±0.89	1.15±0.24	49.22±1.07
12%Ni/ HZSM-5	29.19±0.07	29.79±1.04	1.52±0.14	39.50±0.67

* Not available

Table 2.3 Chemical composition of biofuels

Compounds relative content (%)	No catalyst	HZSM-5	1%Ni/HZSM-5	6%Ni/HZSM-5	12%Ni/HZSM-5
Phenols	11.22	32.53	46.97	0	0
Ethers	0.45	0	2.1	7.16	3.85
Furans	10.14	0.36	3.63	0	0
Ester	0	23.31	3.67	4.78	8.69
Alcohols	10.97	0.67	3.52	14.58	10.43
Aldehydes	4.85	0	0	0	0
Ketones	19.75	2.94	0	0	0
Light hydrocarbons (C4-C12)	2.37	8.32	28.27	30.42	32.45
Heavy hydrocarbons (C13-C24)	0	30.75	6.64	0	3.53

Table 2.4 Gas distribution of different Treatments

Gas (Vol.%)	No catalyst	HZSM-5	1%Ni/HZSM-5	6%Ni/HZSM-5	12%Ni/HZSM-5
H_2	16.73	5.47	8.06	8.39	6.14
CO_2	26.32	18.51	53.70	47.94	55.12
CO	21.82	44.50	17.41	26.62	23.68
CH_4	19.51	10.57	11.49	6.72	5.99
C_2H_6	7.61	6.52	3.96	3.46	2.38
C_2H_4	3.11	4.94	1.65	2.51	2.76
C_3H_8	1.59	3.75	1.16	1.02	1.05
C_3H_6	2.15	1.78	1.76	2.83	2.49
C_4H_{10}	0.36	1.74	0.25	0.21	0.20
C_4H_8	0.80	2.19	0.53	0.30	0.20
C_5H_{12}	0.00	0.04	0.02	0.00	0.00

Table 2.5 Physical properties of Bio-chars

Treatment	No catalyst	HZSM-5	1%Ni/HZSM-5	6%Ni/HZSM-5	12%Ni/HZSM-5
HHV(MJ/Kg)	28.48	26.92	27.94	27.91	29.11
Carbon(wt.%)	74.75	69.42	71.34	73.29	76.26
Hydrogen (wt.%)	2.61	3.18	2.99	3.32	2.86
Nitrogen(wt.%)	3.17	3.14	3.42	3.55	3.64
Rest[b](wt.%)	19.47	24.26	22.25	19.84	17.24

[b] Rest includes oxygen and traces of other elements.

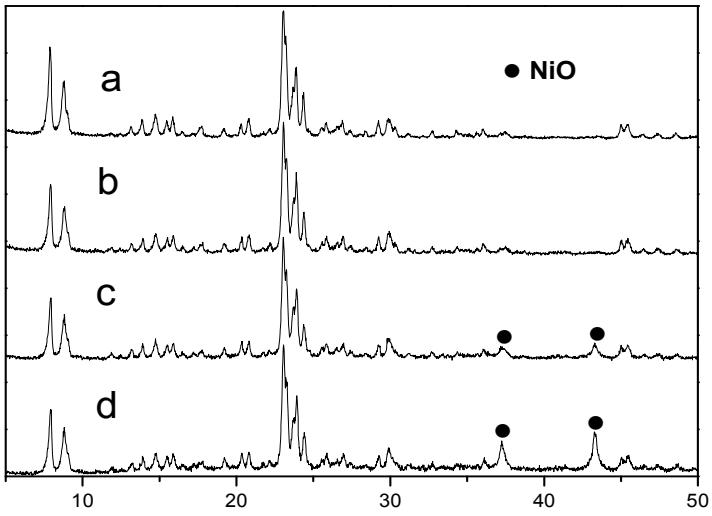

Figure 2.1 XRD patterns of fresh Catalysts (a-HZSM-5, b-f 1%Ni/HZSM-5, c-6%Ni/HZSM-5, d-12%Ni/HZSM-5).

CHAPTER 3

Converting prairie cordgrass to hydrocarbon biofuel over Co-Mo/HZSM-5 using a two-stage reactor system

3.1 Abstract

A series of Co-Mo/HZSM-5 catalysts were prepared for prairie cordgrass (PCG) thermal conversion using an impregnation method. The catalysts were characterized by Brunauer-Emmett-Teller (BET), X-ray diffraction (XRD), Fourier transform infrared spectrometer (FT-IR) and Transmission electron microscope (TEM). These Co-Mo/HZSM-5 catalysts were tested in prairie cordgrass thermal conversion to produce hydrocarbon biofuel in a two-stage catalytic pyrolysis system. The products including non-condensable gas, biofuel and biochar were analyzed. Compared to non-catalytic biofuel, the chemical composition, water content, higher heating value (HHV), viscosity and density of catalytic biofuels were improved. The results indicated that the 4%Mo-2%Co/HZSM-5 catalyst showed a robust ability in the PCG catalytic cracking with highest yield of hydrocarbons at 41.08 %.

3.2 Introduction

Due to the development of economic globalization, the energy demand of the world increases continually. The main source of energy is satisfied by depleting fossil fuels, which are unsustainable and related to air pollution and climate change

[63]. On the other hand, the use of renewable energy such as biofuel is growing, because it can improve energy security and reduce greenhouse gas emissions [64]. Biofuel can be produced from a wide range of lingo-cellulosic biomass, including agricultural waste, wood, forest residues, energy crops et al. One of the energy crops: prairie cordgrass (PCG) is indigenous throughout North America, and it has high potential for biomass production [64, 65]. Fast pyrolysis is an advanced thermochemical method that can effectively convert biomass such as prairie cordgrass to biochar, gas and liquid biofuel (bio-oil), and the bio-oil produced can be readily stored and transported for the use as energy, chemicals or an energy carrier. However, the raw bio-oil has some unfavorable characteristics such as high viscosity and corrosiveness, low chemical stability and heating values due to its oxygen-rich composition, which impedes its direct use as transport fuels. Therefore, the upgrading of the oxygenated compounds in bio-oils to hydrocarbon biofuels is needed to produce a liquid product that can meet the requirements of the engine fuels. There are two main routes that have been developed to reduce the oxygen content in bio-oils, namely hydrodeoxygenation (HDO) and catalytic cracking. Bio-oil HDO is conducted in the presence of hydrogen and catalysts under high hydrogen pressure (80-300 bars), and this increased its capital and operation costs [66]. Alternately, catalytic cracking of bio-oil seems to be an economical route to upgrade bio-oil, since this process can be operated under atmospheric pressure without the consumption of hydrogen. Different types of microporous materials such as HZSM-5,USY, HY, ferrierite, βzeolite, mordenite, rare-earth Y zeolite and

silicate have been investigated for bio-oil catalytic cracking [67]. Due to its strong acidity and shape selectivity, HZSM-5 is the most effective catalyst for hydrocarbon biofuel production from the pyrolytic vapors of biomass [19]. The HZSM-5 zeolite was an acid catalyst with Brønsted acid sites and Lewis acid sites [68]. The HZSM-5 zeolite performed the catalytic activity of bio-oil upgrading by its acidic sites, which promoted deoxygenation, decarboxylation, decarbonylation, cracking, oligomerisation, alkylation, isomerisation and cyclisation of the pyrolytic oil from biomass pyrolysis. However, the strong acidity of HZSM-5 led to the decrease of the yield of the organic fraction in bio-oil and coke formation. Zeolite could be modified by incorporation of metals as promoter. The Co or Mo modified HZSM-5 increased the yields of hydrocarbons and reduced coke formation in catalytic upgrading of biomass pyrolysis vapors in comparison with HZSM-5, which was attributed to the dehydrogenating sites introduced though these transition metals [69]. Mo doped HZSM-5 was also one promising catalyst that was able to convert methane to aromatic hydrocarbons through methane aromatization [70], and the presence of carbon monoxide and carbon dioxide resulted in the promotion of aromatic hydrocarbon formation and a remarkable improvement of the catalyst stability [71]. The gas phase generated from catalytic cracking of biomass pyrolysis contained methane, carbon monoxide and carbon dioxide. Therefore, the methane can be converted to aromatic hydrocarbons over Mo/HZSM-5. The metal-acid catalysts (Co-Mo/HZSM-5) designed in this study were one type of bifunctional catalysts. It combined the catalytic activity of acid HZSM-5, the dehydrogenating

effect of metal Co and Mo, and the methane aromatization function of metal Mo. The purpose of this bifunctional catalyst was to increase hydrocarbon yield and reduce coke formation during biomass catalytic pyrolysis.

In this work, bifunctional Co-Mo/HZSM-5 catalysts were firstly developed for PCG catalytic fast pyrolysis in the two stage fixed-bed reactor to produce hydrocarbon bio-fuels. The aim of this study was to determine optimal Co and Mo loading ratio HZSM-5 catalysts to obtain better yield and quality of hydrocarbon biofuel using the two stage reaction system. The gas distribution and biochar properties will also be discussed.

3.3 Experimental Section

3.3.1 Feedstock and catalysts

The prairie cordgrass (PCG) was harvested from SDSU agriculture extension farm nearby South Dakota State University.

Cobalt (II) nitrate hexahydrate (98 wt.%) and ammonium molybdate tetrahydrate (83 wt.%MoO_3 basis) were purchased from Sigma-Aldrich Inc. The HZSM-5 zeolite with Si/Al molar ratio of 30 was provided by Zeolyst International Company. A series of Co-Mo/HZSM-5 catalysts with different Co/Mo mass ratios (2%Co/HZSM-5,2%Mo/HZSM-5,2%Mo-2%Co/HZSM-5, 2%Mo-4%Co/HZSM-5,4%Mo-2%Co/HZSM-5) were prepared by the wet impregnation method using aqueous solutions of cobalt (II) nitrate hexahydrate and ammonium molybdate

tetrahydrate at room temperature (20 ºC). Then all catalysts were dried at 120 ºC for 4 h and calcined at 500 ºC in air for 6 h before use.

3.3.2 Catalyst characterizations

The BET specific surface area and porosity texture of catalysts were determined by Tristar 3000 micropore analyzer at 77 K. The catalyst sample was degassed at 573 K before the nitrogen adsorption and desorption experiment. The Brunauer–Emmett–Teller (BET) surface areas were calculated from the BET equation. Total pore volume was calculated based on the amount of nitrogen vapor adsorbed at a P/P_0 of 0.99. Density functional theory (DFT) was utilized to determine the micropore, mesopore and pore size distribution.

The structural phase and crystallinity of catalysts were analyzed by X-ray diffraction (XRD). XRD analysis was conducted on a Rigaku Smartlab with CuKα radiation operating at 40 kV and 44 mA. The X-ray pattern was scanned with a step size of 0.02 ° (2θ) from 5 to 80 ° (2theta) and a scanning speed of 4 ° min^{-1}.

The Fourier transform infrared spectrometer (FT-IR) analysis was carried out in a Nicolet 6700 FT-IR spectrometer using KBr pellets. The wavenumber of the IR spectra was recorded from 4000 cm^{-1} to 400 cm^{-1}.

Transmission electron microscope (TEM, JEOL JEM-2100 LaB6) with an accelerating voltage of 200KV was used for the TEM analysis of prepared catalysts.[24] The catalyst powders were dispersed in isopropyl alcohol using an ultrasonic apparatus. Then, a few drops of the sonicated solution were deposited

onto a carbon-film supported Cu grid and allowed to evaporate under ambient conditions.

3.3.3 Product characterizations

The moisture content of the PCG was determined by following the ASABE standard (ASAES358.2 DEC1988 (R2008)). The elemental compositions (carbon, hydrogen and nitrogen) of the feedstock were analyzed by the CE-440 Elemental Analyzer. The higher heating value（HHV）of PCG samples was tested by the bomb calorimeter (Parr Instrument Company C2000).

The properties (density, dynamic viscosity, water content, higher heating value and chemical composition) of upgraded biofuel were also characterized. Density was measured by the ratio of mass to volume of samples at room temperature (20 °C). A viscosity analyzer (REOLOGICA, Instruments AB Company) was employed to analyze the dynamic viscosity of biofuels at 20 °C. Water content was analyzed by a Karl Fischer Titrator V20 (Mettler Toledo Company) in accordance with ASTM E1064. The higher heating value of biofuels was determined by the same the bomb calorimeter as the PCG. The elemental analysis (carbon, hydrogen and nitrogen) of biofuel samples was also measured by the CE-440 elemental analyzer.

The major components of biofuel were analyzed by GC–MS (AgilentGC-7890A (DB-5 column: 30 m × 0.25 mm × 0.25 μm)) and MSD-5975C (electron ionization at 70 eV, mass range of 50–5000 m z^{-1}, semi-quantitation based on TIC,

mass chromatograms).The carrier gas was hydrogen with a flow rate of 1 mL min^{-1}. The injection temperature and the injection volume were 300 °C and 1μL respectively. The initial column temperature was 60 °C and it was held for 1 min. Then, the column temperature increased by following ramp 1 at 3 °C min^{-1} to 140 °C, ramp 2 at 10 °C min^{-1} to 180 °C, ramp 3 at 3 °C min^{-1} to 260 °C, and ramp 4 at 10 °C min^{-1} to 300 °C. The temperature was maintained for an additional 2 min after each ramp. The major compositions of biofuel were identified based on the NIST Mass Spectral library and literature. The relative content of each compound in the oil phase was calculated by the percent of the peak area for each compound in the total peak areas in the GC–MS spectroscopy.

The gas chromatography system (Agilent GC 7890A) with a 50 m× 0.53 mm × 15 μm 19095P-S25 column was employed to analyze compositions of non-condensable gas. The thermal conductivity detector (TCD) was utilized for the determination of H_2, CO, CO_2 and N_2, and the flame ionization detector (FID) was used for the analysis of light hydrocarbons (C_1–C_5). Standard gas mixtures were used for calibration, and argon was employed as the carrier gas.

3.3.4 Experimental apparatus and procedure

As shown in Figure 3.1, a two-stage reaction system for the production of upgraded biofuel from prairie cordgrass was designed and operated under atmospheric pressure. The system consisted of three units: a pyrolysis reactor (inner diameter: 5.08 cm, length: 45.72 cm) for the pyrolysis of PCG, a catalytic reactor

for catalytic cracking of bio-oil (inner diameter: 2.54 cm, length: 40.64 cm) and a condenser (cooling temperature: -10±2°C). 100.00 g of prairie grass was loaded in the pyrolysis reactor, and 10.00 g of catalysts was added in the catalytic reactor. Before each run, the system was flushed with nitrogen to remove air at a flow rate of 15 mL min^{-1} for 0.5 h. A series of bio-oil upgrading treatments were conducted in the catalytic reactor, which included non-catalytic reaction at 600 °C using sand and a series of catalytic reactions at 600 °C using HZSM-5, 2%Mo/HZSM-5, 2%Co/HZSM-5, 2%Mo-2%Co/HZSM-5, 2%Mo-4%Co/HZSM-5 and 4%Mo-2%Co/HZSM-5. The catalytic reactor was heated to 600 °C at a rate of 45 °C min^{-1} by a furnace. The flow rate of nitrogen was maintained at 5 mL min^{-1}. Then the pyrolysis reactor was heated to 600 °C at a rate of 40 °C /min by a furnace, and then non-condensable gas (syngas) was collected and analyzed. The reactor system was turned off after the pyrolysis reactor was kept at 600 °C for 1.5 h. Another 2 h was allowed to cool the system after each test. Then, the biofuel was collected from the condenser. The biochar was obtained by disassembling the pyrolysis reactor, and the coke was calculated by the weight difference of the catalytic reactor with catalyst before and after test. The gas was calculated by subtracting the weights of biofuel, biochar and coke from the original weight of prairie cordgrass. The mass yields of gas, biochar, coke, aqueous phase and oil phase were measured in Equation (1) and in Equation (2):

$$Y\ product\ (wt\%) = m\ product(g) / m\ PCG(g) \times 100 \quad (1)$$

$$Y\ gas\ (wt\%) = 100 - Y\ biochar - Y\ coke - Y\ aqueous\ phase - Y\ oil\ phase \quad (2)$$

where Y product and m product were the yield of the upgraded products (biochar, coke, aqueous phase and oil phase) and the mass of the upgraded products respectively.

Each test was performed twice in order to obtain the objective experiment results, and average values were reported. Two decimals were used for all data.

3.4 Results and Discussion

Physical properties of prairie cordgrass are depicted in Table 3.1. The moisture content of the feedstock was less than 10 %, and the low water content can minimize the water content in biofuel product. The mean particle size of the grass is 0.73 mm. The small particle size is beneficial for improving the heating transfer rate during biomass pyrolysis process, and this is due to its high surface area [72].

Table 3.2 lists BET surface areas and pore volumes of HZSM-5 and how they are affected by the addition of Co and/or Mo. The surface area and pore volume decreased when Co and/or Mo was added to the HZSM-5 supports, and this was probably due to the existence of metal oxides aggregates on the external zeolite surface [73], or the deposition of some metal oxides in internal pores and channels [74].

There are two possible reasons for the increases of average pore sizes in 2%Mo-2%Co/HZSM-5(4.59 nm) and 4%Mo-2%Co/HZSM-5 (4.63 nm) in comparison with HZSM-5(4.43 nm). One possible reason was the formation of some larger mesopores caused by the interparticle voids, which may result from Co

and/or Mo metal oxide aggregates that deposited on the external surface of HZSM-5. Another possible reason was the partial blocking of the micropores caused by the deposition of some Co and/or Mo metal oxides in the inside pores and channels of HZSM-5 [74].

The XRD patterns of all catalysts in the angle region (5–80°) are presented in Figure 3.2. The similarity of the XRD patterns between fresh HZSM-5 and Co and/or Mo loaded zeolites indicated that the framework of HZSM-5 still existed after loading Co and/or Mo, because the presences of typical peaks of HZSM-5 (around 8 °, 9 °, 23-25 °) were still maintained [75]. However, the crystallite peaks of metal oxides could not be observed in the XRD patterns of Co and/or Mo loaded HZSM-5, and it indicates that Co and/or Mo metal oxides crystallites are highly dispersed on HZSM-5 surface and/or in its channels [76].

The valence state of Co over fresh Co/HZSM-5 should be attributed to Co_3O_4.After the prairie cordgrass catalytic pyrolysis test, Co_3O_4 might be reduced to CoO or metallic Co in the reductive atmosphere.The valence state of Mo over fresh Mo/HZSM-5 should be attributed to MoO_3. After the reactions, partial MoO_3 might be converted to Mo_2C (in the form of molybdenum oxycarbide) or Mo^{5+} species in methane aromatization reactions. This was proven in the XPS analysis of Mo/HZSM-5 used in the methane conversion process by L. Chen et al [77].

The FT-IR spectra of the parent HZSM-5 zeolite and the Co and/or Mo modified HZSM-5 catalysts are shown in Figure 3.3. The fresh ZSM-5 exhibited the

characteristic peaks of MFI structure at around: 1220 cm^{-1} (external asymmetric stretch), 1100 cm^{-1} (internal asymmetric stretch), 800 cm^{-1} (external symmetric stretch), 550 cm^{-1} (double ring) and 450 cm^{-1} (T-O bending vibration of internal tetrahedral) [78]. The absorption band at 450 cm^{-1} was due to the T–O bending vibrations of the SiO_4 and AlO_4 internal tetrahedra. The fresh Co and/or Mo-loaded HZSM-5 also exhibited the characteristic peaks of MFI structure in the FT-IR spectra, which indicates that the introduction of Co and/or Mo to HZSM-5 had no significant influence on the framework of the parent HZSM-5. Bands of all catalysts at around 3609 cm^{-1} assigned to strong Brønsted acid sites (Si-OH-Al) were also observed [59].

TEM images (50 nm or 100 nm) of all fresh catalysts are shown in Figure 3.4. Fresh HZSM-5 and Co and/or Mo loaded HZSM-5 showed clear lattice fringes of HZSM-5 (large visible dark area), which confirmed high crystallinity of the zeolite particles. The HZSM-5 did not show obvious small dark spots because there was no metal oxides loading on it. In addition, there were no small dark spots observed for fresh 2%Co/HZSM-5, 2%Mo/HZSM-5 and 2%Mo-2%Co/HZSM-5 catalysts, which confirmed that Co and/or Mo metal oxides were well dispersed on the HZSM-5 support. When more Co and Mo were loaded over HZSM-5, many small dark spots appeared in the TEM images of 2%Mo-4%Co/HZSM-5 and 4%Mo-2%Co/HZSM-5. They might be attributed to Co and/or Mo metal oxide aggregates.

Three main products (biofuel, biochar and non-condensable gas) were generated from the decomposition of cellulose, hemicellulose and lignin in PCG. The mass

balances of non-catalytic and catalytic treatments are presented in Table 3.3. The biochar yields of all treatments showed no significant difference due to the same reaction condition in the pyrolysis reactor. Biofuel included aqueous phase and oil phase. Compared to non-catalytic treatment, the total liquid yield decreased in all catalytic treatments, and this was due to the cracking, dehydration, decarbonylation, decarboxylation reactions catalyzed by the Bronsted acid sites over HZSM-5 and Co-Mo/HZSM-5. Besides, all Co or Mo loading HZSM-5 increased biofuel yields compared to HZSM-5. This is probably because of the reduced cracking behavior of HZSM-5 caused by the addition of Co and Mo. 2%Mo-2%Co/HZSM-5 generated the highest biofuel yield at 38.23 % in all catalytic treatments. The catalysts can be easily deactivated by coke, which was due to the polymerization over zeolites [69]. Compared to HZSM-5, the Co-Mo/HZSM-5 catalysts decreased the coke yield, and this is consistent with the research results of R.French [79].

The biofuel was composed of aqueous phase and oil phase. The aqueous phase mainly contained water, and it was a light yellow liquid. In comparison, the targeted oil phase was mainly composed of organic compounds, and it was dark brown liquid with unpleasant odor. The physicochemical properties of biofuels generated in different treatments are shown in Table 3.4. It shows properties of the catalytic and non-catalytic biofuels, including higher heating values (HHV), density, viscosity and water contents for both aqueous phase and oil phase. The yield of oil phase for the non-catalytic treatment was 15.27 % (Table 3). The catalytic treatments reduced the oil phase yield and increased gas yield. This may be due to

the deoxygenation of organic compounds over HZSM-5 and Co-Mo/HZSM-5, which generated H_2O, CO and CO_2 that were transferred to aqueous phase and non-condensable gas. The HHV of oil-phase generated by catalysts were higher than the oil phase of non-catalytic treatment. The 4%Mo-2%Co/HZSM-5 generated oil phase with the highest HHV at 26.96 $MJkg^{-1}$. This indicated that Co-Mo/HZSM-5 catalysts can improve the higher heating values of biofuels. The water content affected the HHV, viscosity, density and acidity of biofuels. The water content of catalytic biofuels reduced to less than 9.73 % in comparison with the non-catalytic biofuel (10.80 %). The catalytic cracking of HZSM-5 and Co-Mo/HZSM-5 led to lower water content and the formation of lower molecular weight organic compounds [62], and this resulted in the lower density and viscosity of the catalytic oil phase compared to these properties in the oil phase of non-catalytic treatment.

In order to evaluate the catalytic effect of different catalysts on the product distribution of oil phase, the chemical compositions of oil phases for all treatments were analyzed using GC-MS. More than 180 compounds were found in the oil phase, and these chemicals originated from the degradation of cellulose, hemicellulose and lignin presented in prairie cordgrass. The oil phases produced were classified into different chemical groups, namely phenols, ethers, ketones, esters, aldehydes, furans, alcohols, acids and hydrocarbons. These chemical groups for non-catalytic and catalytic PCG biofuels are present in Table 3.5.

In non-catalytic treatment, the PCG oil phase produced was mainly composed of ketones (22.44 %), phenols (20.81 %), alcohols (17.17 %) and esters (10.31 %).

It also contained undesirable aldehydes (8.25 %) and acids (7.55 %), which are responsible for low stability and low higher heating value. The content of desirable hydrocarbons was only 5.32 %.

The organic compositions of biofuel changed significantly after catalytic cracking reaction over HZSM-5 and Co-Mo/HZSM-5 catalysts. After the reaction, the content of phenols increased in all catalytic treatments. Similar results were found by M. S. A. Bakar et al [80]. 4%Co-2%Mo/HZSM-5 catalyst generated the oil phase with the highest phenol content at 74.80 %. The improvement of phenols was due to the formation of alkyl-phenols such as 2-methyl-phenol and 3,4-dimethyl-phenol that occurred on HZSM-5 and Co-Mo/HZSM-5 catalysts. This is possibly caused by the alkylation reactions between phenol and alcohols, and following by cracking, demethoxylation, demethylation and hydrogenation that generated alkylated phenols [81]. The biofuel obtained by Co-Mo/HZSM-5 catalysts contained more phenols than the biofuel produced from HZSM-5 catalyst, which indicated that loading Co and Mo to HZSM-5 benefited in improving the performance of alkyl-phenols formation.

The ketones content in the oil phase decreased in all catalytic treatments, and this is caused by secondary degradation reactions over zeolite catalysts. It seemed that the addition of Mo to HZSM-5 significantly helped in reducing the ketone content, especially the 2%Co-2%Mo/HZSM-5 catalyst obtained biofuel without ketones. The content of aldehydes also reduced in all catalytic treatments, and carboxylic acids were eliminated with the use of catalysts compared to the non-

catalytic pyrolysis. The transformation of aldehydes and acids mainly occurs through decarboxylation and dehydration over HZSM-5 and Co-Mo/HZSM-5 catalysts [82].

The contents of esters and alcohols in the oil phase of catalytic treatments also decreased compared to non-catalytic treatments. This may be due to the transformation of esters and alcohols to hydrocarbons caused by dehydration, cracking and oligomerization reactions that occurred over HZSM-5 and Co-Mo/HZSM-5 catalysts.

Hydrocarbons are the main targeted products that most research focused on. Compared to non-catalytic treatments, the hydrocarbons content increased in all catalytic treatments. This resulted from the thermo-catalytic effects (deoxygenation, cracking, cyclization, isomerization and polymerization) of HZSM-5 and Co-Mo/HZSM-5 catalysts. Especially, the 4%Mo-2%Co/HZSM-5 produced the upgraded biofuel with the highest hydrocarbon content at 41.08 %. This was probably due to the additional aromatization behavior of Mo/HZSM-5 that converted CH_4 in the non-condensable gas to hydrocarbons in the biofuel liquid [70].

Gas distributions of all treatments are listed in Table 3.6. Compared to non-catalytic treatment, all catalysts increased total amount of carbon dioxide and carbon monoxide. This is due to the decarboxylation and decarbonylation reactions that occurred on zeolite catalysts respectively. CH_4 content in Mo modified HZSM-

5 treatments decreased compared to other treatments, and this might due to the effect of Mo/HZSM-5 in methane aromatization that converts CH_4 into liquid hydrocarbons [83].

Biochar is a solid material gained from the carbonization of biomass. The char may be used as solid fuel or soil enhancer [84]. Physical properties of biochars in all treatments are presented in Table 3.7. Since all biochars were obtained in the same pyrolysis conditions in the pyrolysis reactor, there is no significant difference in their HHV and elemental analysis.

3.5 Conclusions

In this study, Co-Mo/HZSM-5 catalysts with different Co/Mo ratio were prepared by the impregnation method. These catalysts were characterized by BET, XRD, FT-IR and TEM. All Co-Mo/HZSM-5 catalysts were used for prairie cordgrass catalytic pyrolysis in the two stage reactor system. The catalytic effect of different Co-Mo loading HZSM-5 on product (biofuel, biochar and gas) yields and product distribution were analyzed. The HHV, water content, density, viscosity and pH of catalytic biofuel were improved compared to non-catalytic biofuel. 4%Mo-2%Co/HZSM-5 treatment yielded the highest amount of hydrocarbons at 41.08 %, exhibited an excellent ability to upgrade biofuel vapor, and showed no significant difference in the properties of biochar when compared to other treatments in the same pyrolysis conditions.

Table 3.1 Properties of prairie cordgrass

Analysis [a]	Data
Moisture content [wt.%]	7.14±0.18
Elemental analysis [wt.%]	
Carbon	44.27±0.62
Hydrogen	5.82±0.04
Nitrogen	1.50±0.20
Oxygen [a]	48.41±0.14
Higher heating value[MJ kg^{-1}]	17.42±0.31

[a] Calculated by 100%- carbon- hydrogen- nitrogen

Table 3.2 BET parameters of fresh catalysts

Catalyst	Surface area [$m^2 g^{-1}$]	Pore Size [nm]	Pore volume [$cm^3 g^{-1}$]		
	BET	Average	Total[b]	Micropores	Mesopores
HZSM-5	598.8	4.43	0.66	0.46	0.20
2%Co/HZSM-5	517.6	4.15	0.58	0.37	0.21
2%Mo/HZSM-5	521.1	4.14	0.59	0.39	0.20
2%Mo-2%Co/HZSM-5	495.9	4.59	0.57	0.41	0.16
4%Mo-2%Co/HZSM-5	474.7	4.63	0.55	0.50	0.05
2%Mo-4%Co/HZSM-5	475.0	4.33	0.51	0.33	0.18

[b] Total pore volume, measured at $P/P_0 = 0.99$

Table 3.3 Product yields of different treatments

Treatments	Liquid [wt.%]			Solid [wt.%]		Gas [wt.%]
	Total	Oil phase	Aqueous phase	Biochar	Coke	
Sand	40.38±1.71	15.27±1.10	25.11±1.62	27.33±0.13	0.00±0.00	32.39±1.59
HZSM-5	22.48±0.72	9.57±0.45	12.91±1.27	30.33±1.56	0.99±0.08	46.20±0.67
2 %Co/HZSM-5	26.61±1.28	10.31±0.22	16.30±1.50	28.61±0.14	0.33±0.01	44.45±1.44
2%Mo/HZSM-5	30.79±1.28	10.86±0.10	19.33±1.35	30.08±0.12	0.26±0.31	38.87±1.34
2%Mo-2%Co/HZSM-5	38.23±1.30	14.31±0.90	23.92±1.40	30.06±0.38	0.75±0.10	30.97±1.39
4%Mo-2%Co/HZSM-5	31.62±1.36	10.86±0.02	20.76±1.34	29.81±0.38	0.79±0.06	37.78±0.85
2%Mo-4%Co/HZSM-5	32.57±1.28	12.02±1.13	20.55±0.16	29.91±0.42	0.79±0.07	36.73±1.82

Table 3.4 Physicochemical properties of different biofuels

Treatments	HHV [MJ kg^{-1}]		Water content [%]		Density [g mL^{-1}]		Viscosity [cP]	
	Oil phase	Aqueous phase	Oil phase	Aqueous phase	Oil phase	Aqueous phase	Oil phase	Aqueous phase
Sand	18.61±0.16	5.46±0.49	10.80±0.14	87.08±2.35	1.25±0.01	0.91±0.02	6.90±0.01	2.24±0.11
HZSM-5	19.45±0.14	3.13±0.19	9.73±0.04	95.16±2.46	0.89±0.01	0.90±0.02	1.87±0.01	1.56±0.02
2 %Co/HZSM-5	19.96±0.01	2.36±0.10	9.10±0.14	89.92±0.91	0.90±0.01	0.90±0.04	1.72±0.03	1.52±0.04
2%Mo/HZSM-5	23.64±1.21	2.90±0.14	6.74±0.03	86.69±0.04	0.88±0.02	0.90±0.05	1.61±0.01	1.47±0.02
2%Mo-2%Co/HZSM-5	22.85±0.43	0.84±0.02	7.86±0.03	85.99±2.07	0.79±0.01	0.92±0.05	1.73±0.04	1.55±0.02
4%Mo-2%Co/HZSM-5	26.96±0.01	2.26±0.20	5.49±0.03	83.70±2.24	0.87±0.02	0.90±0.03	3.28±0.01	1.72±0.04
2%Mo-4%Co/HZSM-5	20.79±0.05	2.44±0.21	8.92±0.03	87.62±2.06	0.84±0.05	0.90±0.04	2.51±0.03	1.52±0.02

Table 3.5 Chemical composition of different oil phases

Compounds relative content [%]	Sand	HZSM-5	2%Co /HZSM-5	2%Mo /HZSM-5	2%Mo-2%Co /HZSM-5	4%Mo-2%Co /HZSM-5	2%Mo-4%Co /HZSM-5
Phenols	20.81	24.42	33.45	39.64	57.17	45.80	74.80
Ethers	0	0	1.34	0.83	0.78	0	0
Ketones	22.44	10.15	8.26	0.82	0	0.58	0.54
Aldehydes	8.25	0	0	0	1.39	0	0
Furans	2.77	0	2.01	0	0.54	0	0
Esters	10.31	8.89	6.53	9.99	0.90	8.19	2.10
Alcohols	17.17	14.92	10.04	9.38	1.90	1.51	4.02
Acids	7.55	0	0	0	0	0	0
Hydrocarbons	5.32	24.51	30.33	26.65	36.07	41.08	16.73
Others	5.38	17.11	8.04	12.69	1.25	2.84	1.81

Table 3.6 Gas distributions of different treatments

Gas [vol.%]	Sand	HZSM-5	2%Co /HZSM-5	2%Mo /HZSM-5	2%Mo-2%Co /HZSM-5	4%Mo-2%Co /HZSM-5	2%Mo-4%Co /HZSM-5
H_2	18.344±1.12	13.254±2.61	11.33±0.98	11.34±0.88	14.48±2.23	14.13±2.08	10.43±1.10
CO_2	26.44±2.51	41.45±3.47	40.31±3.03	36.33±1.77	37.14±1.13	31.25±0.53	32.94±4.42
CO	24.21±2.50	19.16±1.74	25.47±0.44	32.52±3.09	27.68±2.97	33.64±2.71	35.77±2.65
CH_4	17.65±1.32	14.80±0.35	14.60±3.46	12.48±1.43	10.57±0.09	11.91±0.60	11.10±0.14
C_2H_6	5.31±0.16	5.46±0.70	3.31±0.53	3.00±0.99	4.76±0.82	3.88±0.22	3.80±0.12
C_2H_4	3.25±0.10	1.63±0.19	1.70±0.48	1.60±1.07	1.56±0.27	1.65±0.12	1.91±0.03
C_3H_8	1.05±0.03	1.35±0.34	0.74±0.09	0.60±0.26	1.08±0.19	0.85±0.04	0.87±0.05
C_3H_6	2.55±0.09	1.89±0.02	1.73±0.51	1.50±0.91	1.84±0.32	1.84±0.15	2.17±0.07
C_4H_{10}	0.11±0.10	0.28±0.03	0.13±0.02	0.10±0.05	0.18±0.03	0.27±0.18	0.15±0.01
C_4H_8	0.75±0.30	0.68±0.21	0.63±0.23	0.50±0.34	0.68±0.12	0.44±0.30	0.81±0.06
C_5H_{12}	0.35±0.01	0.06±0.01	0.04±0.01	0.03±0.01	0.05±0.01	0.15±0.15	0.05±0.00

Table 3.7 Physical properties of different biochars

Treatment	Sand	HZSM-5	2%Co /HZSM-5	2%Mo /HZSM-5	2%Mo-2%Co /HZSM-5	4%Mo-2%Co /HZSM-5	2%Mo-4%Co /HZSM-5
HHV [MJ Kg^{-1}]	26.40±0.10	27.06±0.06	27.77±0.02	26.69±0.2	28.07±0.4 0	26.91±0.10	27.42±0.26
Carbon [wt.%]	69.33±1.63	71.40±0.68	73.26±0.69	73.12±0.8 9	73.04±2.6 7	72.46±1.36	72.25±0.12
Hydrogen [wt.%]	2.92±0.34	3.36±0.06	3.25±0.13	2.89±1.86	3.35±0.02	3.48±0.71	3.34±0.08
Nitrogen [wt.%]	3.51±0.16	3.53±0.07	3.70±0.12	3.58±0.18	3.60±0.26	3.37±0.18	3.28±0.14
Oxygen[c] [wt.%]	24.24±1.13	21.71±0.55	19.80±0.69	20.42±2.5 7	20.03±2.3 8	20.70±0.48	21.14±0.35

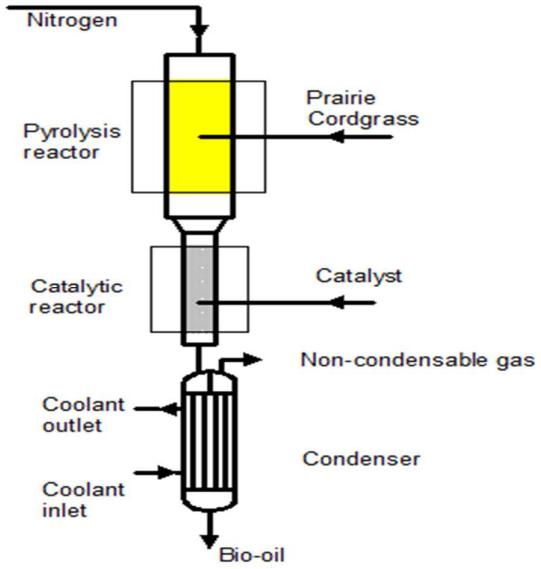

Figure 3.1 The diagram of the two-stage reactor system

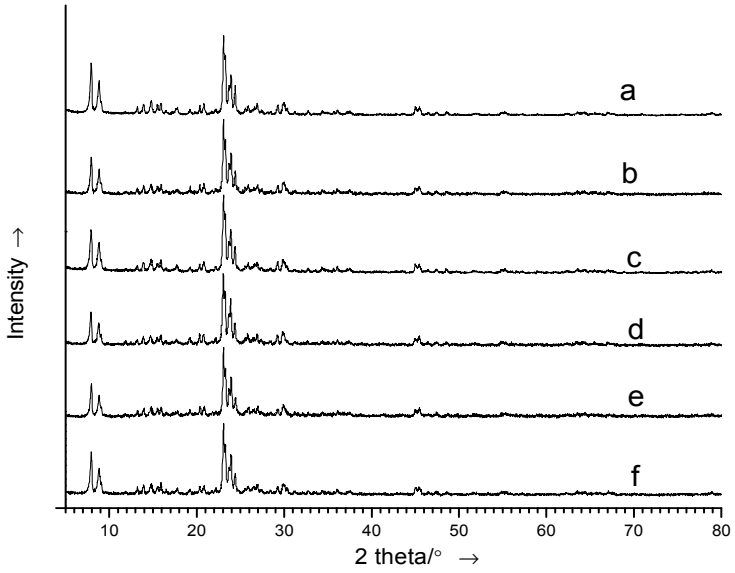

Figure 3.2 XRD patterns of fresh catalysts (a-HZSM-5, b-2%Co/HZSM-5, c-2%Mo/HZSM-5,d-2%Mo-2%Co/HZSM-5,e-2%Mo-4%Co/HZSM-5,f-4%Mo-2%Co/HZSM-5)

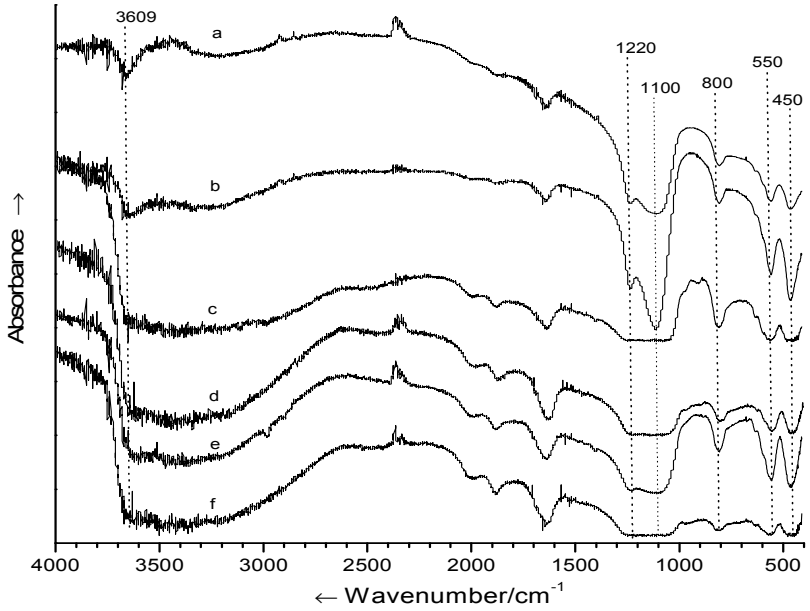

Figure 3.3 FT-IR spectra of fresh catalysts (a-HZSM-5, b-2%Co/HZSM-5, c-2%Mo/HZSM-5,d-2%Mo-2%Co/HZSM-5,e-2%Mo-4%Co/HZSM-5,f-4%Mo-2%Co/HZSM-5)

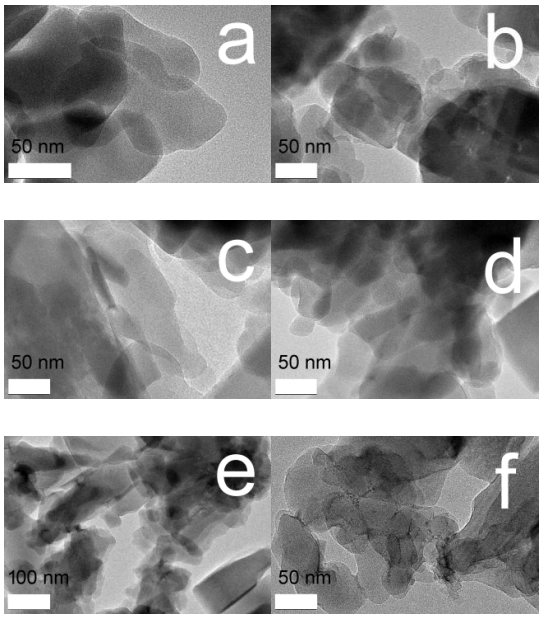

Figure 3.4 TEM images of all fresh catalysts (a-HZSM-5, b-2%Co/HZSM-5,c-2%Mo/HZSM-5,d-2%Mo-2%Co/HZSM-5,e-2%Mo-4%Co/HZSM-5,f-4%Mo-2%Co/HZSM-5)

CHAPTER 4

Hydro-deoxygenation of prairie cordgrass bio-oil over Ni based activated carbon synergistic catalysts combined with different metals

4.1 Abstract

Bio-oil can be upgraded through hydrodeoxygenation(HDO). Low-cost and effective catalysts are crucial for the HDO process. In this study, four inexpensive combinations of Ni based activated carbon synergistic catalysts including Ni/AC, Ni-Fe/AC, Ni-Mo/AC and Ni-Cu/AC were evaluated for HDO of prairie cordgrass (PCG) bio-oil. The tests were carried out in the autoclave under mild operating conditions with 500 psig of H_2 pressure and 350□ temperature. The catalysts were characterized by X-ray Diffraction (XRD), Brunauer–Emmett–Teller (BET) and Transmission electron microscope (TEM). The results show that all synergistic catalysts had significant improvements on the physicochemical properties (water content, pH, oxygen content, higher heating value and chemical compositions) of the upgraded PCG biofuel. The higher heating value of the upgraded biofuel (ranging from 29.65MJ/kg to 31.61MJ/kg) improved significantly in comparison with the raw bio-oil (11.33MJ/kg), while the oxygen content reduced to only 21.70-25.88% from 68.81% of the raw bio-oil. Compare to raw bio-oil (8.78% hydrocarbons and no alkyl-phenols), the Ni/AC catalysts produced the highest content of gasoline range hydrocarbons (C6-C12) at 32.63% in the upgraded biofuel,

while Ni-Mo/AC generated the upgraded biofuel with the highest content of gasoline blending alkyl-phenols at 38.41%.

4.2 Introduction

The world's energy consumption is increasing due to population growth and economic developments. More than 80% of the world primary energy consumption is derived from the utilization of depleting fossil fuels [1]. However, the massive application of fossil fuels causes many global problems such as global warming. Renewable biomass, which is carbon neutral, is a reasonable and promising energy source which can reduce the world's dependence on fossil fuels. Fast pyrolysis is an effective method to convert biomass to liquid bio-oil, and it is the thermochemical process in which biomass is heated to 400–600 °C in the absence of air at a short vapor residence time. However, the bio-oil produced has a high water and oxygen content. As a result, it exhibits acidic and corrosive properties and has a relatively low higher heating values compared with conventional petroleum-derived fuels, making it unusable as transport fuels. Consequently, bio-oil upgrading is needed to reduce its water and oxygen content. Hydrodeoxygenation (HDO) is considered an effective method for bio-oil upgrading, and it involves the stabilization and selective removal of oxygen from untreated bio-oil through its catalytic reaction with hydrogen [85]. Catalysts play a critical role in bio-oil HDO, and many catalysts have been investigated. For instance, hydrodesulfurization (HDS) catalysts such as sulfided Co-Mo and Ni-Mo supported

on alumina have been tested [31]. But the sulfided catalysts are less suitable for bio-oil HDO due to the economic factors of using sulfur, product contamination and the poor stability of alumina support (deactivation by water) . Also, noble metal catalysts, such as Pd/C, Rh/ZrO_2, Pt/C, and Ru/C were used for in bio-oil upgrading studies [86]. However, the availability and high cost of noble metals are main challenges for their application. Recently, non-noble catalysts such as metallic Ni, Cu, Fe or their bimetallic combination supported on Al_2O_3 were tested, and they are very active in bio-oil HDO [87]. However, the problem of alumina's poor tolerance to water still existed in these tests, which can easily cause catalyst deactivation.

Cu can retard the catalyst deactivation caused by coking and prevent methanization of oxygen-containing compounds in bio-oil hydrodeoxygenation process [88]. Fe had a high selectivity for the formation of hydrocarbons without much aromatic ring hydrogenation in the HDO of guaiacol [40]. Mo served as an active element in the hydrodeoxygenation of bio-oil model compound (2-ethylphenol) [89], and Mo catalysts were more active supported on activated carbon (AC) than on alumina or silica due to the weak acidity.

Catalyst supports played a crucial role in dispersing and stabilizing active phases of catalysts, decreasing the cost of catalysts. The alumina (Al_2O_3) support can partially transform into boehmite (AlO(OH)) in presence of water. The alumina can also oxidize active metals such as Ni to metal oxides, which caused catalyst deactivation. In comparison, activated carbon (AC) can be utilized as a support for catalysts due to its low affinity for carbon deposition and economical features [90].

Besides, activated carbon (AC) support can provide an increasing selectivity for direct oxygen removal at low hydrogen consumption. Moreover, the hydrophobic nature of activated carbon support can resist the deactivation of metal catalysts from water produced in the hydrodeoxygenation reaction. Furthermore, AC could be produced from bio-char, one of the main products generated in biomass fast pyrolysis process. To our best knowledge, few studies have been reported to use bimetallic Ni based (Ni combined with Fe, Mo and Cu) catalysts supported on activated carbon (AC) for bio-oil hydrodeoxygenation.

Existing bio-oil hydrodeoxygenation methods suffered from serious drawbacks such as the requirement of extreme reaction conditions (high pressure ranging from 1088 to 4351 psig), which resulted in high hydrogen consumption and severe design standard of HDO reactors. However, the monometallic and bimetallic Ni catalysts were found to be highly selective for oxygen removal under mild HDO conditions [91], which can reduce the hydrogen consumption and equipment cost.

In this study, non-precious monometallic (Ni) and bimetallic (Ni combined with Fe, Mo and Cu) catalysts supported on activated carbon were utilized for PCG bio-oil HDO process to produce upgraded biofuels under low operating pressure (500 psig). The objective of the study is to investigate the catalyst selectivity of oxygen removal at lower catalysts cost (non-noble metals), lower operating cost (low hydrogen pressure) and lower coke formation (AC support).

The PCG bio-oil upgrading experiments were conducted in the autoclave in order to identify catalytic effects of different catalysts on product yields and quality. The catalysts are evaluated with focus on their ability to reduce the oxygen content of the biofuel, while maintaining the organic fraction yield at acceptable levels. In order to evaluate the catalysts' selectivity towards desirable gasoline range products including alkyl phenols and hydrocarbons, the composition of the organic fraction was also studied.

4.3 Materials and Methods

Prairie cordgrass bio-oil was used as the feedstock, and it was produced from prairie cordgrass (PCG) pyrolysis in a fixed bed reactor at 500□. The properties of the bio-oil are listed in Table 4.1. In each test, 100 g of bio-oil was added to the autoclave.

The activated carbon (AC) was provided by Norit Company. The nickel (II) nitrate hexahydrate (crystalline), ammonium molybdate tetrahydrate (81-83wt.%), iron(III) nitrate nonahydrate (98 wt.%), copper (II) nitrate hemi (pentahydrate) (99 wt.%) were purchased from Sigma-Aldrich and used as received. The Ni/AC, Ni-Fe/AC, Ni-Mo/AC and Ni-Cu/AC catalysts were prepared by the wet impregnation method. AC powers were impregnated with aqueous solutions of a given amount of nickel (II) nitrate hexahydrate, ammonium molybdate tetrahydrate, iron(III) nitrate nonahydrate and copper (II) nitrate hemi (pentahydrate). The catalysts were dried in oven at 120□for 4h, and then calcined in furnace in inert nitrogen at 550□ for

5h. All AC catalysts were based on 6% metal content. 5 g of catalysts was used in each test.

The 500ml Parr 4575 autoclave reactor was used to carry out batch PCG bio-oil hydrodeoxygenation experiments. The reactor's allowable maximum pressure and temperature were 5000psi and 500°C respectively. The Parr controller was used to control the vessel temperature and impeller mixing speed, and it also monitored the vessel pressure. The impeller mixing speed was set at 1000 rpm through all tests. Hydrogen was supplied from a hydrogen cylinder via a pressure regulator.

4.4 Experiment Design

4.4.1 Catalyst Reduction

Water and catalyst slurry was used to reduce the catalysts. 5g catalysts (6%Ni/AC, 6%Ni-6%Fe/AC, 6%Ni-6%Mo/AC and 6%Ni-6%Cu/AC) and 150g deionized water were firstly loaded into the autoclave vessel. The vessel was then shut completely and flushed with hydrogen at 40psig for 3 times to remove the air inside. After charging the vessel with hydrogen at 500 psig, the catalyst and water slurry was stirred at 1000 rpm, and the vessel was heated to the temperature of 350 °C by a furnace at a heating rate of 5°C /min. After 3.5h, the heater was removed and the vessel was cooled to room temperature at 20 °C. Then the autoclave vessel with reduced catalysts was dried in vacuum drying oven for 12h.

4.4.2 Bio-oil HDO Test

100g raw PCG bio-oil was added in the vessel which contained the reduced catalysts. After installing the vessel and purging the air with hydrogen as shown in the reduction of catalyst, the vessel was charged with 500 psig hydrogen and heated to 350°C at the heating rate of 4°C /min. 5h later, the heater was shut down and the reactor was gradually cooled to room temperature. Then non-condensable gases (NCG) were collected in sample bags for further analysis. The aqueous phase (AP) and oil phase (OP) of upgraded products were poured to the sample bottles. The targeted oil phase (OP) was subjected to further analysis. The suspended catalysts with char in AP and OP was separated by filtration (using 0.2μm PTFE filter), and then dried in the drying oven at 110°C for 3h. The catalysts left in the vessel were washed with ethanol and then dried at 110°C for 3h. Experiments were conducted in duplicate for each catalyst. The weight difference between the used catalysts and fresh catalysts was the mass of char generated in the bio-oil HDO process. The yield of char, aqueous phase and oil phase were defined using the following equations:

$$Y\ product\ (\%) = M\ product(g)/\ M\ bio\text{-}oil(g) \times 100 \quad (1)$$

$$Y\ gas\ (\%) = 100 - (Y\ char + Y\ aqueous\ phase + Y\ oil\ phase) \quad (2)$$

where Y product and M product are the yield of the upgraded products (char, aqueous phase and oil phase) and the mass of the products, respectively.

In order to evaluate the HDO effect of each catalytic treatment, the degree of deoxygenation (DOD) was defined as follows:

DOD=(1−wt%O oil phase/wt%O bio-oil)×100 (3)

where wt%O oil phase and wt%O bio-oil are the weight percent of oxygen in the upgraded oil phase and raw PCG bio-oil, respectively.

4.4.3 Catalyst Characterization

After catalyst reduction, the catalysts samples in the autoclave vessel were cooled to room temperature (20□). Then the catalysts were flushed with N_2 for 30 minutes. Prior to exposure to air, the catalysts were passivated by purging autoclave vessel with 1% O_2/N_2 for 5 h at room temperature.

The passivated catalysts were disassembled from the autoclave vessel, and transferred to black plastic sample bags (The air in the sample bags was removed before usage). Then the sample bags were stored in a vacuum desiccator immediately. The catalyst samples were transferred to the characterization instruments (XRD, BET and TEM), where the catalysts were quickly taken out from sample bags for characterization.

X-ray diffractometer (XRD, SmartLab, Rigaku Corporation) with Cu Kα radiation was used for the determination of catalyst crystallinity[38]. The X-ray tube was set as 40 kV (tube voltage) and 44 mA (tube current). The X-ray pattern was scanned from 5° to 90° (2θ) with a scan speed of 4°/min and a step of 0.02°.

Tristar 3000 micropore analyzer was employed to analyze BET specific surface area and porosity texture of catalysts. The nitrogen adsorption was

measured at 77.2 K. The catalysts were first degassed at 573 K for around 6 h and then studied by a static volumetric technique. The specific surface area of catalysts was calculated according to the Brunauer–Emmett–Teller (BET) method, and the total pore volume was confirmed at a relative pressure P/P_0 = 0.995. Density functional theory (DFT) was utilized to determine the micropore, mesopore and pore size distribution.

Transmission electron microscope (TEM, JEOL JEM-2100 LaB6) was performed with 200 kV of the accelerating voltage. A few micrograms of catalyst samples was dispersed in isopropyl alcohol (0.5–1.0 mL) and shaked in ultrasonic for about 2 min. Then, a few drops of suspension were dropped on a carbon-coated 200-mesh copper grid and allowed to dry.

4.4.4 Physicochemical Characterization

The properties (pH, water content, higher heating value, elemental compositions and chemical components) of raw bio-oil and upgraded biofuel were characterized. The pH value of the biofuel was tested by a pH meter (AB15, Accumet Company). Water content was analyzed using a Karl Fischer Titrator V20 (Mettler Toledo Company) in accordance with ASTM E1064. The higher heating value (HHV) of samples was determined using a Calorimeter System (C2000, IKA-Works, Inc.) which is based on ASTM D4809. The samples' elemental analysis (carbon, hydrogen and nitrogen) was measured by the CE-440 elemental analyzer.

The major components of liquid products (oil phase) were analyzed by gas chromatography–mass spectrometry (GC–MS) (Agilent GC-7890A and MSD-5975C). Hydrogen was used as carrier gas with a flow rate of 1 mL/min. The injection temperature was 300°C, and the injection volume was 1μL. The initial column temperature was 60 °C and this temperature was held for 1 min. Then, the increase of column temperature followed ramp 1 at 3°C/min to 140°C, ramp 2 at 10°C/min to 180°C, ramp 3 at 3°C/min to 260°C, and ramp 4 at 10°C/min to 300°C. The temperature was kept for an additional 2 min after each ramp. Major compositions of samples were identified based on the NIST Mass Spectral library and literature [42].

The gas chromatography system (Agilent GC 7890A) with a 50 m × 0.53 mm × 15 μm column was used to determine compositions of non-condensable gas. The thermal conductivity detector (TCD) was used for the analysis of H_2 and CO_2. The flame ionization detector (FID) was used for the identification of light hydrocarbons (C1–C5). Standard gas mixtures were used for calibration, and argon was employed as the carrier gas.

4.5 Results and Discussion

4.5.1 Catalyst Characterization

X-ray Diffraction (XRD) was employed to identify the crystalline phases in the investigated catalysts. The XRD patterns of different metal loaded AC catalysts are shown in Figure 4.1. The specific pattern of AC support maintained in all catalysts,

since the small sharp peak (26.6°) of graphitic carbon existed in all catalysts [92]. There are two peaks (44.2°and 51.7°) identified in all metal AC catalysts, corresponding to the presence of metallic Ni particles on the crystalline structure of impregnated catalysts [93]. In the Ni-Cu/AC catalyst, the existence of Cu particles can be detected from peaks at around 43°and 50°. However, they overlapped the reflection peaks of the metallic Ni phase, which is due to the segregation of some of the metallic Cu particles from the Ni-Cu alloy particles formed after the thermal treatment. The diffraction peaks at 35.5°, 43.1°and 62.6°associated to cubic iron oxide phases (Fe_2O_3) are determined in Ni-Fe/AC catalysts [94]. MoO_2 crystallites along with α-$NiMoO_4$ and β-$NiMoO_4$ mixed phases are identified in Ni-Mo/AC catalysts [92].

The textural properties of the AC support catalysts with different metals are listed in Table 4.2. Surface areas of metal loaded AC catalysts are lower than the surface area of the activated carbon. The addition of the metals (Ni, Fe, Mo and Cu) on the AC support resulted in a decrease of the surface area and total pore volumes for all metal loaded catalysts, which is probably due to the filling or blocking of the metal and metal oxides (Ni, Cu, Fe_2O_3, MoO_2,α-$NiMoO_4$ and β-$NiMoO_4$) in the pores of the corresponding AC support.

Figure 4.2 shows the bright field high resolution TEM images of catalysts. As seen in Figure 4.2a, there were no dark spots shown for pure AC, because there was no metal loading on it. However, fresh 6%Ni/AC showed obvious dark spots

in Figure 4.2b, which was attributed to the presence of Ni particles. As was shown in Figure 4.2c, TEM images of Ni-Cu/AC also showed obvious dark spots due to the presence of Ni-Cu alloy particles. Dark spots were also found in the TEM images of Ni-Fe/AC (Figure 4.2d), which indicated the existence of metal Ni or Fe_2O_3. Ni, MoO_2, α-NiMoO4 or β-NiMoO4 crystallites are also detected as dark spots in the TEM images of Ni-Mo/AC (Figure 4.2e).

The histograms on the particle size distribution were calculated by counting particles appeared in the TEM images of prepared catalysts. The histograms on the particles distributions in the four prepared catalysts were built towards a random selection of particles (from 711 to 882 depending on the catalyst samples). The histograms in Figure 4.3 show the particle size distribution of the four prepared catalyst. The 6%Ni/AC catalyst (Figure 4.3a) has a narrow particle size distribution with a maximal size ranging from 6 nm to 7 nm, and there are a very few large particles or agglomerates with size above 28 nm. The 6%Ni-6%Cu/AC (Figure 4.3b) also has a narrow size distribution with a maximum at 8 nm - 9 nm, and some large particles or aggregates were found with size larger than 28 nm. The 6%Ni-6%Fe/AC (Figure 4.3c) has a wider size distribution with a maximum between 10 nm and 11 nm, and some large particles or aggregates were detected with size above 36 nm. The 6%Ni-6%Mo/AC (Figure 4.3d) has the widest size distribution with a maximum at 8 nm - 9 nm, and there are even some large particles or aggregates with size over 72 nm. Besides, the average particle sizes of the bimetallic Ni based catalysts are larger than the monometallic Ni based catalyst.

The metal dispersion ((%)) was defined as the ratio of the number of metal atoms at the catalyst surface to the total number of metal atoms in the catalyst sample . The dispersion DM was calculated according to the following equation [95]:

$$DM\ (\%)=N_{(S)M}/N_{(T)M}\times 100=(6\times\alpha_M)/(d\times V_M)\times 100=(6\times\alpha_M\times M_w)/(d\times\rho_M\times N_0)\times 100 \quad (4)$$

where $N_{(S)M}$ is the number of metal atoms at the catalyst surface, $N_{(T)M}$ is the total number of metal atoms in the catalyst sample, α_M (m^{-2}) is the number of surface atoms per unit area, d (nm) is the average metal particle size, V_M (cm^3) is the volume per metal atom in the bulk, M_w ($g\ mol^{-1}$) is the metal atomic weight, ρ_M ($g\ cm^{-3}$) is the metal density and N_0 (mol^{-1}) is the Avogadro's number. The average particle size and metal dispersion are shown in the Table 4.3. The dispersions of the four prepared catalysts were varying in a range of 6.39%-10.68%. Compared to monometallic 6%Ni/AC, the addition of Cu, Fe and Mo reduced metal dispersions of bimetallic 6%Ni-6%Cu/AC, 6%Ni-6%Fe/AC and 6%Ni-6%Mo/AC. This might be due to the larger average particle sizes of bimetallic catalysts, which might result from the higher proportion of metal particles or aggregations with larger sizes on the surface of the bimetallic catalysts.

4.5.2 Product Yield

The yield of the bio-oil HDO products (aqueous phase, oil phase, char and gas), based on the weight of the raw bio-oil, are shown in Table 4.4. Compared with

Ni/AC treatment, the Ni-Fe/AC catalyst obtained the lowest oil phase yield and char yield, and produced the highest gas yield. This trend may result from the further decomposition of organic compounds in the liquid phase due to the addition of Fe, such as deoxygenation to form carbon dioxide in the gas (20.01% in further gas analysis). The addition of Mo to Ni/AC generated the higher oil phase yield and lower char yield, and it indicated that Ni-Mo/AC slightly reduced the formation of polyaromatic species due to the polymerization and polycondensation reaction, which result in the lower char forming (8.78%) . The addition of Cu also improved the HDO effect of Ni/AC in terms of increasing oil phase yield and decreasing char yield. The aqueous phase yield of all treatments is similar at around 50%, this might be the result of the de-moisturization of the organic compound in the oil phase to the aqueous phase with high water content (around 90%).

4.5.3 Biofuel analysis

The physicochemical properties of different upgraded biofuels, such as water content, pH, elemental compositions and higher heating values, are measured and listed in Table 4.5. The water content of the oil phase reduced significantly from 48.91% in the raw bio-oil to the figure ranging from 6.12% to 11.98% through hydrodeoxygenation and transferring water to aqueous phase. The HHV of the oil phase (ranging from 29.65 MJ/kg to 31.61 MJ/kg) also improved greatly in comparison with the raw bio-oil (11.33MJ/kg), which is due to its much lower water

and oxygen content. The pH of oil phase is slightly higher than raw bio-oil, which may result from the transformation of acids to esters in the upgraded products.

Compared to the carbon and oxygen contents in raw bio-oil (20.01% and 68.81% separately), the carbon content in the upgraded biofuel (64.29-67.64%) increased significantly, while the oxygen content deceased to only 21.70-25.88%. This was mainly caused by the hydrodeoxygenation and decarboxylation reactions of oxygenated compounds that remove oxygen in the form of H_2O and CO_2, which were then transferred to aqueous phase and gas respectively. The decrease of oxygen levels also lead to the high degree of deoxygenation (DOD), which ranged from 62.39% to 68.46%. This DOD is comparable to the DOD of noble Pt/C catalysts (64%) for the HDO of bio-oil [96].

One of the major objectives for this study was to explore the effects of different catalysts on the distribution of organic compounds in the upgraded liquid products. Therefore, the chemical compositions of upgraded biofuel (OP) are determined by GC-MS. The various components present in the original bio-oil were also analyzed for comparison. The main chemical compounds of raw bio-oil and upgraded biofuels, as analyzed by GC-MS, are shown in Table 4.6. The compositions were classified into different categories: phenols, ethers, ketones, esters, alcohols, acids and hydrocarbons.

In raw PCG bio-oil, the type and proportion of organic components are in agreement with those reported by others [97]. The PCG bio-oil produced was rich

in phenols (55.88%), and it also contained undesirable carboxylic acids (3.05%) and ketones (8.55%). The content of hydrocarbons was only 8.78%.

The organic compositions of upgraded biofuel changed significantly after mild HDO processes over different AC supported catalysts. After the reaction, the content of phenols increased in all catalytic treatments except Ni/AC. The improvement of phenols is due to the formation of alkyl-phenols such as 2-methyl-phenol and 3, 4-dimethyl-phenol. The Ni/AC was not very active for the hydrogenation of phenol ring, therefore most of the phenol rings were maintained in all treatments. The addition of Fe, Cu and Mo to Ni/AC might promote the alkylation reactions between phenol and alcohols or light olefins, and then the following reactions of demethoxylation, demethylation and hydrogenation lead to the generation of phenolic derivatives such as alkyl-phenols. By comparison, the Ni-Mo/AC generated the upgraded biofuel with the highest alkyl-phenol content at 38.41%. The alkyl-phenols have been found to possess high blending octane numbers. Therefore, it might have potential to be an excellent gasoline blendstock.

The undesirable acids in biofuel are significantly reduced by all HDO processes over different AC supported catalysts. The acids may be converted into relatively stable esters through decarbonylation, dehydroxylation and ring opening [81]. In addition, some carboxylic acids may be transferred from the oil phase to the aqueous phase. Acids even disappeared totally in Ni-Fe/AC and Ni-Cu/AC treatments. The decreasing of acid content is beneficial for refineries to further

processing the upgraded HDO biofuels in terms of reducing corrosion and materials of construction.

Ketones, which are responsible for the low heating value and instability of raw bio-oil, were also reduced in all HDO processes. Micromolecule ketones were decomposed through decarboxylation to form CO_2 and hydrocarbons, while macromolecule ketones were transferred to other ketones [98]. Alcohols were easily transformed to hydrocarbons and phenol derivatives by HDO, which leads to the decrease of alcohol content in all catalytic treatments.

The content of hydrocarbons in oil phase increased because of the HDO effect of oxygenated organic compounds in all catalytic treatments, and Ni/AC generated the upgraded biofuel with the highest hydrocarbon content at 39.42%. The lower yield of hydrocarbons over Ni-Fe/AC, Ni-Cu/AC and Ni-Mo/AC catalysts might results from the competition reaction to form phenolic derivatives, which reduced the proportion of alcohols that can be used to produce hydrocarbons. The alkylation reactions between phenol and light olefins also consumed partial hydrocarbons. However, the main proportion of hydrocarbons is still light hydrocarbons (C6-C12), which has the potential to be utilized as gasoline additives.

4.5.4 Gas analysis

The composition of non-condensable gas (NCG) provides valuable information on the types of reactions that occurred in the HDO processes. The

compositions of syngas are listed in Table 4.7. As is shown in the table, there are 10 gas compounds detected in the non-condensable gas. As expected, the main component is hydrogen, which was the unreacted hydrogen that fed into the autoclave at the beginning of the experiment. The presence of unreacted hydrogen also indicates that the reactions were not conducted under hydrogen starvation conditions. The second highest composition of gas is always CO_2, which suggested effective decarboxylation of such as ketones and esters followed by water gas shift or disproportionation (Boudouard reaction) over the AC supported catalysts in all bio-oil HDO processes [99]. For each case, small amount of CH_4 were formed as well, which was probably as result of the demethylation of phenolic derivatives.

4.5.5 Correlation of catalyst composition and bio-oil HDO activity

Ni based catalyst was very active in the hydrogenation reactions. However, monometallic Ni-based catalyst showed higher coking levels in hydrodeoxygenation process. In this study, the coking (char) yield of the Ni/AC treatment was as high as 8.86%.

Compared to the monometallic Ni catalysts, the addition of a second metal such as Mo, Fe and Cu reduced the coke formation and increased catalyst activity. Bimetallic Ni–Cu catalysts are found to be more active than single Ni catalysts in hydrodeoxygenation process under mild conditions. The coking (char) yield of Ni-Cu/AC catalyst (4.80%) was lower than Ni/AC catalyst (8.86%). The reason might

be that the copper addition facilitated the reduction of nickel oxide and improved resistance to coke formation on Ni–Cu catalysts [100].

In Ni-Fe bimetallic catalysts, the addition of Fe can promote the C=O hydrogenation and inhibit the C-C breaking [101], which might result in the higher yield of phenols in Ni-Fe/AC treatment in comparison with Ni/AC treatment. The Ni-Fe/AC treatment also led to lower coking (char) yield (3.09%) than Ni/AC treatment (8.86%).

Bimetallic Ni-Mo catalyst was highly active and stable. The Ni-Mo/AC catalysts can promote C-O activation and inhibit the C-C breaking [102], which might result in the higher DOD (degree of deoxygenation) of Ni-Mo treatment (66.02%) than Ni/AC treatment (63.60%).

4.6 Conclusions

The HDO upgrading of PCG raw bio-oil over different metal AC catalysts under mild conditions were carried out in the autoclave reactor. The effects of the different catalysts are evaluated in terms of organic liquid product yield and selectivity towards alkyl phenols and hydrocarbons. The results show that all catalysts had significant improvements on the physicochemical properties (water content, pH, oxygen content, higher heating value and chemical compositions) of the upgraded PCG biofuel. All AC supported catalysts increased the hydrocarbon yield in upgraded biofuel in comparison to raw bio-oil, while the Ni/AC catalysts

produced the highest light hydrocarbons content at 32.63% in upgraded biofuel. The addition of Fe, Cu and Mo to Ni/AC increased the yields of alkyl-phenols, and Ni-Mo/AC generated the upgraded biofuel with the highest content of alkyl-phenols at 38.41%.

Table 4.1 Properties of the PCG bio-oil at 20□

Properties	Data
Water content (wt.%)	48.91±1.41
pH	2.41±0.01
Carbon content (wt.%)	20.01±1.87
Hydrogen content (wt.%)	10.31±0.57
Nitrogen content wt.%)	0.87±0.05
Oxygen content[a] (wt.%)	68.81±2.49
Higher heating value(MJ/kg)	11.33±0.08

[a] Calculated by difference.

Table 4.2 BET parameters of different Catalysts

Catalyst	Surface area (m^2/g)	Pore Size (nm)	Pore volume (cm^3/g)		
	BET	**Average**	**Total[b]**	**Micropores**	**Mesopores**
AC	730.61	5.14	0.92	0.53	0.39
Ni/AC	723.14	4.92	0.87	0.51	0.36
Ni-Fe/AC	687.96	4.84	0.83	0.42	0.41
Ni-Cu/AC	682.83	4.74	0.81	0.48	0.33
Ni-Mo/AC	626.66	4.78	0.81	0.47	0.34

Table 4.3 Average metal particle size and dispersion of the four prepared catalysts

Catalyst	Average metal particle size (nm)	Total metal dispersion (%)
6%Ni/AC	9.45	10.68
6%Ni-6%Cu/AC	10.40	9.86
6%Ni-6%Fe/AC	13.11	8.25
6%Ni-6%Mo/AC	18.90	6.39

Table 4.4 Mass balance of upgrading products from different catalytic treatments

	Biofuel		Char	Gas
Treatments	**Oil phase （wt.%）**	**Aqueous phase（wt.%）**	**Char（wt.%）**	**Gas（wt.%）**
Ni/AC	20.17	51.35	8.86	19.63
Ni-Fe/AC	17.35	51.34	3.09	28.24
Ni-Cu/AC	21.57	51.62	4.80	22.02
Ni-Mo/AC	21.91	49.37	8.78	19.96

Table 4.5 Physicochemical properties of different biofuels

Treatments	Ni/AC	Ni-Fe/AC	Ni-Cu/AC	Ni-Mo/AC
Water content (wt.%)	8.10±0.77	11.98±1.10	6.12±0.33	6.52±1.30
pH	3.63±0.06	3.48±0.03	3.13±0.01	3.50±0.01
Carbon (wt.%)	65.13±0.23	67.64±0.98	64.29±1.19	66.55±1.94
Hydrogen (wt.%)	8.28±0.36	9.30±0.84	8.54±1.14	8.72±0.88
Nirogen (wt.%)	1.55±0.20	1.36±0.02	1.29±0.06	1.35±0.04
Oxygen[b] (wt.%)	25.04±0.79	21.70±0.15	25.88±0.01	23.38±1.09
HHV(MJ/kg)	29.65±0.32	31.61±1.17	31.50±1.37	31.58±1.08
DOD	63.60±1.15	68.46±0.23	62.39±0.02	66.02±1.59

[b] Calculated by difference

Table 4.6 Chemical composition analysis of upgraded biofuels (OP) by GC-MS

Relative content (%)	**Raw bio-oil**	**Ni/AC**	**Ni-Fe/AC**	**Ni-Cu/AC**	**Ni-Mo/AC**
Phenols	55.88	54.65	71.28	65.98	69.99
Alkyl-phenols [c]	0	0.86	33.84	31.46	38.41
Ethers	2.83	0	0.29	0	2.00
Ketones	8.55	0.68	0.63	0.36	1.87
Esters	3.98	0	0.36	0	2.61
Alcohols	7.49	3.2	1.67	5.72	3.40
Acids	3.05	0.43	0	0	0.46
Hydrocarbons [d]	8.78	39.42	24.98	26.60	16.37
Hydrocarbons (C6-C12)	6.32	32.63	23.01	24.62	13.80
Hydrocarbons (C13-C35)	2.46	6.79	1.97	1.98	2.57

[c] Alkyl-phenols are included in phenols, [d] Sum of light hydrocarbons and heavy hydrocarbons

Table 4.7 NCG distributions of different treatments

Gas (Vol.%)	Ni/AC	Ni-Fe/AC	Ni-Cu/AC	Ni-Mo/AC
H_2	75.29	61.16	70.58	68.08
CO_2	9.86	20.01	11.70	12.73
CH_4	1.97	3.46	3.78	4.27
C_2H_6	0.72	1.45	1.66	1.55
C_2H_4	7.12	0.08	0.09	0.09
C_3H_8	1.59	5.84	5.40	5.80
C_3H_6	2.81	7.63	6.39	7.05
C_4H_{10}	0.54	0.22	0.30	0.25
C_4H_8	0.01	0.11	0.07	0.13
C_5H_{12}	0.09	0.04	0.03	0.05

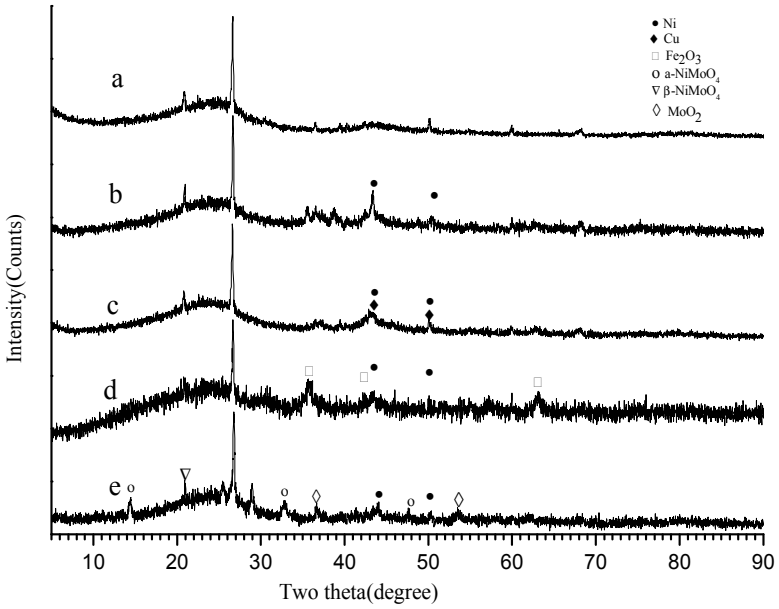

Figure 4.1 XRD patterns of different AC catalysts (a-AC, b-6% Ni/AC, c-6%Ni-6%Cu/AC, d-6%Ni-6%Fe/AC and e-6%Ni-6%Mo/AC)

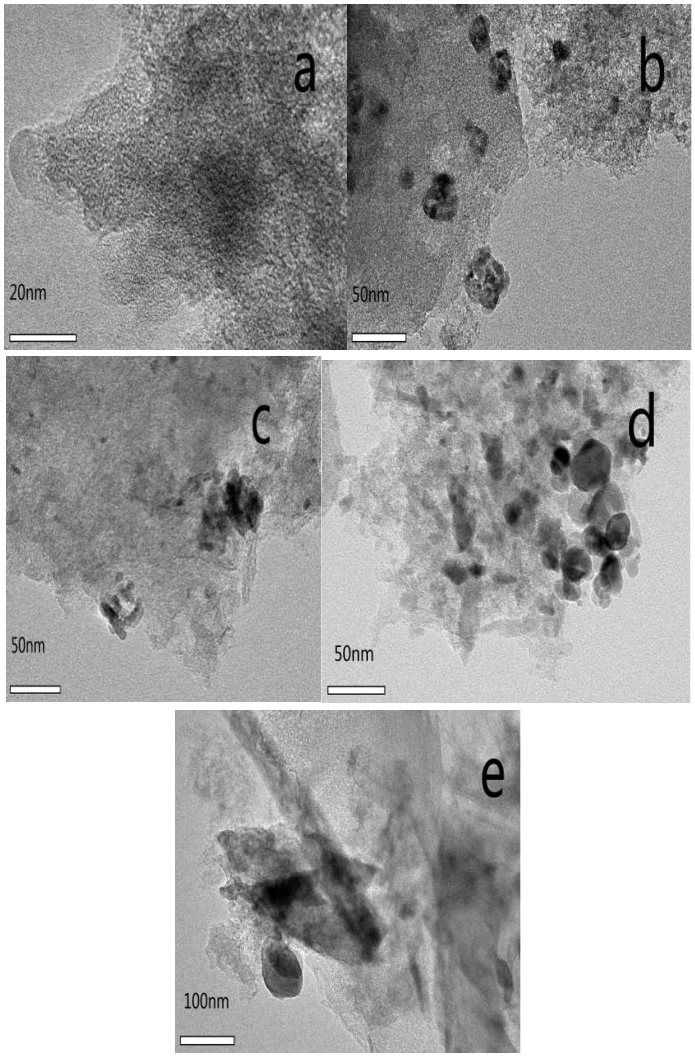

Figure 4.2 TEM images of all metal AC catalysts (a-AC, b-6%Ni/AC, c-6%Ni-6%Cu/AC, d-6%Ni-6%Fe/AC and e-6%Ni-6%Mo/AC)

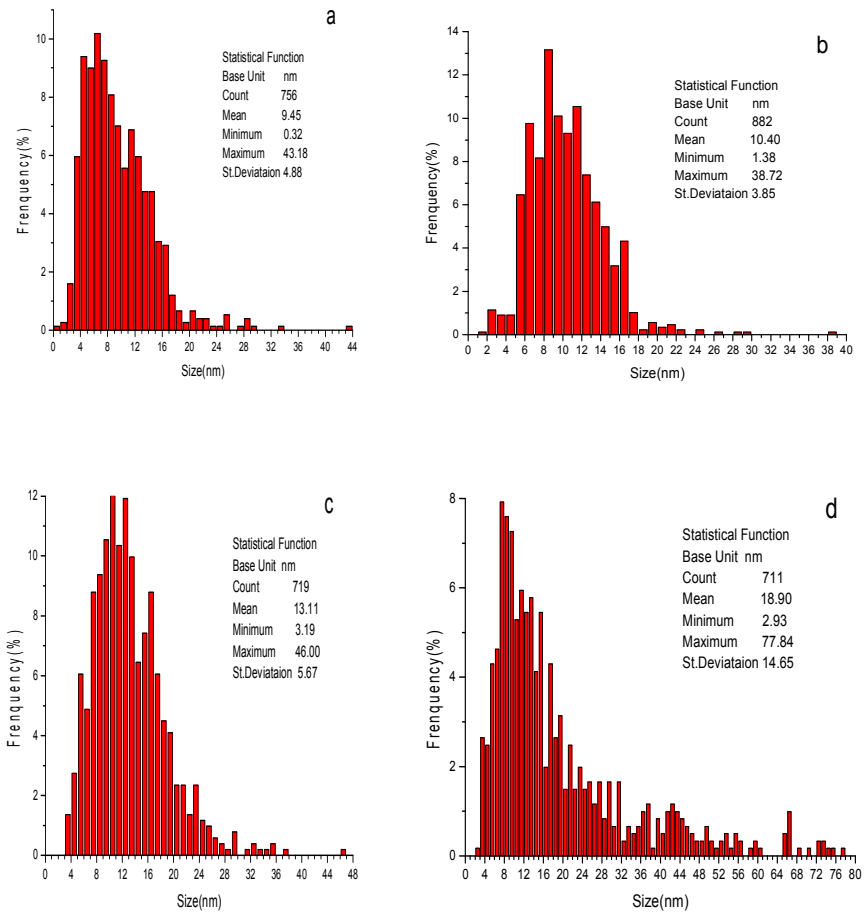

Figure 4.3 The histograms of particle size distribution for the four prepared catalysts: a-6%Ni/AC, b-6%Ni-6%Cu/AC, c-6%Ni-6%Fe/AC and d-6%Ni-6%Mo/AC

CHAPTER 5

In-situ hydrodeoxygenation upgrading of pine sawdust bio-oil to hydrocarbon biofuel using Pd/C catalyst

5.1 Abstract

Hydrodeoxygenation (HDO) is effective for upgrading bio-oil to biofuel. However, the upgrading cost increased due to the high consumption of external hydrogen. In this paper, the hydrogen generated from cheap water using zinc hydrolysis for in-situ bio-oil HDO was reported. The effect of different temperatures (200 °C, 250 °C and 300 °C) on bio-oil HDO over Pd/C catalyst was investigated in a batch reactor. The results show that 250 °C yielded biofuel with the highest heating value at 30.17 MJ/kg and the highest hydrocarbons content at 24.09%. Physicochemical properties including heating value, total acid number and chemical compositions of the produced biofuels improved significantly in comparison with that of the original bio-oil.

5.2 Introduction

Due to increased energy need and rapid consumption of fossil fuels, biomass is considered as an alternative energy resource due to its renewable properties. Biomass can be efficiently transformed to bio-oil through fast pyrolysis, which rapidly heats biomass to 400-600 °C in absence of air. However, the raw bio-oil cannot directly be used as fuel oil because of the undesirable properties including

high oxygen content, strong acidity, low heating value and instability, which was due to high content of oxygenated components. For instance, acids compounds resulted in strong corrosiveness of bio-oil. Ketones, aldehydes and phenols led to instability and low heating value of bio-oil. The low quality bio-oil can be improved by the transformation of these oxygenated compounds to desired compounds such as hydrocarbons. Hydrodeoxygenation (HDO) is one effective technique for bio-oil upgrading, and it improves bio-oil quality through removing oxygen in the oxygenated compounds in bio-oil as H_2O, CO and/or CO_2 using heterogeneous catalysts in presence of hydrogen. Noble metal based catalysts such as Pd/C, Pt/C, Ru/C and Rh/ZrO_2 were efficient for bio-oil HDO. However, the severe hydrogen operating pressure (7.5 - 30 MPa) led to high consumption of hydrogen, and this resulted in the high operation cost of bio-oil HDO. In order to reduce bio-oil HDO cost, more economical method for hydrogen generation needs to be determined.

In-situ hydrodeoxygenation is a new route for bio-oil upgrading without external hydrogen supply. This method decreases the cost of expensive transportation and storage of external gaseous hydrogen. Generally, the internal hydrogen used for in situ HDO is generated using hydrogen donors including alcohols or formic acid. Recently, a promising method of Zn/ZnO thermochemical cycle to produce hydrogen from cheap and available water using zinc hydrolysis was reported [103]. In this technique, hydrogen was generated through reaction of zinc hydrolysis: $Zn + H_2O = ZnO + H_2$ [104]. Bio-oil has a high water content ranging from 15 wt. % to 30 wt. %. Therefore, the water presented in bio-oil may be used to generate

hydrogen for bio-oil HDO. Few studies were found to upgrade real bio-oil using in-situ hydrogen generated from water using zinc hydrolysis reaction over Pd/C catalyst.

Pine sawdust bio-oil upgrading by in situ HDO using zinc hydrolysis coupled with Pd/C catalyst was investigated in this study. The main objective was to explore the effectiveness of temperature on the yield and properties of hydrocarbons biofuel such as water content, total acid number, viscosity, higher heating value and chemical compositions over Pd/C catalyst. Besides, the effect of temperature on reactor pressure and gas compositions was determined. This study can provide an economical approach to produce hydrogen for in situ bio-oil HDO process.

5.3 Material and methods

5.3.1 Materials

Zinc powder with zero valence and 5.00 wt. % Pd/C catalyst were purchased from Fisher Scientific and Sigma Aldrich, respectively. Pine sawdust (PSD) bio-oil was produced using a pyrolysis reactor in the Advanced Biofuel Development Lab at South Dakota State University. The properties of PSD bio-oil are shown in Table 5.1.

5.3.2 Bio-oil HDO experiment

The bio-oil upgrading experiments were performed in a mechanically stirred 500 mL autoclave reactor (Parr 4575). The schematic diagram of bio-oil upgrading

system is shown in Figure 5.1. Solvent plays a critical role in bio-oil upgrading. Water can be an excellent solvent with very low cost in a HDO process of pyrolysis bio-oil upgrading, since it can lower the activation barrier and increase the proton diffusion coefficient. The use of methanol solvent promoted hydrogenation reactions, and it resulted in reduced coke formation on catalysts. Although the crude bio-oil contained 14.5 wt% water, it might be not enough to act as good solvent for the total reactants (6 g zinc powder, 5 g Pd/C catalyst, 50 g PSD bio-oil) to form a supercritical reaction system in the desired temperature. The supercritical reaction can increase mass and heat transfer and produce a high density, low viscosity, and a high diffusion coefficient of the reactant and solvents in the reactor system. Besides, a higher solvent to bio-oil ratio was helpful for bio-oil heating value improvement and lower coke yield. Therefore, appropriate water and methanol were added into the reactor for the in-situ bio-oil HDO process.

In a typical run, 6 g zinc powder, 5 g Pd/C catalyst, 50 g PSD bio-oil, 50 mL deionized water and 63 mL methanol as solvents were loaded in the reactor. The reactor was firstly flushed by nitrogen (0.68 MPa) for 6 times to remove inside air. Then the reactor was heated to the designed temperature (200 °C, 250 °C or 300 °C) by a heater at 5 °C/min under a stirring speed of 1000 rpm. The reactions were proceeded for 5 h at the set temperature. The “5 h” reaction time for the bio-oil HDO process was determined according to out preliminary tests. One reason for this reaction time was that the prolonged reaction time was advantageous to the hydrogenation reaction. Another reason was that longer reaction time can yield

more hydrogen for bio-oil hydrodeoxygenation, since the zinc and water hydrolysis reaction that generated hydrogen at around 250 °C was a slow reaction. Finally, the heater was removed and the reactor was rapidly cooled down to ambient temperature (20 °C) by an electric fan 25 min later. Non-condensable gas product was collected slowly from the reactor.

The bio-oil upgrading product was poured out from the reactor and transferred to a separatory funnel. After statically keeping the product over 6 hours, it was separated into two phases: a top light yellow aqueous phase (AP) and a bottom dark brown oil phase (OP, biofuel). The AP and OP can be easily separated using a phase separating method with the funnel. The bottom bio-oil upgrading product withdrawn from the funnel was oil phase. The top bio-oil upgrading product left in the funnel was aqueous phase. Solid residues including used Pd/C catalyst, zinc oxide and coke presented in AP (S2) and in OP (S3) were separated by filtration (using 0.2μm PTFE filter), washed by ethanol and dried. After pouring out liquid bio-oil product, some solid residue including used Pd/C catalyst, zinc oxide and coke was stuck on the bottom of the reactor due to the sticky property of these solid compounds. Solid residues left in the reactor (S4) was then washed by ethanol and dried.

The residual water and methanol that were added into the reactor went to the aqueous phase of upgraded biofuel after HDO reactions. The yield of aqueous phase was not calculated as the ratio of the mass of the aqueous phase and the mass of crude PSD bio-oil, since the water and methanol present in aqueous phase was not

only derived from the crude bio-oil. Instead, the yield of aqueous phase was calculated as the ratio of the mass of aqueous phase (including solvents of the residual water and methanol) and the mass of liquid (including crude PSD bio-oil, deionized water and methanol) in equation (2). The yield of gas (YG), aqueous phase (YA), oil phase (YO) and coke (YC) were defined in these equations:

$$YG = (L + S1 - AP - OP- S2 - S3 - S4) / L \times 100\% \quad (1)$$

$$YA = AP / L \times 100\% \quad (2)$$

$$YO = OP / L \times 100\% \quad (3)$$

$$YC = (1- YG - YA -YO) \times 100\% \quad (4)$$

where L is the mass of PSD bio-oil, deionized water and methanol, S1 is the mass of zinc and Pd/C catalyst, AP is the mass of aqueous phase after filtration, OP is the mass of oil phase after filtration, S2 is the mass of solid residues in aqueous phase, S3 is the mass of solid residues in oil phase, S4 is the mass of solid residue left in the reactor.

5.3.3 Product analysis

Properties of biofuel and bio-oil samples were determined. Karl Fischer Titrator V20 was conducted to test water content based on ASTM E1064. A MicroTan Titrator was employed to test TAN in accordance with ASTM D664. Dynamic viscosity was analyzed at 20 °C using a viscosity analyzer. A Calorimeter System was employed to test HHV according to ASTM D4809. CE-440 elemental analyzer

was used to determine the elemental compositions of bio-oil and biofuels (carbon, hydrogen and nitrogen).

Biofuel and bio-oil products was analyzed by GC–MS to determine main chemical compounds. The gas chromatography instrument was Agilent GC-7890A with a Agilent DB column (30 m × 0.25 μm ×0.25 mm). The mass spectrometry used was Agilent 5975C (electron ionization of 70 eV, mass range of 50–500 m/z). The oven temperature was programmed to stay at 60 ℃ for 1 min, and then increased following ramp 1 at 3 ℃ /min to 140 ℃, ramp 2 at 10 ℃ /min to 180 ℃, ramp 3 at 3 ℃ /min to 260 ℃ and ramp 4 at 10 ℃ /min to 300 ℃. The main compositions of samples were determined based on NIST library. The relative contents of compounds in samples were determined based on GC-MS peak areas.

Non-condensable gas compositions were analyzed by Agilent GC 7890A equipped with a Hp-5 column (50 m × 0.53 mm × 15 μm). FID and TCD detectors were employed to analyze light hydrocarbons (C1–C4), H_2, CO, CO_2 and N_2. Standard gas was used for calibration, and argon was used as carrier gas.

5.4 Results and discussion

5.4.1 Product yields

The yields of bio-oil HDO products including biofuel, AP, gas and coke at different reaction temperatures are shown in Figure 5.2. The yield of each product was considerably influenced by bio-oil HDO temperature. Compared to 200 ℃

treatment, the higher temperature treatments (250 °C and 300 °C) decreased the biofuel yields and increased gas yields. The hydrogen output increased with increased temperature, and this resulted in the higher hydrogen pressure in the reactor. Therefore, the catalytic activity of Pd/C catalyst was promoted as a result of the hydrogen-enriched atmosphere, which converted more oxygenated compounds in bio-oil to hydrocarbons and gaseous products through hydrodeoxygenation, hydrogenation and decarbonylation reactions. This is confirmed by the increased yields of light gases such as CH_4 and CO in gas products at higher temperature treatments. Catalyst deactivation was mainly attributed to the coke deposition on the catalyst that blocked catalyst pores and masked active sites on catalyst surface, and temperature has a significant influence on coke formation. The coke yield increased with higher reaction temperature. The possible reason was that higher temperature promoted polymerization and polycondensation reactions that formed coke over Pd/C catalyst [105].

5.4.2 Biofuel physicochemical properties

Physicochemical properties of biofuel products such as water content, total acid number (TAN), viscosity and higher heating values (HHV) are listed in Table 5.2. The combustion performance of biofuel in engines is negatively affected by water content of biofuel. Water content of biofuel was lower than raw bio-oil, which was due to the higher proportion of hydrophobic compounds such as hydrocarbons presented in biofuel. Water content decreased with increased reaction temperature,

especially from 10.05 wt.% (200 ℃) to 6.26-6.96 wt.% (250 °C and 300 °C). This tendency was attributed to the improved dehydration of the biofuel improved with increased temperature. The TAN value, a main parameter indicating the corrosiveness of liquids, was as high as 320.03 mg KOH/g in raw bio-oil. After bio-oil HDO, the TAN of biofuels decreased significantly to the figure ranging from 59.63 to 89.30 mg KOH/g. This was probably due to the conversion of acids compounds into other compounds such as esters. The lower contents of water and oxygenated compounds of biofuels led to higher HHV compared to raw bio-oil. Biofuel HHV tend to increase at higher temperatures (250 °C and 300 °C) in comparison with 200 °C temperature. This indicated that deoxygenation reactions became more predominant with increased reaction temperature. The biofuel with the highest HHV (30.17 MJ/kg) was achieved by 250 °C treatment, which was due to the lowest water content and highest hydrocarbons content.

Bio-oil HDO temperatures have a significant effect on biofuel viscosity. The raw bio-oil had a lower viscosity (4.52 Pa·s), and this was attributed to the relative high water content and the homogeneity of the water bio-oil mixture. The viscosity of the upgraded bio-oil at 200 °C and 250 °C increased significantly compared to that of crude bio-oil. One possible reason was that the polymerization reactions of aldehydes, ketones, acids and phenols resulted in increase of bio-oil viscosity at longer heating time (5 h) and higher temperature. Another possible reason was that the removal of partial amounts of water from bio-oil led to the increase of the viscosity of the upgraded bio-oil [106]. However, the viscosity of

biofuel decreased at higher temperature treatment (300 °C) due to the decomposition of higher molecular-weight compounds to low molecular-weight compounds in HDO reactions such as hydrocracking.

The elemental compositions of raw bio-oil and upgraded bio-oil (biofuel) is shown in Table 5.3. The carbon and hydrogen content of upgraded biofuel increased in comparison with crude bio-oil. The oxygen content of upgraded bio-oil (30.20-36.85 wt.%) decreased compared to crude bio-oil (48.78 wt.%). This was due to the bio-oil oxygen removal reactions including hydrodeoxygenation, deoxygenation, decarbonylation and decarboxylation that reduced the oxygen content in the upgraded biofuel. The results showed the effectiveness of deoxygenation on Pd/C catalyst.

5.4.3 Biofuel compositions

The main chemical compounds of biofuel and bio-oil determined by GC–MS include phenols, aldehydes, ketones, esters, alcohols, acids and hydrocarbons. The details (compounds names and molecular formulas) of these compounds and their classifications are listed in Table 5.4.

Raw bio-oil was mainly composed of oxygenated compounds including ketones, acids, phenols, alcohols, aldehydes and hydrocarbons, which derived from the decompositions of biomass components including cellulose, hemicellulose and lignin in pyrolysis process. These oxygenated compounds are responsible for low

quality of bio-oil such as high oxygen content, corrosiveness, low heating values and instability. The desired hydrocarbons content of raw bio-oil was only 11.01%.

After bio-oil HDO, there was a considerable change in chemical compositions of biofuels compared to raw bio-oil. The content of desirable hydrocarbons in biofuels increased because of the hydrodeoxygenation, hydrogenation, decarboxylation and decarbonylation reactions that occurred over Pd/C catalysts. High reaction temperatures (250 °C and 300 °C) increased hydrocarbons content of biofuels. 250 °C treatment produced biofuel with the highest hydrocarbons content at 24.09%. The possible reason was that high temperature improved hydrogen yield from zinc hydrolysis reaction, and this resulted in the higher hydrogen pressure that made Pd/C catalyst more active in bio-oil HDO. However, the 300 °C treatment produced biofuel with lower hydrocarbon content compared to 250 °C treatment. This is probably due to strengthened breakdown reactions of some high molecule-weight hydrocarbons to low molecule-weight gaseous hydrocarbons such as CH_4 at high reaction temperature (300 °C).

The high acidity and strong corrosiveness of biofuel resulted from the presences of acids compounds. The acids contents of biofuels decreased in comparison with raw bio-oil. The acid compounds were probably transformed into stable esters through esterification reactions. The decrease of acids contents resulted in the lower TAN value and decreased corrosiveness of biofuels, which reduced cost of processing biofuel in terms of reducing corrosion for transportation pipelines and

storage vessels. Ketones and aldehydes that led to instability and low heating value of biofuels also decreased after bio-oil HDO reactions. The possible reason might be that ketones and aldehydes were transformed to alcohols in hydrogenation reactions, which might be then converted to esters by esterification in bio-oil HDO process. The contents of phenols in biofuels dropped at all treatments, which was probably due to the hydrodeoxygenation reactions that converted phenols to hydrocarbons such as alkanes [107]. In contrast, the esters content of biofuels increased significantly in all treatments due to the strong esterification reactions between alcohols and acids.

5.4.4 Correlation of catalyst and bio-oil upgrading activities

Pd/C catalyst was proven an effective catalyst for bio-oil hydrodeoxygenation (HDO). It is highly active in bio-oil upgrading reactions including hydrodeoxygenation, hydrogenation, deoxygenation, decarbonylation, decarboxylation and hydrocracking. Bio-oil HDO over metal catalysts such as Pd/C needs to consume hydrogen to complete HDO reactions [108]. The main role of Zn was to supply hydrogen for bio-oil HDO through zinc and water hydrolysis reaction.

5.4.5 Gas compositions

The gas compositions are shown in Figure 5.3. One main gas product was hydrogen generated from zinc hydrolysis, and the existence of unreacted hydrogen indicated that the generated hydrogen was abundant for bio-oil HDO reactions. The

hydrogen content in the reactor increased at higher temperature treatments. This was due to the promoted zinc hydrolysis reactions at higher reaction temperatures. CO_2 was another main gas produced due to effective decarboxylation of organic acids by Pd/C catalyst. Decarbonylation reactions in bio-oil HDO was responsible for the production of CO that was detected in the gas product. The contents of light hydrocarbons such as CH_4 increased with higher temperature, and this was attributed to enhanced decomposition of hydrocarbons and the methoxy groups in organic compounds such as alcohols [109].

5.4.6 Reactor pressures

The pressure of HDO reactor is listed in Table 5.5. Initial pressure was the nitrogen pressure charged in the HDO reactor before HDO experiments. Maximum pressure is the maximum reactor pressure when the experiment was running at the designed temperature. Final pressure is the reactor pressure when the reactor is cooled to ambient temperature. The maximum and final pressures of the reactor increased with temperatures due to the improved hydrogen production from zinc hydrolysis. The increased reactor pressure indicated higher hydrogen pressure for bio-oil HDO reactions, which is beneficial to the improved HDO performance of Pd/C catalyst to convert unfavorable oxygenated compositions in biofuels. This is confirmed by the reduced contents of oxygenated compounds including acids, aldehydes, ketones and phenols in biofuels produced at higher temperature treatments.

5.5 Conclusions

In situ upgrading of pine sawdust bio-oil using Pd/C catalyst under different temperatures (200 °C, 250 °C and 300 °C) were carried out in the HDO reactor. The catalytic effects of different temperatures were evaluated for improving biofuel quality and yield. Higher temperatures (250 °C and 300 °C) improved bio-oil HDO performance of Pd/C catalyst due to increased hydrogen yield. Specifically, 250 °C treatment produced biofuel with the highest heating value and hydrocarbons content. The contents of undesirable oxygenated compounds such as aldehydes, ketones, acids and phenols were significantly decreased in biofuels in comparison with raw bio-oil.

Table 5.1 Properties of PSD bio-oil

Properties	Data
Water content (wt.%)	14.50±0.03
TAN (mg KOH/g)	320.03±35.96
Viscosity (Pa·s)	4.52±0.05
HHV (MJ/kg)	22.38±0.53

Table 5.2 Physicochemical properties of different biofuels

Treatments	200 °C	250 °C	300 °C
Water content (wt.%)	10.05±0.40	6.26±0.09	6.95±0.03
TAN (mg KOH/g)	59.63±8.84	89.30±1.00	62.35±0.15
Viscosity (Pa·s)	110.23±2.45	56.10±2.80	2.29±0.07
HHV (MJ/kg)	27.23±0.64	30.17±0.05	29.79±0.20

Table 5.3 Elemental compositions of raw bio-oil and biofuels

Treatments	Raw bio-oil	200 °C	250 °C	300 °C
C(wt.%)	45.38±0.02	55.94±0.14	62.22±0.49	61.21±0.01
H(wt.%)	5.12±0.02	6.17±0.04	6.71±0.01	6.48±0.02
N(wt.%)	0.73±0.03	1.05±0.05	0.88±0.03	0.92±0.01
O*(wt.%)	48.78±0.02	36.85±0.15	30.20±0.50	31.40±0.02

* Calculated by difference

Table 5.4 Chemical compositions of different biofuels and raw bio-oil

Relative content (%)	Raw bio-oil	200 °C	250 °C	300 °C
Phenols	10.69	10.05	2.07	2.00
Aldehydes	5.69	1.61	0.00	0.00
Ketones	19.97	5.48	1.77	2.64
Esters	9.53	49.09	62.30	68.92
Alcohols	6.13	4.63	0.42	2.33
Acids	11.59	10.25	3.45	2.19
Hydrocarbons	11.01	12.47	24.09	19.36
Others	25.39	6.42	5.90	2.56

Table 5.5 Reactor pressure of different treatments

Treatment		200 °C	250 °C	300 °C
Pressure (MPa)	Initial	0.07±0.00	0.07±0.00	0.07±0.00
	Maximum	2.69±0.00	6.42±0.20	14.35±1.43
	Final	0.27±0.00	0.96±0.00	4.45±0.52

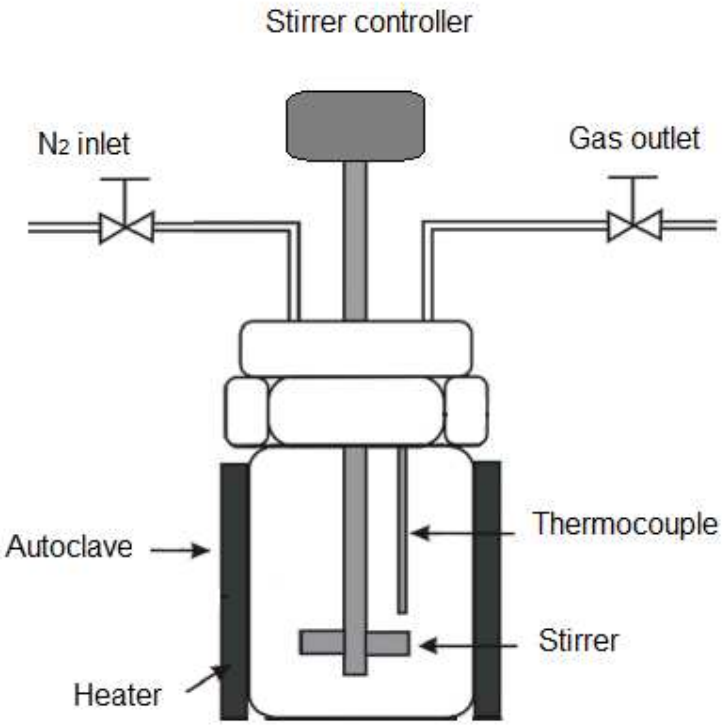

Figure 5.1The schematic diagram of bio-oil HDO system

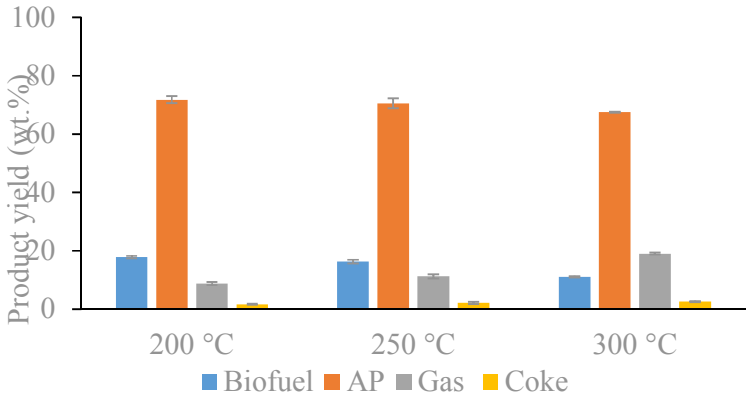

Figure 5.2 Product yields of different treatments

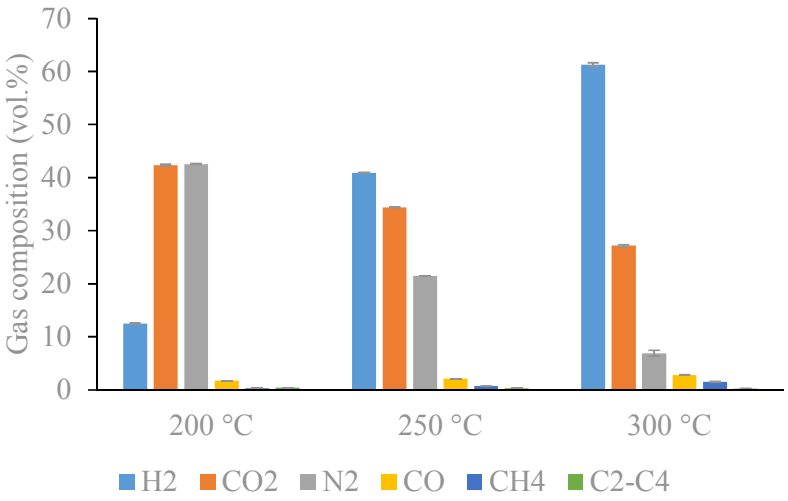

Figure 5.3 Gas distributions of different treatments

CHAPTER 6

Hydrodeoxygenation upgrading of pine sawdust bio-oil using zinc metal with zero valency

6.1 Abstract

Hydrodeoxygenation (HDO) is an effective method for bio-oil upgrading. However, the high hydrogen consumption resulted in high bio-oil upgrading cost. In this study, an novel method of hydrogen generation from water for bio-oil HDO was reported. Zinc metal with zero valency was used to generate hydrogen through zinc hydrolysis reaction in the bio-oil HDO process. The effects of different temperatures (20°C, 250°C , 300°C , 350°C , 400°C) on in situ bio-oil HDO was investigated. The results showed that high temperatures resulted in high hydrogen yield that led to promoted HDO activity over zinc metal-based materials. Although 20°C bio-oil HDO process generated the highest oil phase yield at 14.07%, 400°C bio-oil upgrading process produced upgraded bio-oil with highest hydrocarbons content at 68.95%. Physicochemical properties of raw bio-oil improved significantly after bio-oil HDO upgrading at higher temperatures (250°C, 300°C, 350°C and 400°C). The pH of upgraded bio-oils (5.70-6.49) increased significantly compared to raw bio-oil (3.24). The higher heating value of upgraded bio-oils (28.67-33.43MJ/kg) increased significantly compared to raw bio-oil (15.54 MJ/kg), and valuable hydrocarbons content improved significantly from 16.94% in raw bio-oil to 37.86 – 68.95% in upgraded bio-oils.

6.2 Introduction

A predicted shortage of fossil fuels and environmental issues of global warming resulted from massive fossil fuel consumption led to great interest in the research of developing renewable resources such as biomass to partly replace fossil fuels. Fast pyrolysis is an effective method to convert biomass to bio-oil, which has the potential to be used as transportation fuel. However, the raw bio-oil product has high oxygen contents (35-40 wt.%), which was due to the presence of water and organic compounds such as aldehydes, ketones, carboxylic acids, ethers and esters in raw bio-oil. As a result，the bio-oil has a strong acidity (pH values of around 3) and a low energy density (lower than 19MJ/kg) compared to conventional petroleum-derived fuels (43MJ/kg), hindering its direct use as fuels. The quality of bio-oil can be improved by the partial elimination of the oxygenated components. HDO is effective for bio-oil upgrading, and it involves the stabilization and selective removal of oxygen from raw bio-oil through its catalytic reaction with hydrogen. The high hydrogen pressure (7.5-30MPa), temperature (250-450°C) and metal catalysts such as Pt/C, Ru/C, Pd/C, Rh/ZrO_2, $Ni\text{-}Mo/Al_2O_3$ and $Co\text{-}Mo/Al_2O_3$ were commonly used for bio-oil HDO. However, the harsh operation conditions resulted in the high hydrogen consumption and severe design standard of HDO reactors, which led to unfavorable economic evaluation of bio-oil HDO. Besides, the availability and high cost of noble metals (Pt, Ru, Pd and Rh) are main challenges for their application and the sulfided catalysts ($Ni\text{-}MoS_2/Al_2O_3$ and $Co\text{-}MoS_2/Al_2O_3$) are less suitable for bio-oil HDO due to the economic factors of using

sulfur and product contamination. In order to avoid these disadvantages, more economical and effective catalyst and operation condition should be established to upgrade bio-oil.

Recently, zinc metal with zero valency were used to upgrade bio-oil at atmospheric pressure and room temperature due to its reaction with organic acids in bio-oil to generate active hydrogen [110]. This method significantly reduced operation cost of bio-oil HDO process. However, the catalytic effect of bio-oil upgrading is limited (heating value of bio-oil increased slightly from 12.5 MJ/kg to 13.4 MJ/kg), which might be due to the low hydrogen pressure in the study. On the other hand, the hydrolysis of metal was a promising approach for large-scale production of hydrogen. For instance, the hydrogen can be produced from the cheap and available water via zinc metal hydrolysis reaction, which can be presented as follows: $Zn + H_2O = ZnO + H_2$ [104]. The reaction was found to start at about 250°C. Bio-oil has a content of water as high as 15-30 wt.%, so it can be used to generate hydrogen for bio-oil HDO from zinc hydrolysis. Besides, the generated zinc oxide (ZnO) can be used as an effective catalyst for acetic acid (bio-oil model compound) HDO in the presence of hydrogen [111]. To the best of our knowledge, few studies have been reported to use in-situ hydrogen generation from zinc hydrolysis for real bio-oil HDO process.

In this work, the zinc hydrolysis reaction coupled with the catalytic effect of zinc oxide were used for pine sawdust bio-oil hydrodeoxygenation. Emphasis was put on the effect of temperatures on the yield and quality of upgraded bio-oil (water

content, pH, higher heating value and chemical compositions) over zinc metal-based material.

6.3 Materials and method

6.3.1 Materials

The zinc metal with zero valency and zinc oxide were purchased from Fisher Scientific and used as received. Anhydrous methanol was purchased from Sigma Aldrich and used as received. The pine sawdust (PSD) bio-oil was produced in a proprietary pyrolysis pilot reactor in the Advanced Biofuel Development Lab at South Dakota State University.

6.3.2 Method

The batch bio-oil HDO experiments were performed in a 500 ml Parr 4575 autoclave reactor. The stirrer mixing speed used in the experiment was 1000 rpm.

Water is an excellent solvent in upgrading of pyrolysis bio-oil, and it can also be used to promote zinc hydrolysis reaction for hydrogen generation. In this study, 6 g zinc metal with zero valency, 60 g PSD bio-oil and 100 g deionized water were firstly loaded into the autoclave vessel. In the control experiment, The vessel with reactant was installed and flushed with nitrogen (0.34 MPa) for 3 times to remove the inside air. Then the vessel was heated up to the targeted temperature at 250 °C, 300 °C, 350 °C and 400 °C by a furnace at a heating rate of 5°C/min. The room temperature (20°C) control experiment was conducted without heating. In the

control 1 treatment, 6 g zinc metal with zero valency, 60 g PSD bio-oil and 100 g anhydrous methanol were loaded into the autoclave vessel, the nitrogen (0.34 MPa) was used to remove the inside air, and the vessel was heated to the targeted 300 °C. In the control 2 treatment, 6 g zinc oxide (ZnO), 60 g PSD bio-oil and 100g deionized water was loaded into the autoclave vessel. Hydrogen (0.34 MPa) was used to remove the inside air and then pressurized to 3.45 MPa before bio-oil HDO test, and then the vessel was heated to the targeted 300 °C. The designed temperature was kept stable for 5 h. After the reaction, the furnace was removed and the vessel was quickly cooled to room temperature by a cooling fan. Non-condensable gas (NCG) products were collected in sample bags. The upgraded bio-oil product included two phases: aqueous phase (AP) and targeted oil phase (OP). The two bio-oil phases were separated by a separating funnel. The suspended zinc material with coke product in aqueous phase and oil phase were separated by filtration (using 0.2μm PTFE filter), washed with ethanol and then dried at 110°C for 3h in air in a drying oven. The used zinc material with coke product left in the vessel was filtrated, washed with ethanol and then dried at 110°C in air for 3h. The following abbreviations were defined to determine products (gas, aqueous phase, oil phase and coke) yields: Solid 1(S1) is fresh zinc metal with zero valency for 20 °C, 250 °C, 300 °C, 350 °C, 400 °C and control 1 treatment or ZnO for control 2 treatment. Solid 2 (S2) is used zinc material with coke in aqueous phase, Solid 3 (S3) is used zinc material with coke in oil phase. Solid 4 (S4) is used zinc material with coke left in the vessel. Liquid (L) is defined as raw bio-oil and used solvent

(water for 20 ℃, 250 ℃, 300 ℃, 350 ℃, 400 ℃ and control 2 treatment, or methanol for control 1 treatment). Aqueous phase (AP) is defined as aqueous phase after filtration. Oil phase (OP) is defined as oil phase after filtration. Gas (G) is defined as gas product. Coke (C) is defined as coke product. The yields of products including gas (Y_G), aqueous phase (Y_{AP}), oil phase (Y_{OP}) and coke (Y_C) were calculated based on the following equations:

$$Y_G\ (\text{wt.}\%) = (M_L + M_{S1} - M_{AP} - M_{OP} - M_{S2} - M_{S3} - M_{S4}) / M_L \times 100\% \quad (1)$$

$$Y_{AP}\ (\text{wt.}\%) = M_{AP} / M_L \times 100\% \quad (2)$$

$$Y_{OP}\ (\text{wt.}\%) = M_{OP} / M_L \times 100\% \quad (3)$$

$$Y_C\ (\text{wt.}\%) = (1 - Y_G - Y_{AP} - Y_{OP}) \times 100\% \quad (4)$$

where M_L, M_{S1}, M_{AP}, M_{OP}, M_{S2}, M_{S3}, M_{S4} were the mass of Liquid, Solid 1, Aqueous phase, Oil phase, Solid 2, Solid 3 and Solid 4 respectively.

6.3.3 Zinc-based material characterization

X-ray Diffractometer (XRD, MiniFlex, Rigaku Corporation) was used to determine zinc crystallinity. The filtered Cu-Kα radiation was employed in the XRD analysis. The X-ray tube was set as 30 kV (tube voltage) and 15 mA (tube current). The scan range of X-ray pattern was 30-90° (2 theta) and the scan speed was 2 °/min. The step size of X-ray pattern was 0.02° (2 theta).

Transmission electron microscope (JEOL, JEM-2100 LaB6) was used at 200 kV to determine zinc based material morphology. EDS (Energy Dispersive X-Ray Spectroscopy) data of elemental composition for fresh and used zinc based material samples were acquired in the TEM using an Oxford Inca energy-dispersive silicon-drift X-ray (EDX) spectrometer.

The XPS measurements of zinc sample were performed on a PHI Versa Probe III XPS system (ULVAC-PHI) using a monochromated Al K_α X-ray source (1486.6 eV). The zinc sample was mounted on a stainless steel holder using a piece of carbon sticking tape. The sample was conductive and no charge neutralization was needed. The X-ray spot size was 0.1 x 0.1 mm^2 with a power of 25 W. The high resolution spectra were collected using 0.05 eV/step and a pass energy of 13 eV for Zn 2p peaks and 26 eV for O 1s elements.

6.3.4 Product characterization

Physicochemical properties of bio-oils such as water content, pH, higher heating value (HHV) and chemical compositions were determined. Water content was determined by a Karl Fischer Titrator V20 (Mettler Toledo Company) based on ASTM E1064. Bio-oil pH value was analyzed by a pH meter (AB15, Accumet Company). HHV was tested by a Calorimeter System (C2000, IKA-Works) in accord with ASTM D4809.

The major components of bio-oil products (oil phase) were analyzed by gas chromatography–mass spectrometry (GC–MS). The used gas chromatography was

Agilent GC-7890A (Agilent DB column: 30 m× 0.25 mm × 0.25 μm) and the used mass spectrometry was Agilent 5975C (electron ionization at 70 eV, mass range of 50–500 m/z). The injection volume and injection temperature were 1 μL and 300 °C respectively. The column temperature was first set at 60 °C and then held at this temperature for 1 min. Then, the column temperature increased following ramp 1 at 3 °C /min to 140 °C, ramp 2 at 10 °C /min to 180 °C, ramp 3 at 3 °C /min to 260 °C and ramp 4 at 10 °C /min to 300 °C. The set temperature was maintained for an additional two minutes after each ramp. Helium was employed as carrier gas at a flow rate of 1 mL /min. The main compositions of samples were determined from NIST Mass Spectral library and related literatures. The contents of compounds reported in this study were their area percentages in the GC-MS spectroscopy.

Compositions of non-condensable gas was determined by Agilent GC 7890A (Hp-5 column: 50 m × 0.53 mm × 15 μm). H_2, CO, CO_2 and N_2 were identified by the thermal conductivity detector (TCD). Light hydrocarbons (C_1–C_5) were determined by the flame ionization detector (FID). The carrier gas used in GC was argon, and calibration was conducted by using standard gas mixtures with known composition.

6.4 Results and discussion

6.4.1 Zinc material Characterization

The XRD patterns of fresh and used zinc materials are shown in Figure 6.1. The fresh zinc metal material showed typical peaks of zinc (zero valency) at 39.06°,

43.30°, 54.44°, 70.20°, 70.68°, 82.18° and 86.58°. The fresh zinc metal also displayed some peaks of zinc oxide (ZnO) (32.07°, 34.47°, 36.53°, 47.79°, 56.17° and 63.10°) (PDF card No. 1011258), which was due to the existence of zinc oxide in the fresh zinc metal material [112]. The typical peaks of zinc maintained in the used zinc (20°C) metal, which indicated that the low zinc conversion ratio in its reaction with acids presented in bio-oil, and this reaction did not consume all the fresh zinc material. In contrast, the peaks of zinc disappeared in used zinc metal materials at higher temperatures (250°C, 300°C, 350°C and 400°C), and only typical peaks of zinc oxide (32.07°, 34.47°,36.53°,47.79°,56.17°,63.10°,67.07°,68.49°and 69.78°) (PDF card No. 1011258) appeared in these used zinc metal materials. This was probably due to the strong hydrolysis and redox reactions between zinc and oxygen presented in water and/or bio-oil at higher temperature (≥250°C) that converted zinc to zinc oxide completely.

Figure 6.2 shows the high resolution TEM images of fresh and used zinc metal materials. In fresh zinc metal, small and disperse dark spots were shown in the TEM image (Figure 6.2a), which might be attributed to metal zinc (zero valency). The gray zone in Figure 6.2a might be attributed to ZnO impurities that was determined by XRD analysis. After reaction, the dark spots appeared in the TEM images of the used zinc powder in Figure 6.2b might be attributed to zinc and/or zinc oxide species based on XRD analysis. The dark spots appeared in the TEM images of the used zinc powder in Figure 6.2c, Figure 6.2d, Figure 6.2e and Figure 6.2f might be

attributed to zinc oxide species according to XRD analysis. The TEM results of fresh and used Zn materials are consistent with the XRD results about the presence of peak phases such as zinc and zinc oxide.

The EDS elemental analysis of fresh and used zinc materials is shown in Table 6.1. The oxygen element was found in fresh zinc metal material, and it confirmed the presence of zinc oxide. This is in agreement with the existence of XRD peaks of zinc oxide in fresh zinc metal. The oxygen content in used zinc metal materials increased at higher temperatures (250°C, 300°C, 350°C and 400°C), and it suggested that more zinc was transformed to zinc oxide due to strengthened zinc hydrolysis and redox reactions at higher temperatures.

The molar ratio of Zn/O in used catalysts samples is lower than 1:1. One possible reason was that ZnO has strong ability to absorb oxygen to form oxygen interstitials defects on the surface. When the used catalysts were dried in the air, oxygen is abundant and the concentration of oxygen interstitials on the surface increased, which lead to the lower molar ratio of Zn/O in EDS analysis results (<1:1). Another possible reason was that EDS has limited depth penetrations of samples, and it focused on the sample surface [113].

The XPS spectra of Zn $2p_{1/2}$ (A), Zn $2p_{3/2}$ (B) and O 1s (C) for fresh zinc sample are shown in Figure 6.3. The two fitting peaks at binding energies of 1044.6 eV and 1021.5 eV were attributed to Zn $2p_{1/2}$ and Zn $2p_{3/2}$ peaks of Zn^{2+} ions, respectively [114]. The data of O 1s was fitted to two peaks. The first peak at 530.2 eV was

ascribed to the O atoms in ZnO matrix, and the second peak at 531.6 eV might be attributed to the oxygen adsorbed on the surface of ZnO. These XPS results indicated that there was some ZnO impurity contained in fresh zinc sample.

6.4.2 Product distribution

The upgraded bio-oil liquid can be separated to two phases: targeted oil phase product (mainly composed of organic compounds) and aqueous phase (contained main water and a few organic compounds). The yields of bio-oil HDO products (oil phase, aqueous phase, coke and gas) are shown in Table 6.2. Compared to room temperature 20°C, high temperatures treatments including 250°C, 300°C, 350°C, 400°C, control 1 and control 2 treatments reduced the total bio-oil yield (sum of aqueous and oil phase yields) and increased gas yields. This change might be due to the promoted gasification or hydro-cracking reactions of bio-oil due to the increased temperature, which converted organic compounds in bio-oil to gaseous products[109]. The coke yield increased with increased temperature, and this is probably due to high temperature-promoted polymerization and poly-condensation reactions that were responsible for coke formation in bio-oil HDO process. 20°C treatment generated the highest oil phase yield at 14.07% among all treatments. The oil phase yield decreased at higher temperature (250°C, 300°C, 350°C and 400°C) treatments, control 1 and control 2 treatments, which is probably due to the breakdown of some high weight molecule organic compounds in bio-oil to low weight molecule gaseous products such as light hydrocarbons. This is confirmed by

the increase of C_{1-5} hydrocarbons in gas analysis in the higher temperature bio-oil HDO processes (Table 6.5).

6.4.3 Bio-oil physicochemical properties

Physicochemical properties of upgraded bio-oils (oil phase) and raw bio-oil such as water content, pH and higher heating values were shown in Table 6.3. The water content of bio-oil has a negative effect on the combustion performance of bio-oils in engines. The pH value, a main parameter indicating the acidity of a solution, was 5.46 in the upgraded bio-oil produced at 20°C. It is much higher than raw bio-oil (3.24). This is probably due to the redox reaction between Zn and organic acids in bio-oil that reduced the acids content in upgraded bio-oil. For bio-oils generated at high temperatures (250°C, 300°C, 350°C and 400°C) and control 1 treatment, the water content (ranging from 11.21 wt.% to 25.92 wt.%) is lower than raw bio-oil (26.91 wt.%), which is probably due to the consumption of water in zinc hydrolysis reaction and/or the production of more hydrophobic compounds such as hydrocarbons (control 1 treatment) in oil phase. The pH of upgraded bio-oils (ranging from 5.53 to 6.56) generated at higher temperatures and control 1 treatment improved in comparison to raw bio-oil (3.24) and bio-oil generated at 20°C (5.46). This is probably due to the strengthened esterification reactions that transformed more acids in bio-oil to other compounds such as esters in the upgraded bio-oils. This is confirmed by the further GC-MS analysis that the acids contents of upgraded bio-oils generated at these high temperature treatments were lower than raw bio-oil

and upgraded bio-oil produced at 20°C. The lower contents of water and oxygenated compounds in bio-oils produced from high temperatures (250°C, 300°C, 350°C and 400°C) and control 1 treatment led to higher HHV of upgraded bio-oils (ranging from 17.18MJ/kg to 33.43MJ/kg) compared to raw bio-oil (15.54MJ/kg). A higher process temperature has a positive effect on heating value of the upgraded bio-oil products. The highest HHV (33.43 MJ/kg) of the upgraded bio-oil was achieved at 400°C bio-oil HDO treatment.

The water content of upgraded bio-oil produced in control 2 treatment using ZnO catalyst decreased compared to raw bio-oil, and the pH and HHV of upgraded bio-oil increased in comparison with raw bio-oil. This indicated that ZnO catalyst was effective for improving bio-oil quality in bio-oil HDO.

6.4.4 Bio-oil chemical compositions

In order to investigate effects of different reaction temperatures on chemical compositions of upgraded bio-oil products, GC-MS was used to determine chemical components of upgraded bio-oils (oil phase). The raw bio-oil was homogeneous without an aqueous phase and an oil phase. The main chemical compounds of raw bio-oil and upgraded bio-oils are summarized in Table 6.4. Different categories including phenols, ethers, aldehydes, ketones, esters, alcohols, acids, furans and hydrocarbons were identified in raw bio-oil and upgraded bio-oils.

In the raw bio-oil, the main components were oxygenated compounds such as phenols (21.10%), acids (17.62%), ketones (9.77%), esters (6.86%), alcohols (5.64%) and aldehydes (5.40%). These components led to low quality of bio-oil such as the high oxygen content and high acidity, low heating values and low stability. The desirable hydrocarbons content in raw bio-oil was only 16.94%.

After bio-oil HDO processes at different temperatures, the chemical compositions of upgraded bio-oils changed significantly. The content of desired hydrocarbons in oil phases of all treatments increased because of the hydrodeoxygenation reactions of oxygenated organic compounds in all treatments. High temperatures (250°C, 300°C, 350°C and 400°C) increased hydrocarbons content of upgraded bio-oils compared to bio-oil produced from raw bio-oil. High temperature increased the hydrogen production from zinc hydrolysis in 250°C, 300°C, 350°C and 400°C treatments, and this led to the higher hydrogen pressure in the reactor. The resulted hydrogen–rich atmosphere made the bio-oil hydrodeoxygenation activity of zinc oxide more active. 400°C bio-oil HDO treatment generated the upgraded bio-oil with the highest hydrocarbon content at 68.95%. This is probably due to the highest hydrogen pressure in this treatment. The presences of acids are responsible for the high acidity and strong corrosiveness of bio-oil. Compared to raw bio-oil, the acids contents in upgraded bio-oils from all treatments are significantly reduced. The acids might be converted into relatively stable esters through esterification reactions. Besides, some carboxylic acids might be transferred from oil phase to aqueous phase. This decrease of acids resulted in

the improvement of pH value in upgraded bio-oils (Table 6.3). The decreasing of acids content is beneficial for further processing the upgraded bio-oils in terms of reducing corrosion for storage tanks and pipeline materials.

Ketones and aldehydes, which are responsible for the low heating value and instability of raw bio-oil, were also decreased in all treatments. The possible reason might be that ketones and aldehydes could be transformed to alcohols through the reduction of C=O bonds in hydrogenation reactions. The formed alcohols might be then transformed to hydrocarbons or esters in bio-oil HDO process.

The hydrocarbon contents of upgraded bio-oil in the control 2 treatment using ZnO catalyst increased in comparison with raw bio-oil, and ketones and aldehydes contents of upgraded bio-oil decreased compared to raw bio-oil. This was due to the hydrodeoxygenation reactions that occured on zinc oxide catalyst. This indicated that ZnO was an effective catalyst for bio-oil hydrodeoxygenation. Similar catalytic performance of ZnO for bio-oil model compound (acetic acid) HDO upgrading was determined by Hargus *et al* [111].

The phenols content in upgraded bio-oils increased at 20°C, 250°C, 300°C and 350°C, which was due to the newly formed phenolic compounds such as 2-methoxy-3-(2-propenyl) phenol that resulted from the cracking of pyrolytic lignin. However, the phenols might be converted to other compounds such as hydrocarbons at harsh temperature (400°C), which led to the decrease of phenols content in upgraded bio-oil at 400°C treatment.

6.4.5 Correlation of catalyst activities and active centers

The active centers of catalysts at 20 °C treatment might be Zn with zero valence. The oxygen vacancies derived from the bulk of the Zn catalyst was mainly responsible for the hydrogenation of C=O compounds, and this converted ketones and aldehydes in upgraded bio-oil products. The active centers of catalysts at higher reaction temperature (250°C, 300°C, 350°C and 400°C) treatments might be ZnO that generated from Zn hydrolysis. The oxygen vacancies diffused from the bulk of the Zn particle to the formed high-valence ZnO particle surface, and they played the same role of oxygen removal from the adsorbed organic compounds. Since bio-oil HDO on Zn or ZnO catalysts have similar reaction oxygen vacancies based mechanisms, the catalytic performance of Zn catalyst at 20°C or ZnO catalysts at higher reaction temperatures (250°C, 300°C, 350°C and 400°C) was slightly changed.

6.4.6 Proposed scheme of catalyst stability and recycle

The stability and reuse of zinc metal with zero valence catalyst is important. The catalyst stability performance and recycle test were not yet conducted in this experimental design since this study mainly focused on the effect of different temperatures on the catalytic performance of zinc metal with zero valence catalyst in bio-oil HDO. The used catalyst was composed of ZnO according to the EDS analysis after reaction. Zinc oxide in bio-oil HDO reaction cannot be reduced to zinc metal with zero valency, and this will lead to the termination of hydrogen

generation due to the exhaust of zinc metal. It will generate hydrogen at the cost of zinc metal consumption in the sole in-situ bio-oil HDO process using zinc metal. In order to lower the cost of bio-oil HDO, reduce zinc metal consumption and provide continuous hydrogen generation, the Zn regeneration will employed to decompose ZnO to Zn and O_2 using free and renewable solar energy in our following research. The proposed scheme of looped-Zn catalysis for catalyst recycle and bio-oil HDO is shown in Figure 6.4. The upper dash line box in Figure 6.4 showed that the Zn regeneration (conversion of ZnO to Zn) will be conducted in the high temperature solar electrothermal reactor (1350 K) and subsequent condenser. The recovered Zn will be reused for in situ hydrogen production for bio-oil HDO at longer operation time for catalyst stability performance test. In this way, the hydrogen generation from Zn hydrolysis could be recovered. The consumption of Zn and the cost of bio-oil upgrading process might be reduced through using free solar energy.

6.4.7 Economical and environmental comparison of hydrogen production from ZnO/Zn thermochemical cycle and traditional method

The cost of hydrogen produced by the ZnO/Zn thermochemical cycle coupled with a solar tower ranges from 4.33 to 7.98\$ kg^{-1} H_2 for small capacity plants (796 kg h^{-1} H_2 and 250 kg h^{-1} H_2 respectively) [115]. Besides, ZnO needs to be separated from bio-oil HDO system for the regeneration system. However, the production cost of H_2 can be further reduced by the increase of plant size. In addition, the ZnO/Zn thermochemical cycle for hydrogen production does not produce

greenhouse gases such as CO_2. The cost of conventional method for H_2 production from fossil fuels such as natural gas steam reforming was 2.42-2.78 \$ kg^{-1} H_2 (1780-22250 kg h^{-1} H_2 capacity) [116]. But it produced large quantities of CO_2 due to the application of fossil fuels in manufacturing and heating process.

Although the cost of ZnO/Zn thermochemical cycle for hydrogen production used for bio-oil HDO was higher than conventional hydrogen production method due to the small plant scale, the cost of bio-oil HDO using thermochemical ZnO/Zn hydrogen production could be further reduced through increasing plant size, using government subsidies or any credit for CO_2 mitigatio. Bio-oil HDO using thermochemical ZnO/Zn hydrogen production in two separate systems is more complicated than bio-oil HDO on ZnO in the presence of H_2 produced by conventional method. However, the complexity of bio-oil HDO using thermochemical ZnO/Zn hydrogen production could be reduced through using advanced control systems and employing skilled engineers.

On the other hand, the environmental effect of ZnO/Zn thermochemical cycle is better in removing CO_2 emission compared to conventional hydrogen production method. In addition, the solar energy used for H_2 generation in ZnO/Zn thermochemical cycle is free, infinite and renewable compared to depleting and non-renewable fossil fuels subject to fluctuating prices that were used for H_2 generation for bio-oil HDO. Therefore, the ZnO/Zn thermochemical cycle for in-situ bio-oil HDO provides more environmental friendly and renewable route for the integrated H_2 generation and bio-oil upgrading in the long term. Besides, the cost

and complexity of bio-oil HDO using thermochemical ZnO/Zn hydrogen production could be further reduced. In comparison, bio-oil HDO on ZnO in the presence of H_2 produced by conventional method is more economic and easier to perform currently. However, this traditional method generates greenhouse gas (CO_2) emission and consumes non-renewable energy resources.

6.4.8 Gas compositions

After bio-oil HDO reaction, the non-condensable gas product was collected and analyzed by GC. Initial, maximum and final pressures of the HDO reactor were recorded. The pressure of HDO reactor and compositions of gas are listed in Table 6.5. The main component of 20°C, 250°C, 300°C, 350°C, 400°C and control 1 treatments was nitrogen, which was the unreacted nitrogen that fed into the autoclave before experiment. Another main gas determined in 250°C, 300°C, 350°C, 400°C and control 2 treatments is hydrogen, and the presence of unreacted hydrogen indicated that the reactions were not performed under hydrogen starvation conditions. The hydrogen content was higher at higher temperatures for 250°C, 300°C, 350°C and 400°C treatments compared to 20°C treatment, which resulted from the enhanced zinc hydrolysis reaction at higher temperatures. The other main gas product of all treatments was CO_2, which indicated effective decarboxylation of organic acids in bio-oil HDO processes. At higher temperatures (250°C, 300°C, 350°C and 400°C), light hydrocarbons ($C_{1\text{-}5}$) of all treatments were formed, which was probably due to the decomposition of organic compounds such as alcohols.

Control 1 treatment used anhydrous methanol solvent, the hydrogen content in the gas product was very low (only 0.53 vol.%), and this small amount of hydrogen might result from Zn and organic acids reaction in bio-oil [16]. Compared to control 1 treatment, the hydrogen content of the water solvent treatment at 300 °C was much higher (33.97 vol.%). This indicated that the increased hydrogen production resulted from zinc and water solvent hydrolysis reaction at higher temperatures (≥250 °C).

As the temperature increased, the maximum pressure of the HDO reactor increased, which was probably due to the increased hydrogen yield from zinc hydrolysis reaction. The final pressure increased with the higher temperatures, which indicated higher hydrogen pressure for bio-oil HDO reactions. This is helpful for the increased HDO performance of zinc oxide catalysts for the conversion of oxygenated compounds to hydrocarbons in upgraded bio-oils. This is consistent with the reduced content of oxygenated compounds such as aldehydes and ketones in upgraded bio-oils at higher temperatures (Table 6.4).

6.5 Conclusions

The HDO upgrading of pine sawdust bio-oil over zinc metal with zero valency under different temperatures were carried out in the autoclave reactor. The effects of different temperatures (20°C , 250°C , 300°C , 350°C , 400°C) are evaluated in terms of upgraded bio-oil yield and quality. While 20 °C bio-oil upgrading process generated the highest oil phase yield at 14.07%, 400 °C bio-oil upgrading process

produced upgraded bio-oil with the highest hydrocarbons content at 68.95%. High temperatures (250°C, 300°C, 350°C, 400°C) resulted in the promoted bio-oil HDO performance due to increased hydrogen production.

Table 6.1 EDS elemental composition of fresh and used zinc based metal materials

Zinc material	Fresh Zn	used Zn (20°C)	used Zn (250°C)	used Zn (300°C)	used Zn (350°C)	used Zn (400°C)
Zn content (wt.%)	91.18	74.89	73.67	61.16	59.66	47.76
O content (wt.%)	8.82	25.11	26.33	38.84	40.34	52.24

Table 6.2 Product yields of different treatments

Treatments	Liquid			Solid	Gas
	Total	Oil phase (wt.%)	Aqueous phase (wt.%)	Coke(wt.%)	Gas(wt.%)
20°C	92.28±0.73	14.07±0.80	78.21±0.72	1.35±0.27	6.37±0.01
250°C	89.26±0.54	12.23±0.17	77.03±0.74	1.68±0.31	9.06±0.68
300°C	87.01±0.52	12.28±0.22	74.73±0.52	2.21±0.02	10.78±0.41
350°C	82.63±0.34	9.09±0.41	73.54±0.17	2.72±0.04	14.65±0.54
400°C	84.11±0.27	7.37±0.16	76.74±0.29	3.88±0.08	12.01±0.14
Control 1	89.04±0.14	12.02±0.17	77.03±0.34	2.76±0.09	8.20±0.13
Control 2	86.19±0.43	9.89±0.20	76.30±0.56	1.87±0.05	11.94±0.16

Table 6.3 Physicochemical properties of raw bio-oil and upgraded bio-oils at different temperatures

Treatments	Raw bio-oil	20°C	250°C	300°C	350°C	400°C	Control 1	Control 2
Water content (wt.%)	26.91±0.29	25.51±0.95	19.53±0.02	16.29±0.32	17.24±0.33	11.21±0.29	25.92±0.84	11.14±0.28
pH	3.24±0.28	5.46±0.01	5.70±0.01	5.53±0.01	5.86±0.05	6.49±0.23	6.56±0.26	5.48±0.03
HHV(MJ/kg)	15.54±0.04	18.00±0.66	28.67±0.49	31.35±0.11	31.36±0.25	33.43±0.15	17.18±0.49	31.13±0.72

Table 6.4 Chemical composition of raw bio-oil and upgraded bio-oils at different temperatures

Compounds content (%)	Raw bio-oil	20°C	250°C	300°C	350°C	400°C	Control 1	Control 2
Phenols	21.10±0.43	22.38±0.88	30.82±1.02	24.62±0.30	22.17±0.84	19.07±0.64	12.18±1.07	23.45±1.11
Ethers	3.59±1.57	3.92±1.27	2.46±0.44	1.08±0.23	1.12±0.56	0.73±0.37	6.27±1.88	5.73±1.63
Aldehydes	5.40±1.08	4.59±0.92	1.37±0.69	0.79±0.05	1.83±0.74	0.65±0.55	1.14±0.63	4.62±0.49
Ketones	9.77±1.50	7.39±1.20	5.26±3.70	6.11±0.39	6.40±0.71	2.40±0.85	8.18±1.73	5.30±1.14
Esters	6.86±0.72	7.23±1.65	1.79±1.48	2.53±1.00	1.47±0.63	0.91±0.25	37.22±1.82	9.39±2.37
Alcohols	5.64±1.29	5.92±1.02	2.19±0.12	3.40±0.97	2.04±0.13	0.98±0.33	12.02±2.27	15.96±1.73
Acids	17.62±0.78	7.90±1.04	2.62±1.31	1.50±0.75	0.44±0.12	0.00±0.00	0.81±0.27	6.72±0.12
Furans	0.72±0.68	0.78±0.39	0.33±0.05	1.25±0.42	0.49±0.25	0.00±0.00	2.68±1.73	1.18±0.28
Hydrocarbons	16.94±0.41	30.44±0.29	37.86±1.24	48.53±1.02	50.26±1.03	68.95±2.16	18.46±0.57	26.89±2.82
Others	12.36±1.06	9.45±0.85	15.30±1.35	10.19±1.15	13.78±2.01	6.31±1.15	1.04±0.07	0.76±0.34

Table 6.5 Pressure and gas distributions of different treatments

Pressure (psi) & Gas (Vol.%)	20°C	250°C	300°C	350°C	400°C	Control 1	Control 2
Initial (psi)	40±0.00	40±0.00	40±0.00	40±0.00	40±0.00	40±0.00	500±0.0 0
Max (psi)	40±0.00	690±20	1360±30	2530±40	3650±30	2200±20	1290±1 0
Final (psi)	40±0.00	130±10	150±10	230±20	260±20	120±10	220±20
H_2 (Vol.%)	0.05±0.0 1	18.64±0. 72	33.97±0. 65	33.94±0. 71	22.69±0. 34	0.53±0.1 8	93.33±0 .09
CO_2 (Vol.%)	1.60±0.0 0	31.96±0. 39	34.84±0. 40	39.12±0. 71	47.00±0. 65	34.88±1. 26	5.80±0. 09
CO (Vol.%)	0±0.00	1.86±0.0 1	0.67±0.0 1	0.84±0.0 3	1.12±0.0 4	2.42±0.1 1	0.26±0. 00
N_2 (Vol.%)	98.30±0. 01	22.21±0. 32	29.79±0. 42	23.14±0. 65	21.50±0. 57	60.85±1. 24	0.00±0. 00

CH_4 (Vol.%)	0±0.00	16.65±0.01	0.47±0.02	1.33±0.01	4.02±0.03	0.77±0.06	0.02±0.00
C_2H_4 (Vol.%)	0±0.00	0.23±0.00	0.07±0.01	0.20±0.01	0.29±0.02	0.10±0.01	0.03±0.00
C_2H_6 (Vol.%)	0±0.00	5.06±0.02	0.06±0.00	0.26±0.01	1.25±0.03	0.15±0.00	0.06±0.00
C_3H_6 (Vol.%)	0±0.00	0.56±0.00	0.06±0.01	0.94±0.03	1.27±0.02	0.18±0.00	0.18±0.00
C_3H_8 (Vol.%)	0.04±0.0	2.48±0.01	0.06±0.01	0.15±0.02	0.63±0.04	0.05±0.00	0.03±0.00
C_4H_8 (Vol.%)	0.01±0.0	0.26±0.00	0.01±0.00	0.04±0.01	0.06±0.01	0.07±0.00	0.09±0.02
C_4H_{10} (Vol.%)	0±0.00	0.00±0.00	0.00±0.00	0.04±0.00	0.17±0.04	0.00±0.00	0.00±0.00
C_5H_{12} (Vol.%)	0±0.00	0.09±0.00	0.00±0.00	0.00±0.00	0.00±0.00	0.00±0.00	0.00±0.00

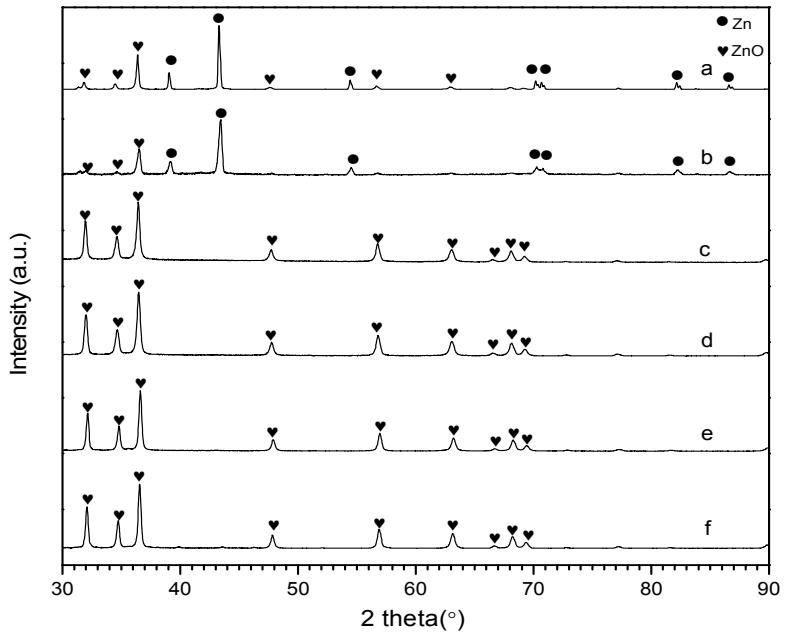

Figure 6.1 XRD patterns of fresh and used zinc based metal materials (a-fresh Zn, b-used Zn (20°C), c-used Zn (250°C), d-used Zn (300°C),e-used Zn (350°C) and f-used Zn (400°C)

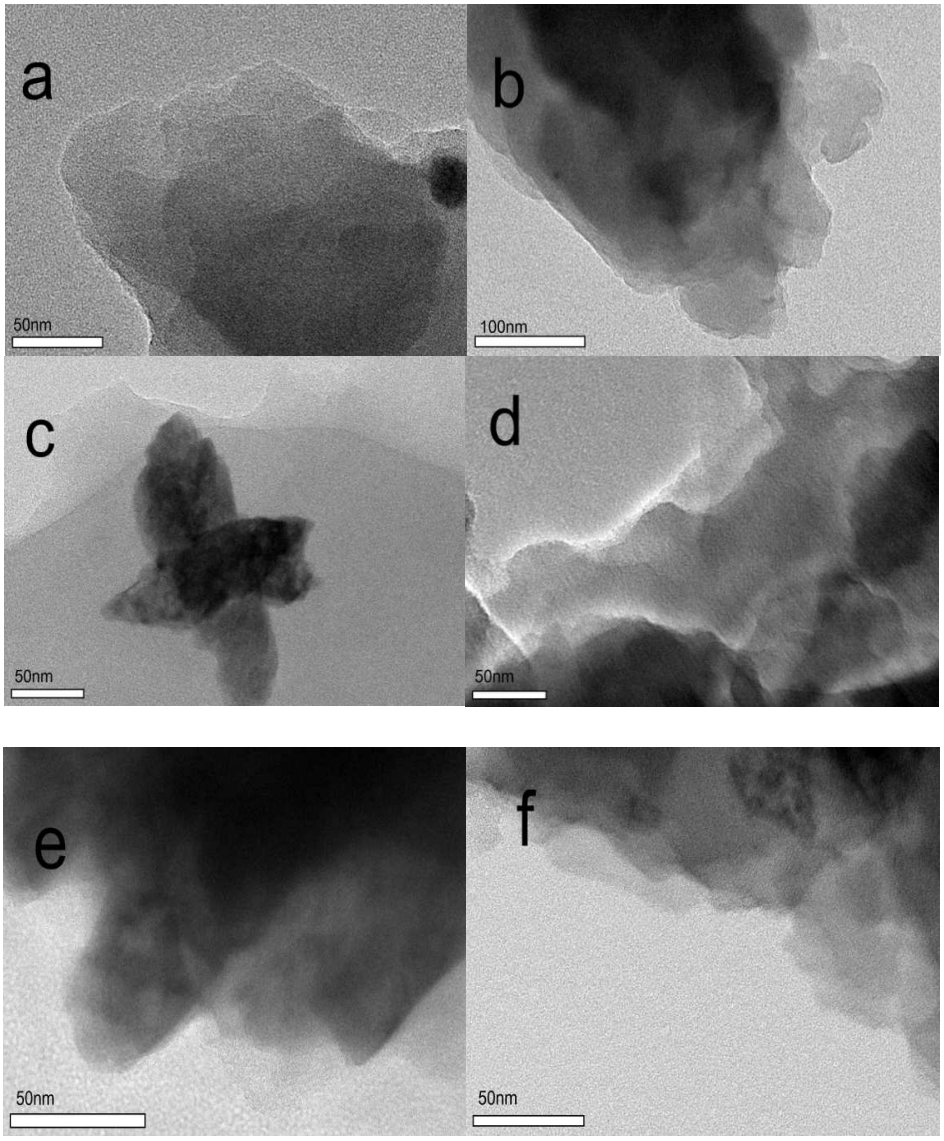

Figure 6.2 TEM images of fresh and used zinc based metal materials (a-Fresh Zn, b-used Zn (20°C), c-used Zn (250°C), d-used Zn (300°C), e-used Zn (350°C) and f-used Zn (400°C)

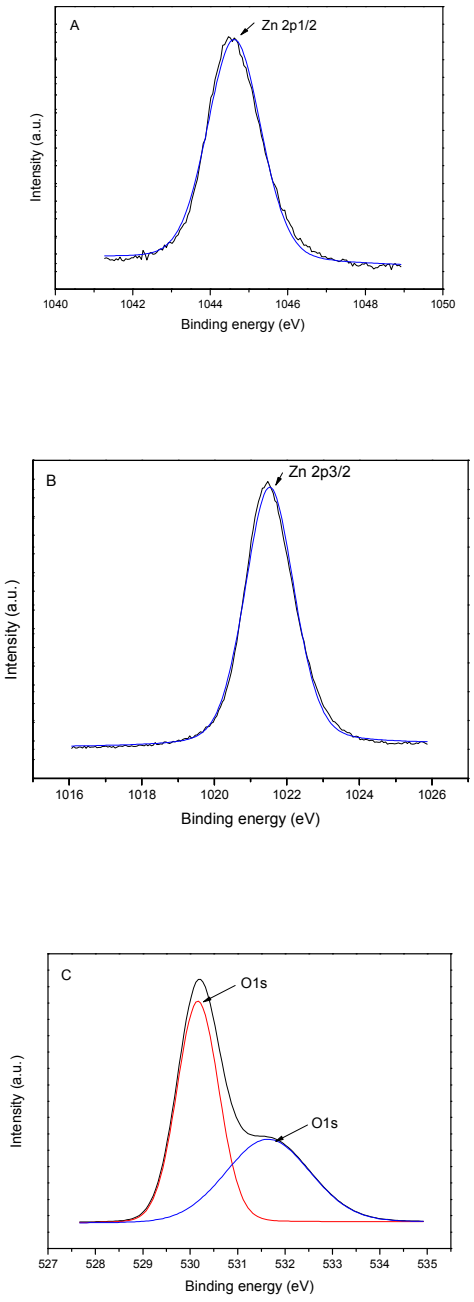

Figure 6.3 XPS spectra of Zn 2p1/2 (A), Zn 2p3/2 (B) and O 1s (C) in fresh zinc sample

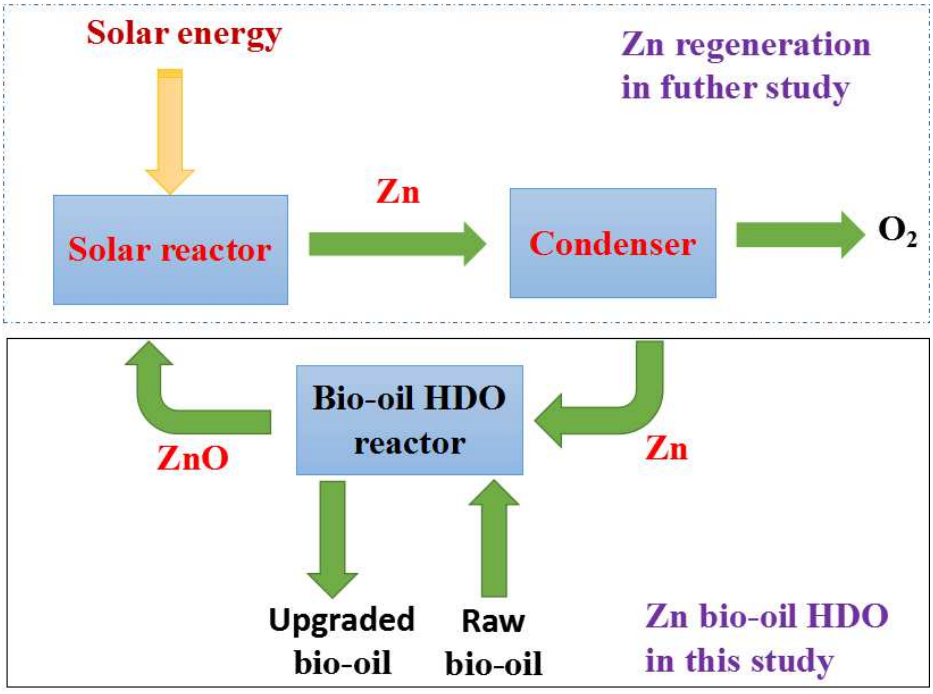

Figure 6.4 Proposed scheme of looped-Zn catalysis for catalyst recycle and bio-oil HDO

CHAPTER 7

Converting Alkali Lignin to Biofuels over NiO/HZSM-5 Catalysts Using a Two-stage Reactor

7.1 Abstract

A series of NiO/HZSM-5 catalysts were used to convert alkali lignin to hydrocarbon biofuels in a two-stage catalytic pyrolysis system. The results indicated that all NiO/HZSM-5 catalysts reduced the content of undesirable phenols, furans and alcohols of biofuel compared to non-catalytic treatments. The 1.27% NiO/HZSM-5 catalyst generated the highest biofuel yield at 27.5% in all catalytic treatments, and it also produced biofuel with the highest content of hydrocarbons at 69.4 %. The emission of carbon dioxides (CO and CO_2) increased in higher NiO loading HZSM-5 treatments (7.64 % and 15.27 %) due to the redox reaction between NiO and the oxygenated compounds in the bio-oil. Ni_2SiO_4 formed in the used NiO/HZSM-5 catalysts during the high temperature pyrolysis process.

7.2 Introduction

The majority of the increasing energy demand in the world is satisfied by increased consumption of depleting fossil fuels, which lead to global problems such as climate change and environmental pollution. Recently, biomass-containing wastes derived from agricultural and industrial resources showed great potential to

partially replace fossil fuels. Black liquor (BL) from pulp and paper industry contains large quantities of alkali lignin [117]. Lignin was a significant resource to produce high-value products due to its high energy content, aromatic structure and the existence of reactive groups. Pyrolysis is a promising thermochemical technology to convert waste lignin to liquid fuel (bio-oil) product.

However, bio-oil produced from lignin pyrolysis cannot be directly utilized as fuel due to its high acidity, viscosity and instability resulted from the high oxygen content (10-50 wt.%) . Bio-oil has to be upgraded. Catalytic cracking is a promising bio-oil upgrading method, since it does not consume hydrogen and can be operated at atmospheric pressure. Zeolite catalysts such as HZSM-5, β-zeolite, MCM-41, SBA-15, USY and H-β have been investigated in lignin bio-oil upgrading. The results indicated that HZSM-5 was the most effective catalyst for bio-oil upgrading due to its excellent ability of reducing the oxygen content in upgraded bio-oils. However, rapid catalyst deactivation and high coking yield were observed for HZSM-5 catalyst used in bio-oil deoxygenation. In the wood-derived bio-oil upgrading process, nickel modified HZSM-5 showed higher yield of hydrocarbons and hydrothermal stability than pure HZSM-5 due to the dehydrogenating activity of nickel and the moderate acid strength of the doped catalyst. However, this study investigated only one nickel-loading level HZSM-5 catalyst for upgrading of pretreated bio-oil without lignin [57]. Few studies were conducted to investigate effects of different nickel-loading HZSM-5 catalysts on lignin-derived bio-oil upgrading.

The traditional catalytic pyrolysis of lignin in a single stage reactor led to high catalyst/lignin ratio (≥0.5/1 or even 15/1), which increased the cost of this technique. This issue can be addressed by the combination of lignin pyrolysis with catalytic cracking in a two-stage reactor system [62]. This integration can greatly reduce catalyst/lignin ratio (0.1/1) and improve energy efficiency. Catalyst/biomass ratio does not affect the yields and selectivity of products in this ex-situ process, which is different from in-situ process that required high catalyst/biomass ratios.

In this study, catalytic cracking of alkali lignin pyrolysis bio-oil over a series of NiO-doped HZSM-5 catalysts (1.27 wt.%, 7.64 wt.% and 15.27 wt.%) was conducted to produce hydrocarbon biofuels in a two-stage reactor system. The goal of this study was to screen optimal NiO loading level HZSM-5 catalyst to obtain higher biofuel yield and quality. The effects of catalysts on biofuel yield and chemical compositions will be discussed. Non-condensable gas distribution and bio-char properties will be analyzed.

7.3 Experimental

7.3.1 Feedstock and Characterizations

The alkali lignin used in this study was purchased from Sigma-Aldrich Inc. ASABE standards (ASAE S358.2 DEC1988 (R2008)) was used to analyze the moisture content of the alkali lignin. The bomb calorimeter (IKA 2000) was used to test the higher heating value (HHV) of alkali lignin. CE-440 elemental analyzer

was used to determine the elemental composition of the biofuels (carbon, hydrogen and nitrogen) .

7.3.2 Catalysts Preparation and Characterizations

The zeolite powder (HZSM-5) was provided by Zeolite International, and the silica/alumina ratio was 30/1. The wet impregnation method was implemented to prepare NiO/HZSM-5 catalysts using aqueous solutions of nickel (II) nitrate hexahydrate ($Ni(NO_3)_2 \bullet 6H_2O$) purchased from Sigma-Aldrich Inc. The NiO-HZSM-5 catalysts (1.27 wt.%, 7.64 wt.% and 15.27 wt.% NiO) were impregnated by aqueous solutions of nickel (II) nitrate hexahydrate at room temperature (20 ºC) for 1 h. The concentration and volume of the aqueous solution of $Ni(NO_3)_2$ used in preparing 1.27 wt.% NiO/HZSM-5 catalysts (40 g) were 0.34 mol L^{-1} and 20.25 mL respectively. The concentration and volume of the aqueous solution of $Ni(NO_3)_2$ used in preparing 7.64 wt.% NiO/HZSM-5 catalysts (40 g) were 3.31 mol L^{-1} and 12.33 mL respectively. The concentration and volume of the aqueous solution of $Ni(NO_3)_2$ used in preparing 15.27 wt.% NiO/HZSM-5 catalysts (40 g) were 3.31 mol L^{-1} and 24.69 mL respectively. The prepared nickel-based catalysts were dried at 120 ºC for 3 h and calcined in air at 550 ºC for 3 h.

BET specific surface area and pore texture of catalysts was analyzed by the automatic Micromeritics ASAP 2020 apparatus with nitrogen adsorption measurements operated at 77.2 K. Specific surface area was determined by

Brunauer–Emmett–Teller method. Density functional theory (DFT) was used to determine micropore, mesopore and pore size distribution of catalysts.

The phase identity for fresh catalysts was determined by the automated multipurpose X-ray diffractometer (Rigaku Smartlab). The Rigaku Smartlab with Cu Kα radiation was operated at 40 kV and 44 mA for XRD analysis. The step size of 0.02 ° (2 theta) from 5 ° to 50 ° (2 theta) and a scanning speed of 2 ° min^{-1} were used in the scanning of X-ray pattern.

The XRD patterns of the used catalysts were investigated by X-ray diffraction in a Rigaku MiniFlex (Japan) with filtered Cu-Ka radiation (30 kV, 15 mA). The X-ray patterns were obtained with a step size of 0.02 ° (2 theta) from 5 ° to 55 ° (2 theta) and a scanning speed of

2 ° min^{-1}.

The acidity of fresh catalysts was determined by Micrometrics Autochem II Chemisorption Analyzer with a thermal conductivity detector (TCD). The catalyst was thermally stable at 700 °C. The fresh catalyst sample (300 mg) was firstly added to ammonium hydroxide (37.1 wt.%, 4.5 g), and the mixture was kept at room temperature (20 ºC) for 3 h. Then, the mixture was dried at 60 ºC for 12 h. The dried sample was used for NH_3-TPD analysis. The helium flow in the chemisorption analyzer was 60 mL min^{-1}. The catalyst sample was heated and maintained at 100 ºC for 30 min to remove the physically absorbed ammonia. Then the sample

temperature was increased from 100 ºC to 700 ºC at a rate of 10 ºC min^{-1}. The final temperature of 700 ºC was held for 30 min.

7.3.3 Experimental Procedure

The experiments were carried out in a two-stage reactor system including a pyrolysis reactor, a catalytic reactor and a condenser. The two-stage catalytic reactor system is depicted in Figure 7.1. Alkali lignin (100.0 g) and catalyst (10.0 g) was loaded in the pyrolysis reactor and catalytic reactor separately. A series of treatments (no catalyst, HZSM-5, 1.27 % NiO/HZSM-5, 7.64 % NiO/HZSM-5 and 15.27 % NiO/HZSM-5) were carried out. Firstly, nitrogen with a rate of 15 mL min^{-1} was introduced into the system for 0.5 h to remove air. Then the nitrogen flow rate was reduced to 5 mL min^{-1}. The catalytic reactor was heated to 500 □ at a rate of 45 □ min^{-1} by a furnace. Then, the pyrolysis reactor was heated to the targeted 500 □ at a rate of 25 □ min^{-1} by another furnace. The non-condensable gas was collected and analyzed after the pyrolysis reactor reached the target temperature. Both furnaces were turned off when the experiment was running at designed temperature for 1 h.

Another 2 h was used to cool the system to collect biofuel from the condenser after each test. The biofuel obtained was a single phase of organic compounds (oxygenates and hydrocarbons) mixture. Bio-char was collected and weighed through disassembling the pyrolysis reactor. The mass of the coke was acquired by

recording the weight difference of the catalyst in the catalytic reactor before and after reaction. The coke yield was measured in Eq.1:

$$Y_{coke} = m_{coke} * m_{alkali\ lignin}^{-1} * 100 \qquad (1)$$

Where Y_{coke} (wt.%) was the coke yield, m_{coke} (g) and $m_{alkali\ lignin}$ (g) were the mass of coke and alkali lignin respectively. The weight of the non-condensable gas was calculated by subtracting total weight of bio-char, coke and biofuel from original alkali lignin weight. Each test was conducted in duplicate and the average data was used.

7.3.4 Product Characterizations

Gas chromatography system was used to determine the composition of gas product. The Agilent GC (7890A, Hp-5 column: 30 m×0.25 mm×0.25 μm) with a thermal conductivity detector (TCD) and a flame ionization detector (FID) was used. H_2, CO and CO_2 was analyzed by TCD, and CH_4 and C_2–C_4 hydrocarbons was determined by FID. Calibration was conducted by standard gas mixtures, and the employed carrier gas was argon.

Gas Chromatography–Mass Spectrometry was used to determine the chemical composition of biofuel. Gas Chromatography was performed using Agilent GC-7890A (DB-5 column: 30 m × 0.25 mm × 0.25 μm). The Mass Spectrometer used was Agilent MSD-5975C (electron ionization at 70 eV, mass range of 50–500 $m \cdot z^{-1}$). The 0.4 mL biofuel was firstly dissolved in 4 ml methanol. The water in the solution was removed by adding sodium sulphate. Then the biofuel sample was

filtered by 0.2μm PTFE filter for GC-MS analysis. The gas chromatograph was programmed at 60 □ for 1 min, followed by ramp 1 at 3 □ min^{-1} to 140 □, ramp 2 at 10 □ min^{-1} to 180 □, ramp 3 at 3 □ min^{-1} to 260 □ and ramp 4 at 10 □min^{-1} to 300 □. The injector temperature and injection volume were 300 □and 1 μL, respectively. The flow rate of the carrier gas (helium, 99.999%) was 1 $mL \cdot min^{-1}$. The relative content of each compound in the biofuel was calculated by taking the ratio of its peak area to the total peak areas in the GC–MS spectrogram. Eq.2 was used to determine the relative content of each compound:

$$x_i = t_i * t^{-1} * 100 \qquad (2)$$

where x_i (%) represented the relative content of each compound, t_i represented its peak area and t represented the total peak areas of compounds appeared in the GC–MS spectrogram.

The ash content of the lignin and bio-char was determined by heating samples at 575 °C until their weight remained constant in a muffle furnace according to NREL standard procedure. Elemental compositions (carbon, hydrogen and nitrogen) and higher heating values of bio-chars were analyzed by the CE-440 elemental analyzer and bomb calorimeter (IKA 2000) respectively.

7.4 Results and Discussion

7.4.1 Feedstock Properties

Moisture content, elemental composition (on a dry basis) and HHV analysis of the alkali lignin used in this study are shown in Table 7.1. The lignin is a brown powder with particle size of approximately 50 μm. The small particle size increased the heating transfer rate in lignin pyrolysis process due to its high surface area.

7.4.2 Catalysts Characterizations

The BET surface areas and pore volumes of fresh catalyst samples are shown in Table 7. 2. The surface area and total pore volume decreased when NiO was loaded on the HZSM-5. This might be due to the deposition of metal oxides (NiO) in the internal pores or the external zeolite surface. The pore size distribution is automatically calculated from the experimental adsorption isotherm using NLDFT (Non-local density functional theory) techniques by the software of Micromeritics.

DFT results (Figure 7.2) showed that HZSM-5 and NiO/HZSM-5 mainly contained pores with size ranging from 1 nm to 20 nm.

ZSM-5 is a well-known zeolite material with microporous structure. The ZSM-5 used in this study was directly purchased from Zeolite International with a mesoporous pore size. The average pore sizes of pure HZSM-5 and NiO/HZSM-5 catalysts ranged from 3.80 nm to 4.22 nm, which was located in the mesopore region. The textural mesopores might result from the interparticle voids, which might result from NiO aggregates deposited on HZSM-5. Another possible reason was the blockage of some micropores of the metal loaded HZSM-5 zeolites by the formed NiO phases.

The XRD spectra of fresh catalysts in the angle region (5–50°) are depicted in Figure 7. 3. Typical peaks of HZSM-5 (23 - 24°) were maintained in all catalysts, and this indicated that the framework of HZSM-5 remained constant after nickel loading. The peaks of NiO (37.2°, 43.3°) were detected in the diffraction patterns of 7.64% NiO/HZSM-5 and 15.27% NiO/HZSM-5. These peaks were in accordance with the standard XRD pattern of NiO (JCPDS 71-1179). This indicated that the formation of NiO on the surface of catalysts. However, the peaks of NiO were not identified in the diffraction pattern of 1.27% NiO/HZSM-5, which indicated that the NiO species might be small and highly dispersed on the catalyst.

The XRD patterns (angle region 5–55°) for used catalysts are presented in Figure 7.4. After the reaction, there is no significant change in the patterns of used HZSM-5 and 1.27%NiO/ HZSM-5 in comparison with fresh HZSM-5 and 1.27%NiO/ HZSM-5. The diffraction peaks of NiO were no longer detected in

1.27%NiO/HZSM-5, 7.64%NiO/HZSM-5 and 15.27%NiO/HZSM-5 catalysts. This indicated that the NiO present in these catalysts was reduced to metallic Ni in the reductive atmosphere at high reaction temperature after reaction. The Ni species might be small and highly dispersed on the catalysts. Then, the Ni may interact with ZSM-5 (SiO_2-Al_2O_3) to form $Ni_xSi_yO_z$ or $Ni_xAl_yO_z$ during high temperature pyrolysis process. Specially, the peak at 50.2° might be attributed to Ni_2SiO_4 based on XRD standard of Ni_2SiO_4 (JCPDS 01-076-1502). There were no Ni peaks identified in the XRD patterns of used catalysts, since Ni (111) and Ni (200) peaks (44.5° and 51.8°) were not determined based on standard XRD pattern of Ni (JCPDS 04-0850) .

The NH_3-TPD profiles of fresh catalysts were shown in Figure 7.5. Two NH_3-TPD peaks at around 100-220 °C and 220-500 °C appeared in all catalysts. This was attributed to weak acid sites (Brønsted acid) and strong acid sites (Lewis acid) respectively [118]. Compared to HZSM-5, the loading of the NiO increased the strong acid sites over NiO/HZSM-5 catalysts. The observed increase of strong acid sites of fresh Ni/HZSM-5 catalyst probably resulted from the Lewis acid sites created by nickel oxides, and the formation of the corresponding nickel oxides functioned as Lewis acidic centers that increased the number of Lewis acid sites. The NiO loading at higher level (7.64% and 15.27%) might tend to replace the Brønsted acid sites in HZSM-5 that were responsible for the hydrocarbon formation reactions, and this led to the decease of Brønsted acid sites in 7.64% NiO/HZSM-5 and 15.27% NiO-HZSM-5 catalysts.

7.4.3 Product Yields

Three main products (biofuel, bio-char and non-condensable gas) were obtained from lignin catalytic pyrolysis. The mass balances of different treatments are shown in Table 7.3. There is no significant difference in the bio-char yields of different treatments, and this was due to the same pyrolysis condition used for all treatments. All catalysts decreased the biofuel yield and increased the gas yield in comparison with non-catalytic treatment. This was due to enhanced secondary cracking reactions that decomposed biofuel to non-condensable gas over HZSM-5 and NiO/HZSM-5 catalysts. Compared to HZSM-5, 1.27%NiO/HZSM-5 increased biofuel yields, which indicated the reduced biofuel cracking performance of HZSM-5. However, when more nickel (7.64% or 15.27%) was loaded on the HZSM-5 catalyst, the biofuel yield decreased significantly. The decrease of biofuel yield was most likely due to the massive formation of metal oxide aggregates (NiO) that reduced organic compounds in biofuel to light gaseous products such as CO_2. Although the coking yield was not high, it can still deactivate catalyst remarkably. Coking formation was due to condensation and polymerization reactions. The addition of NiO to HZSM-5 reduced the coke formation in comparison to pure HZSM-5. This reduction might be due to the higher activity of NiO/HZSM-5 catalysts that converted phenols (coke precursors) into hydrocarbons or gaseous product. Another reason might be the excellent catalyst stability of NiO/HZSM-5 catalyst.

7.4.4 Biofuel Analysis

GC-MS was employed to analyze the compositions of biofuels produced by non-catalytic and catalytic treatments. The compounds in the biofuel can be

classified into different groups: phenols, ethers, furans, esters, alcohols, acids and hydrocarbons. The relative contents of each group for different treatments are presented in Table 7.4.

The main components of the biofuel produced by non-catalytic treatment were alcohols, esters, hydrocarbons, phenols and furans. The bi-functional NiO/HZSM-5 catalysts, showed higher activity and selectivity for the deoxygenation of C-O bonds in alcohols, phenols and furans [119]. The content of alcohols decreased to some degree in the catalyzed biofuel. This decrease was due to the transformation of alcohols to hydrocarbons such as olefins that occurred on HZSM-5 and NiO/HZSM-5 catalysts. The phenol content of biofuel, which was considered as coke precursors, decreased in catalytic treatment, especially in NiO/HSM-5 treatments. The furan contents of biofuel also decreased in all catalytic treatments. The decreased phenols and furans may be converted to hydrocarbons over NiO/HZSM-5 catalysts through a series of cascade reactions including hydrogenation, hydrolysis, dehydration and dehydroaromatization. The esters content of the biofuel reduced when treated with HZSM-5 and 1.27 % NiO/HZSM-5 in comparison to the non-catalytic treatment, but increased significantly when treated with 7.64 % NiO/HZSM-5 and 15.27 % NiO/HZSM-5. It appeared that the more NiO loaded over HZSM-5, the less cracking and aromatization ability of NiO doped HZSM-5 which can convert esters to hydrocarbons.

One of the major objectives of this study was to maximize the yields and selectivity of desirable hydrocarbons in the biofuel product. The Brønsted acid sites in HZSM-5 zeolites facilitated the formation of hydrocarbons through cyclization, alkylation, aromatization, dehydration, isomerization, cracking, decarbonylation, decarboxylation, oligomerization and dehydrogenation reactions [120]. The

hydrocarbon contents of biofuel produced by HZSM-5, 1.27% NiO/HZSM-5 and 7.64% NiO/HZSM-5 treatments increased compared to the non-catalytic treatment, with 1.27% NiO/HZSM-5 having the most effect at 69.4 %. This increase might be due to the Ni promoted hydrogenation and dehydro-aromatization reactions. Most of the hydrocarbons in the biofuel produced were in the gasoline range olefins (C_5-C_{12}), which was due to the shape selectivity (moderate internal pore space and steric hindrance) of HZSM-5 catalyst. Compared to the HZSM-5 treatment, 1.27% NiO/HZSM-5 treatments generated higher content of hydrocarbons in the biofuel. However, 7.64% NiO/HZSM-5 and 15.27% NiO/HZSM-5 treatment obtained biofuel with lower hydrocarbon contents in comparison to 1.27 % NiO/HZSM-5 treatment. When more NiO was loaded on the HZSM-5, the Ni reduced from NiO may preferentially replace the Brønsted acid sites. Therefore, it greatly decreased the Brønsted acid sites in 7.64% NiO/HZSM-5 and 15.27% NiO/HZSM-5, which might lead to the lower formation of hydrocarbons. Another possible reason is that the redox reaction between NiO and the oxygenated organic compounds in the biofuel may transform the organic compounds such as hydrocarbons to gaseous products such as CO_2.

Both NiO and Ni were active phases for upgrading bio-oil to biofuel. Nickel oxide (NiO) was active for bio-oil deoxygenation through decarboxylation reaction pathway on NiO/HZSM-5 catalysts [121], and the CO_2 yields increased in NiO/HZSM-5 treatments. The oxygen present in the bio-oil compounds was also removed through hydrodeoxygenation and hydrogenation reactions that could be activated by Ni metals [122].

7.4.5 Gas Analysis

The detailed gas compositions (based on the weight percent of the original alkali lignin) of all treatments are shown in Table 7.5. The non-condensable gas products contained hydrogen, carbon dioxide, carbon monoxide, methane and C_2-C_4 hydrocarbons. Carbon dioxide and carbon monoxide are the two main components that generated from decarboxylation and decarbonylation reactions that occurred on HZSM-5 catalysts. The carbon oxides (CO and CO_2) content increased significantly in 7.64% NiO/HZSM-5 and 15.27% NiO/HZSM-5 due to the redox reaction between NiO and the oxygenated organic compounds in the bio-oil. In the presence of NiO/HZSM-5, H_2 content increased rapidly, which might be due to in situ H_2 formation reactions (steam reforming and water-gas shift) occurred on Ni loading zeolites [46]. The contents of C_2-C_4 compounds changed slightly in different treatments.

7.4.6 Bio-char Analysis

Bio-char is a pyrolysis product of lignin, cellulose and hemicellulose, and it can be used as a fuel, soil-improver or precursor for activated carbon. Since all bio-chars were obtained in the same pyrolysis condition in the reactor, there is no significant difference in their higher heating values (29.5-32.8 MJ/Kg), elemental analysis (carbon 71.8-74.9 wt.%, hydrogen 2.4-3.0 wt.%, nitrogen 0.4-0.8 wt.% and oxygen 10.7-13.1 wt.%, based on dry basis) and ash content (10.7-12.7 wt.%).

7.5 Conclusions

NiO/HZSM-5 and HZSM-5 catalysts were used to produce hydrocarbon biofuels from alkali lignin catalytic pyrolysis in a two-stage reactor system. The

catalytic effects of different NiO/HZSM-5 catalysts on yields and quality of biofuel, gas and bio-char were investigated. The interaction between Ni and HZSM-5 formed Ni_2SiO_4 during the high temperature pyrolysis process. Compared to non-catalytic treatment, all catalysts decreased the biofuel yields. Among all catalytic treatments, 1.27 %NiO/HZSM-5 generated highest biofuel yield (27.5 %), and it also produced biofuel with the highest amount of hydrocarbons (69.4%). All catalysts showed no significant effect on properties of bio-chars.

The development of a stable and long-life NiO/ZSM-5 catalyst for catalytic pyrolysis of lignin is important. The further stability study of fresh NiO/ZSM-5 catalyst for upgrading lignin pyrolysis bio-oil at longer operation time, the reduced catalyst activity caused by coke deposition, used NiO/ZSM-5 catalyst regeneration by air combustion and recycle will be investigated to develop a stable and long-life NiO/ZSM-5 catalyst in our following research.

Table 7.1 Lignin properties

Analysis	Result
Moisture content (wt.%)	4.1±0.4
Elemental analysis	
Carbon (wt.%)	61.9±0.4
Hydrogen (wt.%)	5.6±0.2
Nitrogen(wt.%)	0.5±0.0
Sodium (wt.%)	0.543%
Ash (wt.%)	2.95±0.3
Oxygen* (wt.%)	28.48±0.6
Higher heating value (MJ kg^{-1})	26.1±0.1

*Calculated by 100%-carbon-hydrogen-nitrogen.

Table 7.2 BET parameters of the different fresh catalysts

Catalyst	BET surface area ($m^2\ g^{-1}$)	Average pore size (nm)	Total pore volume* ($cm^3\ g^{-1}$)
HZSM-5	473.3	4.22	0.46
1.27% NiO/HZSM-5	451.4	3.92	0.44
7.64%NiO/HZSM-5	442.7	3.85	0.42
15.27%NiO/HZSM-5	386.2	3.80	0.36

* Total pore volume, measured at P/P_0= 0.995.

Table 7.3 Product yields of different treatments

Treatments	Liquid (wt.%)	Solid (wt.%)		Gas (wt.%)	Liquid rate (g/gcat/h)
	Bio-oil	Bio-char	Coke		
No catalyst	30.9±0.4	50.5±0.2	0.0±0.0	18.6±0.2	-*
HZSM-5	25.7±0.6	50.0±0.1	1.1±0.1	23.2±0.6	2.4±0.06
1.27%NiO/HZSM-5	27.5±0.1	50.2±0.1	0.3±0.1	22.0±0.2	2.7±0.01
7.64%NiO/HZSM-5	18.8±0.4	50.2±0.1	0.6±0.1	30.4±0.3	1.8±0.05
15.27%NiO/HZSM-5	14.2±0.7	49.4±0.1	0.7±0.1	35.7±0.6	1.3±0.15

* Not available, since no catalyst was used in no catalyst treatment.

Table 7.4 Chemical composition of compounds in biofuels

Compounds relative content (%)	No catalyst	HZSM-5	1.27 %NiO /HZSM-5	7.64 %NiO /HZSM-5	15.27 %NiO /HZSM-5
Phenols	7.9	3.2	0	0	1.3
Ethers	0	0	0	0	2.5
Furans	4.8	0	0	0	1.1
Esters	20.4	8.5	9.3	43.9	55.1
Alcohols	29.8	12.6	4.0	14.1	4.6
Acids	0	0	5.8	1.7	2.1
Hydrocarbons *	31.1	65.3	69.4	36.8	23.5
Light hydrocarbons (C_5-C_{12})	31.1	56.3	66.7	27.2	19.8
Heavy hydrocarbons (C_{13}-C_{19})	0	9.0	2.7	9.5	3.7

* Sum of light hydrocarbons and heavy hydrocarbons.

Table 7.5 Non-condensable gas distribution of different treatments

Gas composition* (wt.%)	No catalyst	HZSM-5	1.27 % NiO/HZSM-5	7.64 % NiO/HZSM-5	15.27 % NiO/HZSM-5
H_2	0.1±0.0	0.1±0.0	0.2±0.0	0.7±0.1	0.7±0.1
CO_2	11.3±0.3	14.1±0.1	14.4±0.1	16.6±0.3	19.9±0.4
CO	3.8±0.1	4.2±0.1	3.8±0.2	8.1±0.4	9.0±0.2
CH_4	2.5±0.1	2.6±0.2	2.3±0.1	2.7±0.3	3.5±0.3
C_2H_6	0.6±0.1	0.6±0.1	0.5±0.1	0.7±0.2	0.8±0.1
C_2H_4	0.2±0.0	0.7±0.0	0.4±0.1	0.7±0.1	0.9±0.2
C_3H_8	0.2±0.0	0.3±0.0	0.2±0.0	0.4±0.1	0.4±0.1
C_3H_6	0.1±0.0	0.5±0.1	0.3±0.1	0.4±0.1	0.6±0.2
C_4H_{10}	0.0	0.0	0.0	0.1±0.0	0.0
C_4H_8	0.0	0.0	0.0	0.1±0.0	0.0

* The gas composition is calculated as the weight percent of the feedstock.

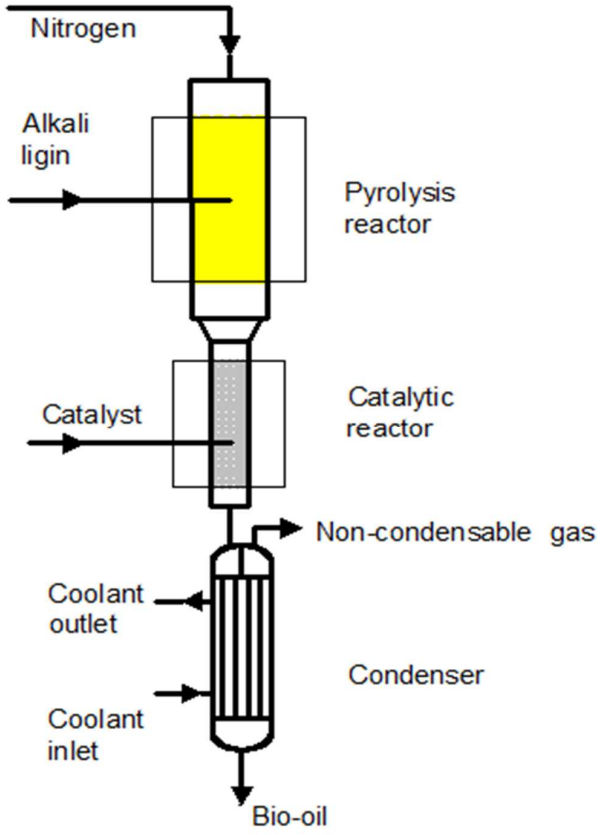

Figure 7.1 Schematic diagram of two-stage reactor system

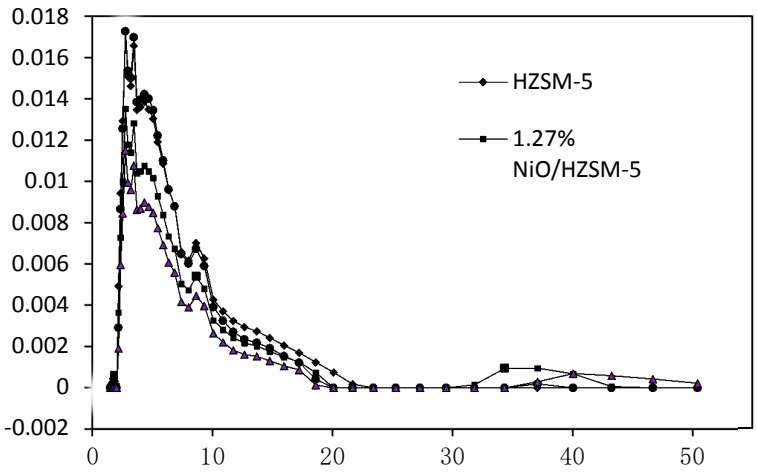

Figure 7.2 Pore size distribution of fresh HZSM-5 and NiO/HZSM-5 catalysts

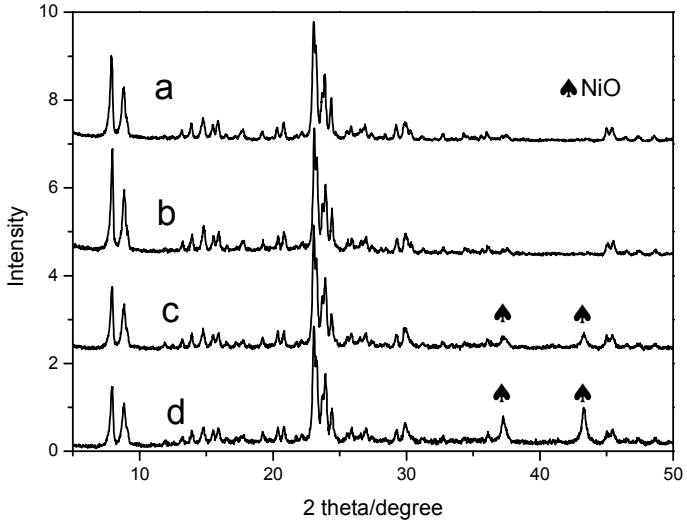

Figure 7.3 XRD spectra of fresh catalysts (a-fresh HZSM-5, b-fresh1.27%NiO/HZSM-5,c-fresh7.64%NiO/HZSM-5,d-fresh15.27%NiO/HZSM-5)

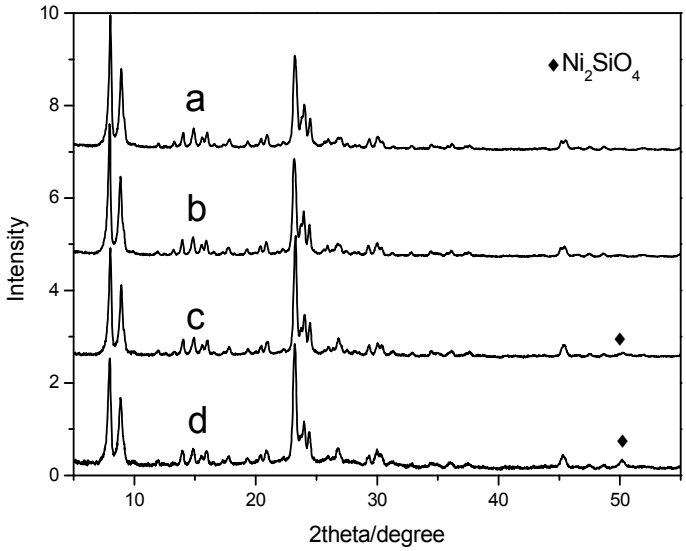

Figure 7.4 XRD spectra of used catalysts (a-used HZSM-5, b-used 1.27%NiO/HZSM-5, c-used 7.64%NiO/HZSM-5, d-used 15.27%NiO/HZSM-5)

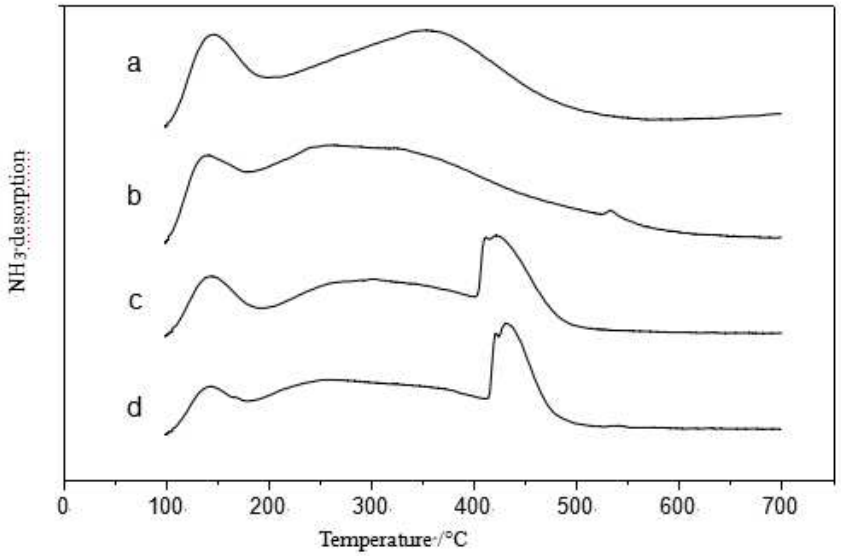

Figure 7.5 NH3-TPD profiles of fresh catalysts (a-fresh HZSM-5, b-fresh 1.27%NiO/HZSM-5, c-fresh7.64%NiO/HZSM-5,d-fresh15.27%NiO/HZSM-5)

CHAPTER 8

Hydrocarbon bio-oil production from pyrolysis bio-oil using non-sulfide Ni-Zn/Al2O3 catalyst

8.1 Abstract

Upgraded bio-oil can partly replace fossil fuels to reduce the environmental issues caused by the massive consumption of fossil fuels. Hydrodeoxygenation is a promising route for upgraded bio-oil production from pyrolysis bio-oil. Non-sulfide catalysts are effective in bio-oil hydrodeoxygenation due to low cost and high activity. Ni-Zn/Al2O3 catalysts were first used to selectively produce hydrocarbon upgraded bio-oil through bio-oil hydrodeoxygenation. Upgrading pine sawdust bio-oil to upgraded hydrocarbon bio-oil was performed using a series of Ni and/or Zn loaded Al2O3 catalysts. The crystalline structure of Al2O3 was maintained after Ni and/or Zn loading, but BET surface area and total pore volume of Ni-Zn/Al2O3 catalysts decreased significantly compared to Al2O3 support. Bimetallic Ni-Zn/Al2O3 catalysts were more effective than monometallic Ni/Al2O3 or Zn/Al2O3 catalyst. Bimetallic 15%Ni-5%Zn/Al2O3 catalyst generated the highest upgraded bio-oil yield at 44.64 wt.% and produced the upgraded bio-oil with the highest hydrocarbon content at 50.12%. Physicochemical properties of upgraded bio-oils including heating value, water content and pH were significantly improved in comparison with raw bio-oil. The improved catalytic performance of bimetallic Ni-Zn/Al2O3 catalyst was associated with the synergistic effect of Ni and Zn on Al2O3 support.

8.2 Introduction

Increased energy demand and diminishing fossil fuels concerns, and the related environmental issues including air pollution and global warming, have sparked great interest in the use of biomass as a partial fossil fuel alternative resources. Liquid upgraded bio-oils derived from renewable biomass sources are an attractive substitute for fossil-derived fuels. Pyrolysis is an effective technology for the conversion of biomass into liquid bio-oil. Pyrolysis involves the rapid heating of biomass to the temperature range of 400–600 °C in an oxygen-free atmosphere. Bio-oil cannot be used directly as a transportation fuel for high-speed combustion engines due to the high oxygen content (35–40 wt.% dry basis), high water content (up to 30 wt.%) and the presence of corrosive organic acids compounds (up to 10 wt.%). Bio-oil upgrading is required before it can be used as fuel (upgraded bio-oil). The upgraded bio-oil (biofuel) is defined as bio-oil with higher quality (lower water content, improved pH and carbon content, higher heating value and improved hydrocarbons content).

Hydrodeoxygenation (HDO) is a promising bio-oil upgrading technology. This technique selectively removes oxygen from pyrolysis bio-oil through a catalytic reaction using hydrogen in the presence of a heterogeneous catalyst. Catalysts play a significant role in bio-oil HDO. Many catalysts with different active phases, promoters and supports have been studied on bio-oil HDO. For instance, noble metal catalysts including Ru/C, Ru/TiO_2, Ru/Al_2O_3, Pt/C and Pd/C have been

widely tested for bio-oil HDO processes. However, scarcity and the high price of noble metals are the main problems for industrial scale application. Conventional hydrodesulfurization (HDS) catalysts such as sulfided $NiMo/Al_2O_3$ and $CoMo/Al_2O_3$ were also tested for bio-oil HDO. However, the sulfided catalysts have problems of sulfur usage and product contamination. Therefore, non-sulfided Ni based catalysts including $MoNi/Al_2O_3$, $NiCu/Al_2O_3$ and $NiFe/Al_2O_3$, have attracted great interest because of their excellent catalytic activities for HDO of pyrolysis bio-oil. Xu et al. found that $MoNi/Al_2O_3$ catalysts considerably improved the upgraded bio-oil properties. These improvements included hydrogen content (increased from 6.25 wt.% to 6.95 wt.%) and acidity (pH increased from 2.33 to 2.77). The addition of Mo metal promoted the dispersion of nickel species and inhibited $NiAl_2O_4$ spinel formation on the $MoNi/Al_2O_3$ catalysts [123]. Bimetallic $Ni\text{-}Cu/Al_2O_3$ catalysts were more active than monometallic Ni/Al_2O_3 catalyst for anisole and pyrolysis bio-oil HDO [34]. Leng et al.demonstrated that $NiFe/Al_2O_3$ improved the bio-oil heating value from 37.8 MJ kg^{-1} to 43.9 MJ kg^{-1}, and the main involved reaction pathway was C-O cleavage rather than C-C cleavage during the bio-oil HDO process [39].

Zinc, a transition metal present in $ZnCl_2$, is cost effective and can used to improve the catalytic performance of zeolite during upgrading vegetable bio-oil to hydrocarbon fuel. Recently, the study of Zhao et al. indicated that Zn modified $Mo\text{-}Zn/Al_2O_3$ catalyst exhibited an excellent catalytic activity and stability for the conversion of oxygenated compounds in vegetable oil to hydrocarbons. This was

due to its acidity and coke resistance properties[124]. To the best of our knowledge, few studies have been performed using non-sulfided Zn promoted Ni-Zn/Al_2O_3 catalysts for HDO of pyrolysis bio-oil.

The purpose of this study was to investigate the effects of Ni-Zn synergy during HDO of pine sawdust bio-oil during the production of hydrocarbon upgraded bio-oil using Ni-Zn/Al_2O_3 catalysts with different Ni and Zn loading ratios at a temperature of 250 °C and pressure of 500 psig. The catalytic effect of different Ni-Zn/Al_2O_3 catalysts on upgraded bio-oil yield and physicochemical properties (water content, pH, higher heating value and chemical compositions) were determined. The catalysts were characterized by BET, XRD, NH_3-TPD and TEM. The compositions of produced gases were analyzed by GC.

8.3 Material and methods

8.3.1 Feedstock

The raw pine sawdust (PSD) bio-oil was produced using a proprietary pyrolysis pilot reactor in our lab. The sawdust was ground into powder with screen of 1 mm using a hammer mill. The sawdust powder was then screened by 200-250 mesh sieve. The average particle size of pine sawdust feedstock was 0.06 mm. The reactor is consisted of a screw feeder, a reaction chamber and a condenser. The feeding rate of PSD through the screw feeder into the reactor was 1.36 kg h^{-1}, and the residence time of PSD in the reactor was approximately 1 s. The temperature of the reaction chamber and the condenser were 538 °C and -10 °C, respectively.

8.3.2 Catalyst preparation

Nickel nitrate hexahydrate and aluminum oxide were provided by Sigma-Aldrich and used as received. Zinc chloride was provided by Fisher Scientific and used as received. A series of Ni-Zn/Al_2O_3 catalysts with differing Ni and/or Zn mass loading ratios (20%Ni/Al_2O_3, 15%Ni-5%Zn/Al_2O_3, 10%Ni-10%Zn/Al_2O_3, 5%Ni-15%Zn/Al_2O_3 and 20%Zn/Al_2O_3) were prepared using a wet impregnation method. The aluminum oxide support was impregnated with a given amount of nickel nitrate hexahydrate and zinc chloride aqueous solution at 20 °C. The prepared catalysts were then dried at 120 °C for 5 h in static air and calcined at 600 °C for 4 h in static air.

8.3.3 Catalysts characterization

A X-ray Diffractometer (XRD, MiniFlex, Rigaku Corporation) was used to determine catalyst crystallinity. The filtered Cu-Kα radiation was employed during the XRD analysis. The X-ray tube was set at 30 kV (tube voltage) and 15 mA (tube current). The scan range of the X-ray pattern was 10-90 ° (2 theta) and the scan speed was 2 ° min^{-1}. The step size of X-ray pattern was 0.02 ° (2 theta).

A transmission electron microscope (JEOL JEM-2100 LaB6) was used at 200 kV to determine TEM images of catalysts. Isopropyl alcohol (0.5–1.0 mL) was employed to disperse the catalyst samples (several micrograms). The dispersed suspension was then mixed using an ultrasonic for 2 minutes. A few suspension droplets were placed on a copper grid (200-mesh, carbon-coated) and dried before

testing. EDS (Energy Dispersive X-Ray Spectroscopy) data of elemental composition for catalysts samples were obtained in the TEM using an Oxford Inca energy-dispersive silicon-drift X-ray (EDX) spectrometer.

BET specific surface area and pore texture of catalysts were analyzed by an automatic Micromeritics ASAP 2020 apparatus with nitrogen adsorption measurements operated at 77.2 K. Specific surface area was determined by Brunauer–Emmett–Teller method.

Acidity of fresh catalysts was determined by a Micrometrics Autochem II Chemisorption Analyzer with a thermal conductivity detector (TCD). The fresh catalyst sample (300 mg) was firstly added to ammonium hydroxide (37.1 wt.%, 4.5 g), and the mixture was kept at room temperature (20 ºC) for 3 h. Then, the mixture was dried at 60 ºC for 12 h. The dried sample was used for NH_3-TPD analysis. The helium flow in the chemisorption analyzer was 60 mL min^{-1}. The catalyst sample was heated and maintained at 100 ºC for 30 min to remove the physically absorbed ammonia. Then the sample temperature was increased from 100 ºC to 700 ºC at a rate of 10 ºC min^{-1}. The final temperature of 700 ºC was held for 30 min. During the period of heating from 100 ºC to 700 ºC, abundant dilute HCl solution (1.0mol/L) was used to collect the chemisorbed ammonia from the catalyst sample. Then, NaOH solution (0.1mol/L) was employed to titrate the HCl solution to determine the total acid sites of the catalyst sample.

8.3.4 Bio-oil HDO test

The batch bio-oil HDO tests were performed in an autoclave reactor (500 mL, Parr 4575). The maximum allowable operating pressure and temperature of the reactor were 5000 psig and 400 °C, respectively. The reactor temperature and impeller mixing speed were continuously controlled by an electronic controller panel. The controller panel also monitored the reactor pressure. The impeller mixing speed used in the experiment was 1000 rpm.

Water was the solvent used during pyrolysis bio-oil upgrading to lower the activation barrier and increase the proton diffusion coefficient. The autoclave reactor was loaded with 6 g of fresh catalyst, 60 g of raw pine sawdust bio-oil and 100 g of deionized water. In control 1 test, 6 g Al_2O_3, 60 g raw pine sawdust bio-oil and 100 g deionized water were loaded in the reactor. In control 2 test, 6 g 15%Ni-5%Zn/Al_2O_3 catalyst, 60 g raw pine sawdust bio-oil and 100 g deionized water were loaded in the reactor. In catalyst recycle test, 6 g used 15%Ni-5%Zn/Al_2O_3 catalyst (washed by ethanol and dried at 120 °C for 12 h), 60 g raw pine sawdust bio-oil and 100 g deionized water were loaded in the reactor. The reactor with reactants was installed and flushed three times with hydrogen at 50 psig (50 psig nitrogen for control 2 test) to remove the inside air. The reactor was then pressurized with hydrogen at 500 psig (or 20 psig nitrogen for control 2 test), and heated to the reaction temperature of 250 °C at a rate of 5 °C min^{-1}. This reaction temperature was maintained for 5 h. These reaction conditions, the catalyst/bio-oil ratio of 1:10,

and mixing rate of 1000 rpm were determined by our preliminary tests. At the end of 5 hours, the furnace turned off and the reactor vessel was allowed to cool to room temperature (20 °C). The liquid bio-oil product separated into the oil phase (upgraded bio-oil) and aqueous phase using a separator funnel. The gas product was collected in gas sample bags. The oil and aqueous phases were filtered (0.2μm PTFE filter) to remove the catalysts and coke. The separated catalysts were washed with ethanol and dried at 110 °C for 3 h in a drying oven. The mass of coke was determined by the mass difference between used and fresh catalyst. The coke yield (Y coke) was calculated by the ratio of coke mass (M coke) to bio-oil mass (M bio-oil) according to equation (1). Oil phase and aqueous phase yields (Y product) were determined by determining the ratio of product mass (M product) to bio-oil mass (M bio-oil) using equations (2). The gas yield was calculated via mass balance following equation (3).

$$Y\ coke = M\ coke / M\ bio\text{-}oil \times 100\% \quad (1)$$

$$Y\ product = M\ product / M\ bio\text{-}oil \times 100\% \quad (2)$$

$$Y\ gas = 100 - (Y\ oil\ phase + Y\ aqueous\ phase + Y\ coke) \quad (3)$$

where Y gas is the yield of gas product.

8.3.5 Physicochemical properties determination

Physicochemical properties of bio-oils including water content, pH, higher heating value (HHV) and chemical compositions were determined. Water content was determined using a Karl Fischer Titrator V20 (Mettler Toledo Company) based on ASTM E1064. Bio-oil pH was determined using a pH meter (Accumet Company). HHV was determined in accordance with ASTM D4809 using a bomb Calorimeter System (C2000, IKA-Works).

Chemical compositions of upgraded bio-oils and raw bio-oil were determined by gas chromatography–mass spectrometry (GC–MS) using anAgilentGC-7890A (DB-5 column: 30 m × 0.25 μm × 0.25 mm) and MSD-5977B (electron ionization of 70 eV, mass range at 50–500 m z^{-1}). The injection temperature and injection volume were 300 °C and 1 μL respectively. The column temperature was initially set at 60 °C and held at this temperature for 1 min. The column temperature was then ramped up at a rate of 3 °C min^{-1} to 140 °C, then at 10 °C min^{-1} to 180 °C, then at 3 °C min^{-1} to 260 °C and finally at 10 °C min^{-1} to 300 °C. The set temperature was maintained for an additional 2 min after each ramp was completed. Helium was the carrier gas at a flow rate of 1 mL min^{-1}. The chemical composition of samples was determined using the NIST mass spectral library. The relative content of compounds in the samples was calculated using the ratio of its peak area to the total peak area of GC–MS spectrogram.

Gas compositions were determined using an Agilent 7890A GC system (19095P-S25 column: 50 m × 15 μm× 0.53 mm). H_2, CO_2 and CO were identified using a thermal conductivity detector. Light hydrocarbons (C_1–C_5) were determined using a flame ionization detector. Argon was the carrier gas. GC calibration was conducted using standardized gas mixtures.

8.4 Results and discussion

8.4.1 XRD characterization

The x-ray diffraction (XRD) spectra of the Al_2O_3 based catalysts are shown in Figure 8.1. In the XRD patterns of all Al_2O_3 based catalysts, diffraction peak positions of Al_2O_3 structure at 25.58°, 35.15°, 37.78°, 43.36°, 52.55°, 57.50°, 61.30°, 66.52°, 68.21° and 77.23° were determined using JCPDS No. 00-046-1212. The results indicate that the crystalline structure of the Al_2O_3 support was maintained after Ni and/or Zn loading. Ni/Al_2O_3 catalysts showed peaks of NiO phase at 37.32°, 63.00°, 75.56° and 79.57° according to PDF Card No.1010381. Zn/Al_2O_3 catalysts showed ZnO with peaks of 32.07°, 36.53° and 81.65° that are consistent with PDF Card No.1011258. Ni-Zn/Al_2O_3 catalysts showed peaks of both NiO and ZnO phases. These results indicate that NiO and ZnO particles formed on Ni-Zn/Al_2O_3 catalysts.

8.4.2 TEM and EDS characterizations

The TEM images of Al_2O_3 catalysts are shown in Figure 8.2. There were no obvious dark spots in Al_2O_3 image (Figure 2a), indicating no NiO and/or ZnO loading take place. Dark spots were found in the TEM image of 20%Ni/Al_2O_3 catalyst (Figure 2b), and these were attributed to NiO particles. Dark spots were found on 20%Zn/Al_2O_3 catalyst (Figure 2f), which was attributed to the loading of ZnO particles. Kasatkin et al. showed similar dark spots on TEM images of Cu-Zn/Al_2O_3. These were attributed to copper oxide and/or zinc oxide [37]. Dark spots were identified in the TEM images of 15%Ni-5%Zn/Al_2O_3 catalyst (Figure 2c), 10%Ni-10%Zn/Al_2O_3 catalyst (Figure 2d) and 5%Ni-15%Zn/Al_2O_3 catalyst (Figure 2e), indicating these might be attributed to the metal oxides particles of NiO and/or ZnO. TEM results of Al_2O_3 based catalysts are in accordance with the XRD results which showed the existence of metal oxides such as NiO and/or ZnO. The metal contents of Ni-Zn/Al_2O_3 catalysts are shown in Table 8.1. The Ni and/or Zn elements were detected in Ni and/or Zn loaded Al_2O_3 catalysts. The Ni and/or Zn metal contents of Ni-Zn/Al_2O_3 catalysts were a bit lower than calculated metal contents, which might be due to a nonquantitative immobilization and non-uniform distribution of the metals on the Al_2O_3 support.

8.4.3 BET and NH3-TPD characterizations

The textural properties and total acidity of the Ni-Zn/Al_2O_3 catalysts are listed in Table 8.2. The BET specific surface area and total pore volume of Ni and/or Zn

loaded Al_2O_3 catalysts decreased significantly compared to Al_2O_3 support. The average pore diameter of Ni-Zn/Al_2O_3 catalysts was lower than that of Al_2O_3 support. Some micropores and mesopores of the Al_2O_3 support were filled with metal oxides after the metal-loading, which might result in the decrease of these textural properties. The total acidity of 20%Ni/Al_2O_3 was lower than Al_2O_3 support. The total acidity of higher Zn loading Al_2O_3 catalysts was higher than Al_2O_3 support, and total acidity of Zn loaded Al_2O_3 catalysts increased with the Zn loading ratio.

8.4.4 Products yields

The bio-oil obtained from the HDO process can be separated into two phases: oil phase (targeted upgraded bio-oil, mainly composed of organic compounds) and aqueous phase (contained mainly water and a few organic compounds). The yields of bio-oil HDO products (upgraded bio-oil (BP), aqueous phase (AP), coke and gas) are shown in Figure 8.3. Bimetallic catalysts such as 15%Ni-5%Zn/Al_2O_3 and 10%Ni-10%Zn/Al_2O_3 increased upgraded bio-oil yields compared to monometallic catalysts (Ni/Al_2O_3 and Zn/Al_2O_3). This change might be due to the hydrodeoxygenation and hydrogenation promoted reactions due to the bimetallic Ni-Zn/Al_2O_3 catalysts increasing the content of hydrophobic hydrocarbons compounds in upgraded bio-oils. The bimetallic Ni-Zn/Al_2O_3 catalysts decreased coke yield when compared to monometallic Ni/Al_2O_3 and Zn/Al_2O_3 catalysts. These results indicate that bimetallic catalysts might inhibit polymerization and poly-condensation reactions that are responsible for coke formation during bio-oil HDO

process. 15%Ni-5%Zn/Al_2O_3 catalyst generated the highest upgraded bio-oil yield at 44.64 wt.% and the lowest coke yield at 4.67 wt.%. The statistical analysis of 15%Ni-5%Zn/Al_2O_3 and 10%Ni-10%Zn/Al_2O_3 catalysts on bio-oil yields was conducted by SPSS statistics software. At 0.05 significant level, the P-value (0.005) < 0.05. Therefore, the effect of 15%Ni-5%Zn/Al_2O_3 and 10%Ni-10%Zn/Al_2O_3 catalysts on bio-oil yields are significantly different. Besides, the mean value of these two catalysts were higher than other Ni-Zn/Al_2O_3 catalyst, and thus bimetallic catalysts such as 15%Ni-5%Zn/Al_2O_3 and 10%Ni-10%Zn/Al_2O_3 increased upgraded bio-oil yields. The yields of upgraded bio-oil of control 1 and control 2 tests were lower than Ni-Zn/Al_2O_3 catalysts due to the lack of metal active centers and enough hydrogen supply, respectively. The upgraded bio-oil yield of reused 15%Ni-5%Zn/Al_2O_3 catalyst was lower than fresh 15%Ni-5%Zn/Al_2O_3 catalyst, and this might be due to the higher coke deposition that deactivated catalyst quickly.

8.4.5 Physicochemical properties of upgraded bio-oil

Physicochemical properties including pH, water content and higher heating value of upgraded bio-oils and raw bio-oil are shown in Table 8.3. Water content has a negative effect on the combustion performance of upgraded bio-oils in engines. The water content of upgraded bio-oil ranged from 11.48 wt.% to 20.43 wt.%, and it was reduced significantly from the water content of 26.91 wt.% present in raw bio-oil. The reduced water content was due to the increased hydrocarbon

hydrophobic products in the oil phase. There is an obvious increase in the higher heating values of upgraded bio-oil (17.13-30.47 MJ kg^{-1}) compared to raw bio-oil (15.54 MJ kg^{-1}). This is attributed to the lower contents of water and oxygenated compounds present in the upgraded bio-oils. The HDO process effectively improved the energy content of upgraded bio-oil products. HHV of upgraded bio-oil produced by Ni-Zn/Al_2O_3 was higher than control 1 and control 2 tests. This indicated that hydrogen was necessary for bio-oil HDO reactions. The loading of Ni and/or Zn on Al_2O_3 improved bio-oil HDO activity. Low pH values of bio-oil have a strong corrosive effect on combustion engines. The pH of upgraded bio-oil (3.27-3.43) increased slightly in comparison with raw bio-oil (3.24). This might be due to the conversion of some acids compounds into other compounds including hydrocarbons in upgraded bio-oils. However, the upgraded bio-oil was was still very acidic with pH comparable to that of bio-oil due to the high content of acidic compounds.

The carbons contents of upgraded bio-oil was higher than raw bio-oil due to the removal of oxygen in bio-oil HDO reactions. The carbon content of upgraded bio-oil produced by Ni-Zn/Al_2O_3 catalysts was higher than control 1 and control 2 tests. The carbon balance of bio-oil HDO processes (Table 3) over Ni-Zn/Al_2O_3 catalysts was ranging from 74.34 wt.% to 94.58 wt.%.

8.4.6 Chemical compositions of upgraded bio-oil

In order to determine catalytic effects of Ni-Zn/Al_2O_3 catalysts on upgraded bio-oil products, GC-MS was used to analyze the chemical compositions of both upgraded bio-oil and raw bio-oil. The major chemical components of the upgraded bio-oils and raw bio-oil are displayed in Table 8.4. Chemical groups identified consisted of phenols, ethers, aldehydes, ketones, esters, alcohols, acids, furans and hydrocarbons.

The raw bio-oil main compositions were organic oxygenated compounds that included phenols (21.10%), acids (17.62%), ketones (9.77%), esters (6.86%), alcohols (5.64%) and aldehydes (5.40%). The total amount of detected oxygenated compounds was 70.70%. These compounds are responsible for the low quality of the raw bio-oil. The amount of valuable hydrocarbons in the raw bio-oil was 16.94%.

The chemical compositions of upgraded bio-oils changed significantly after the raw bio-oil HDO over different Ni-Zn/Al_2O_3 catalysts. The contents of undesirable acids in upgraded bio-oil were decreased. This decrease may be due to the conversion of acids into hydrocarbons caused by decarbonylation, hydrogenation and cracking reactions. Transfer of some carboxylic acids from the oil phase to aqueous phase might also contribute to the decrease of acids content in upgraded bio-oils. This decrease in acid compounds reduces the requirements of special vessels and pipelines that would be used for upgraded bio-oil storage, transportation and processing.

The contents of ketones in upgraded bio-oils decreased during catalytic upgrading treatments. Ketones might be transformed into hydrocarbons and CO_2 through decarboxylation reactions. Alcohols were most probably converted to hydrocarbons and phenols during bio-oil HDO process, resulting in decreased alcohols levels in upgraded bio-oil products. Some esters were transformed into hydrocarbons through hydrogenation, decarboxylation and decarbonylation reactions [125]. This led to the decreased content of esters present in upgraded bio-oil samples. During bio-oil HDO processes, the content of aldehydes and phenols decreased in the upgraded bio-oil products. Aldehydes and phenols might be transformed into coke-like polymers in the presence of acidic catalyst.

Hydrocarbons are the main valuable components in upgraded bio-oil product. The content of hydrocarbons in upgraded bio-oil increased significantly in comparison with raw bio-oil. This was probably due to the bio-oil HDO reactions including cracking, decarbonylation, decarboxylation, hydrocracking, hydrodeoxygenation and hydrogenation that converted oxygenated organic compounds to hydrocarbons on Ni-Zn/Al_2O_3 catalysts. Compared to monometallic catalysts, the bimetallic 15%Ni-5%Zn/Al_2O_3 produced the upgraded bio-oil with the highest hydrocarbons content at 50.12%. This was probably due to the synergistic effect of Ni and Zn on Al_2O_3 support. The hydrocarbons content of upgraded bio-oil produced by control 1 and control 2 test was lower than Ni-Zn/Al_2O_3 catalysts, which indicated the important role of metal active centers and hydrogen consumption for bio-oil HDO reactions. The hydrocarbons content of

upgraded bio-oil produced by reused 15%Ni-5%Zn/Al_2O_3 was lower than fresh 15%Ni-5%Zn/Al_2O_3, and this indicated the reduced catalyst activity for bio-oil HDO reactions in this reused catalyst.

8.4.7 Conversion and selectivity of compounds in bio-oil

The conversion rates of main oxygenated compounds present in bio-oil are shown in Figure 8.4. The high conversion rates of ketones and aldehydes indicate that a large proportion of them were converted into hydrocarbons and coke-like polymers on Ni-Zn/Al_2O_3 catalysts. The massive transformation of alcohols into other compounds such as hydrocarbons resulted in the high conversion rate of alcohols in bio-oil over Ni-Zn/Al_2O_3 catalysts. Similarly, the large amount of acids and esters were transformed into hydrocarbons, and this led to high conversion rates of acids and esters compounds. The selectivities of compounds present in bio-oil are shown in Figure 8.5. The high conversion rate of oxygenated compounds including ketones, alcohols, acids and esters into hydrocarbons compounds on Ni-Zn/Al_2O_3 catalysts led to the high selectivity of hydrocarbons in upgraded bio-oil products.

8.4.8 Synergistic effect of Ni and Zn on Al2O3 support

Metallic Ni and Zn reduced from NiO and ZnO are the catalytic active centers for catalytic hydrogenation reactions on Ni-Zn/Al_2O_3 catalysts. There are three factors which resulted in the improved catalytic activity of binary Ni-Zn/Al_2O_3

(synergistic effect of Ni and Zn) than singular Ni/Al_2O_3, Zn/Al_2O_3 or Al_2O_3 catalyst. Firstly, the incorporation of Zn enhanced the interaction between NiO and alumina and improved the nickel dispersion [126]. Secondly, binary catalysts had higher stability and activity than singular catalyst. Finally, the loading of second metal prevented excessive carbon deposition on metal active sites of singular catalysts, and this led to lower coke formation of binary catalyst than singular catalyst.

8.4.9 Gas distributions

The compositions of gases produced in the HDO processes were determined by GC. The compositions of gas are shown in Table 8.5. The main component of the produced gas was unreacted hydrogen. This indicates abundant hydrogen present for the bio-oil HDO reactions. However, the efficiency of Ni-Zn/Al_2O_3 catalysts still needs to be improved to further reduce the contents of oxygenated compounds in upgraded bio-oil. More research will be conducted to improve the catalyst activity in the future research. The other main gas product was CO_2, which indicates decarboxylation reactions of organic acids on Ni-Zn/Al_2O_3 catalysts during the bio-oil HDO processes [51]. Light hydrocarbons such as CH_4 and C_2-C_5 were detected. These were probably due to the cracking of organic compounds.

In the gas compositions, the hydrogen content of 15%Ni-5%Zn/Al_2O_3 catalyst (90.26 %) was a bit higher than other Ni-Zn/Al_2O_3 catalysts (89.50-89.77%). CO_2 content of this catalyst (9.27%) was lower than other Ni-Zn/Al_2O_3 catalysts (9.73-

10.02%). However, based on the actual H_2 consumption results (calculated from the initial H_2 and final H_2 in the autoclave reactor in Table 6), the relatively higher amount of H_2 (0.18 g) was consumed for 15%Ni-5% Zn/Al_2O_3 catalyst when compared to other Ni-Zn/Al_2O_3 catalysts (0.09-0.19 g). Decarboxylation level of 15%Ni-5%Zn/Al_2O_3 was lower than other catalyst due to the lower CO_2 formation. The rest of consumed hydrogen might be used in other HDO reactions such as hydrocracking, hydrodeoxygenation and hydrogenation. This indicated that the hydrogenation level of 15%Ni-5%Zn/Al_2O_3 might not be lower than other Ni-Zn/Al_2O_3 catalyst due to the higher hydrogen consumption.

8.4.10 Reactor pressures

The reactor pressures monitored during the HDO reactions are shown in Table 8.6. The initial, maximum and final pressures of the HDO reactor were recorded. The initial pressure was the hydrogen pressure measured at 20 °C at the beginning of the test. The maximum pressure was the reactor pressure during the bio-oil HDO process at reaction temperature of 250 °C. The final pressure was the reactor pressure when the HDO reactor was cooled to 20 °C after reaction. The amount of hydrogen consumed in bio-oil HDO processes over Ni-Zn/Al_2O_3 catalysts was calculated and shown in Table 6. Higher amount of hydrogen consumption was found for 15%Ni-5%Zn/Al_2O_3, 10%Ni-10%Zn/Al_2O_3 and 20%Zn/Al_2O_3 catalysts. This indicates the higher hydrogen consumption for bio-oil HDO reactions on these catalysts. This is beneficial for improving catalytic performance of the Ni-Zn/Al_2O_3

catalysts that converted oxygenated compounds into hydrocarbons. The result is higher hydrocarbons contents in upgraded bio-oils produced using these Ni-Zn/Al_2O_3 catalysts.

8.5 Conclusions

Pine sawdust raw bio-oil was upgraded using HDO processes over a series of Ni-Zn/Al_2O_3 catalysts. The HDO processes were carried out in a batch autoclave reactor at 250 °C and 500 psig. The effects of Ni-Zn/Al_2O_3 catalysts are evaluated by determining the products (bio-oil and gas) yield and quality. Bimetallic Ni-Zn/Al_2O_3 was more effective in improving bio-oil yield and quality compared to monometallic Ni/Al_2O_3 or Zn/Al_2O_3 catalyst. The highest upgraded bio-oil yield at 44.64 wt.% and the highest hydrocarbon content at 50.12% were produced using15%Ni-5%Zn/Al_2O_3 catalyst. Physicochemical properties of upgraded bio-oils including pH, water content and higher heating value were improved compared to the raw bio-oil. The hydrocarbon contents of upgraded bio-oils produced over Ni-Zn/Al_2O_3 catalysts improved when compared to the raw bio-oil. Undesirable acids, aldehydes and ketones contents of upgraded bio-oils produced by catalysts reduced when compared to raw bio-oil.

Table 8.1 Metal contents of Ni-Zn/Al2O3 catalysts

Catalysts	20%Ni/Al_2O_3	15%Ni-5%Zn/Al_2O_3	10%Ni-10%Zn/Al_2O_3	5%Ni-15%Zn/Al_2O_3	20%Zn/Al_2O_3
Ni content (wt.%)	16.35	12.83	9.51	4.32	0
Zn content (wt.%)	0	4.46	8.75	13.76	16.48

Table 8.2 Textural properties and acidity of different catalysts

Catalyst	S_{BET} (m^2/g)	$d_{average}$(nm)	Total pore volume (cm^3/g)	Total acidity (mmol NH_3/g_{cat})
Al_2O_3	341.08	3.33	0.28	2.80
20%Ni/Al_2O_3	187.47	3.12	0.16	2.49
15%Ni-5%Zn /Al_2O_3	186.31	3.11	0.14	2.39
10%Ni-10% Zn/Al_2O_3	186.12	3.10	0.13	3.95
5%Ni-15% Zn/Al_2O_3	184.20	3.08	0.12	3.96
20%Zn/Al_2O_3	189.69	3.13	0.17	3.98

Table 8.3 Physicochemical properties of raw bio-oil and different upgraded bio-oils

Treatments	Raw bio-oil	20%Ni /Al_2O_3	15%Ni-5%Zn /Al_2O_3	10%Ni-10%Zn /Al_2O_3	5%Ni-15%Zn /Al_2O_3	20%Zn/ Al_2O_3	Control 1	Control 2	Used 15%Ni-5%Zn /Al_2O_3
Water content (wt.%)	26.91±0.29	17.53±0.22	14.00±0.14	12.98±0.14	15.33±0.21	11.48±0.22	13.02±0.12	20.43±0.14	14.45±0.03
pH	3.24±0.28	3.41±0.01	3.31±0.01	3.34±0.08	3.43±0.03	3.43±0.01	3.33±0.04	3.27±0.05	3.29±0.04
HHV (MJ kg^{-1})	15.54±0.04	28.47±1.34	30.47±0.42	30.39±0.22	29.37±0.79	27.85±1.25	26.67±0.20	17.13±0.17	29.59±0.21
Carbon （wt.%）	40.37±0.04	54.37±0.12	55.92±0.36	55.27±0.15	52.06±0.38	51.05±0.42	48.07±0.31	42.05±0.08	51.07±0.04
Carbon balance(wt.%)	N/A	91.92±0.11	92.75±0.13	94.58±0.16	78.73±0.18	87.46±0.38	74.34±0.23	74.05±0.14	92.53±0.24

Table 8.4 Chemical compositions of different upgraded bio-oils and raw bio-oil

Relative content (%)	Raw bio-oil	20% Ni /Al_2O_3	15%Ni-5%Zn/Al_2O_3	10%Ni-10%Zn /Al_2O_3	5%Ni-15%Zn /Al_2O_3	20%Zn /Al_2O_3	Control 1	Control 2	Used 15%Ni-5%Zn /Al_2O_3
Phenols	21.10	15.48	12.55	19.34	15.46	18.36	16.18	20.03	13.87
Ethers	3.59	1.62	6.21	0.36	0	0.70	0.89	3.23	5.74
Aldehydes	5.40	1.17	0	0.62	0.92	0.48	4.21	5.1	3.04
Ketones	9.77	3.92	0.23	0.28	3.11	4.79	7.61	8.76	6.52
Esters	6.86	3.90	0	3.53	3.72	3.19	5.73	6.02	2.34
Alcohols	5.64	2.18	0.21	1.30	2.23	0.91	4.38	4.98	2.32
Acids	17.62	9.80	6.65	6.39	9.73	6.99	12.34	16.73	10.12
Furans	0.72	0	0	0.35	0	0.23	0.56	0.34	0.63
Hydrocarbons	16.94	38.58	50.12	49.91	39.62	43.86	21.36	17.09	40.12
Others	12.36	23.35	24.03	17.92	25.21	20.49	26.74	17.72	15.3

Table 8.5 Gas compositions of different treatments

Treatments		20 %Ni/ Al_2O_3	15% Ni-5%Zn/Al_2O_3	10%Ni-10%Zn/Al_2O_3	5%Ni-15%Zn/Al_2O_3	20 %Zn /Al_2O_3	Control 1	Control 2	Used 15%Ni-5%Zn /Al_2O_3
Gas composition (vol.%)	H_2	89.77±0.04	90.26±0.05	89.50 ±0.01	89.71±0.03	89.56±0.02	89.80±0.11	0.74±0.26	94.16±0.15
	C O_2	9.73±0.04	9.27± 0.03	10.02 ±0.02	9.84± 0.02	9.80±0.07	9.26±0.07	89.84±0.23	5.62±0.18
	C O	0.36±0.00	0.29± 0.00	0.31± 0.00	0.30± 0.00	0.31±0.00	0.30±0.01	3.05±0.01	0.12±0.00
	C H_4	0.11±0.00	0.09± 0.00	0.10± 0.00	0.09± 0.00	0.10±0.00	0.06±0.00	0.38±0.00	0.02±0.00
	C_2 -C_5	0.03±0.01	0.09± 0.01	0.07± 0.01	0.06± 0.01	0.23±0.02	0.58±0.02	5.99±0.02	0.09±0.03

Table 8.6 Reactor pressures of different treatments

Treatments		20 %Ni /Al_2O_3	15%Ni-5%Zn /Al_2O_3	10%Ni-10%Zn /Al_2O_3	5%Ni-15%Zn /Al_2O_3	20 %Zn /Al_2O_3	Control 1	Control 2	Used 15%Ni-5%Zn /Al_2O_3
Pressure (psig)	Initial	500±0.00	500±0.00	500±0.00	500±0.00	500±0.00	500±0.00	20±0.00	500±0.00
	Maximum	1105±15	1135±35	1145±35	1115±45	1100±10	1010±10	560±10	1050±10
	Final	480±10	470±0	475±5	485±5	465±15	480±10	50±0	485±10
Hydrogen consumption (g)		0.10±0.03	0.18±0.04	0.12±0.02	0.10±0.01	0.19±0.01	0.11±0.01	N/A	0.09±0.01

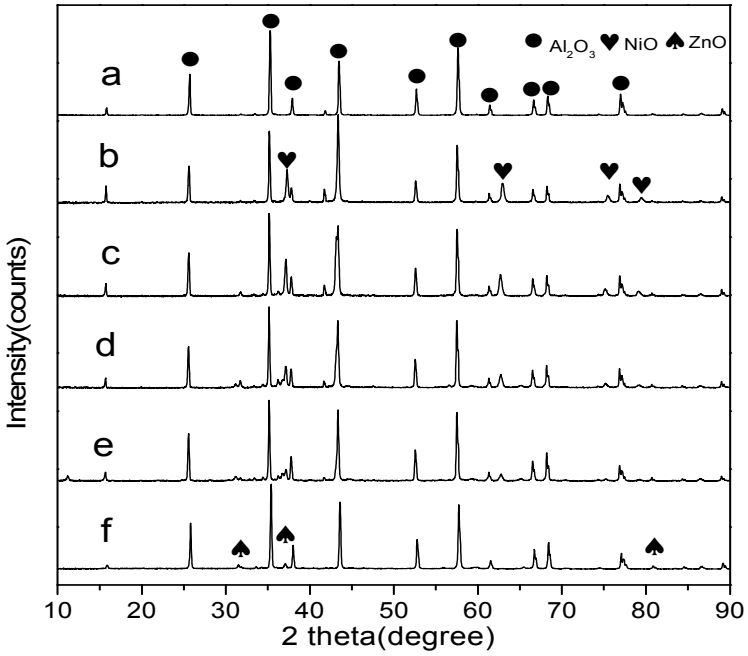

Figure 8.1 (a) Al2O3,(b) 20%Ni/Al2O3, (c) 15%Ni-5%Zn/Al2O3, (d)10%Ni-10%Zn/Al2O3, (e) 5%Ni-15%Zn/Al2O3 and (f) 20%Zn/Al2O3

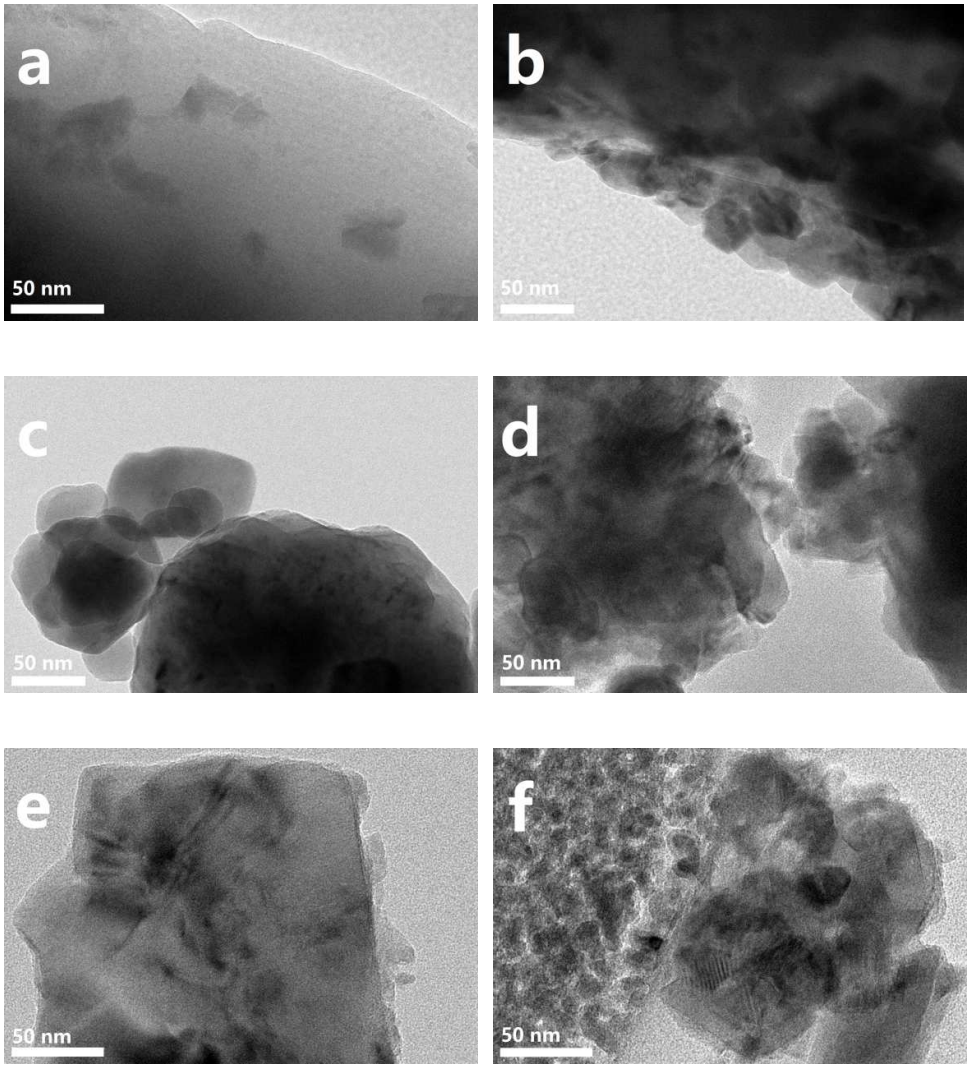

Figure 8.2 TEM images of catalysts: (a) Al2O3,(b) 20%Ni/Al2O3, (c) 15%Ni-5%Zn/Al2O3, (d)10%Ni-10%Zn/Al2O3, (e) 5%Ni-15%Zn/Al2O3 and (f) 20%Zn/Al2O3

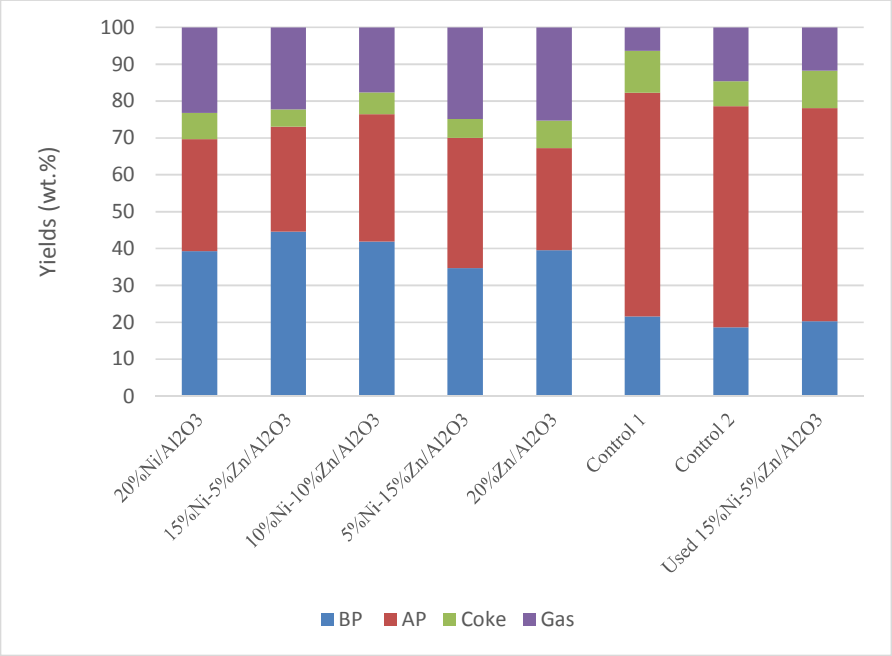

Figure 8.3 Product yields of different treatments

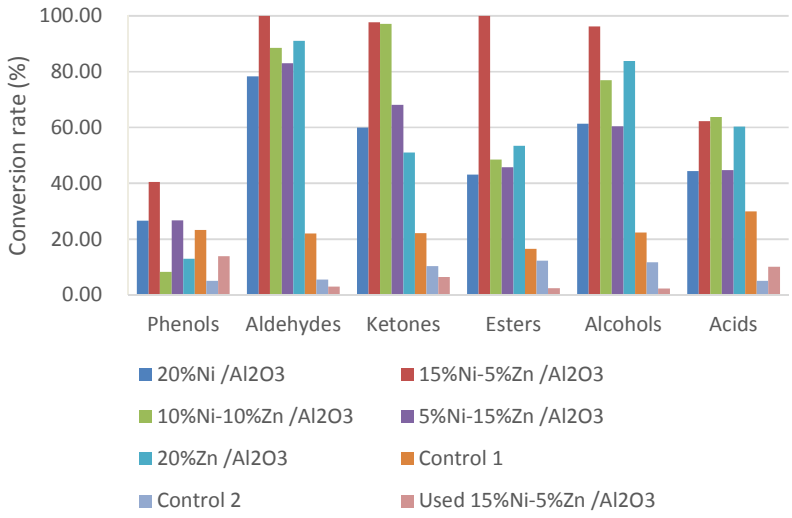

Figure 8.4 Conversion rates of different compounds present in upgraded bio-oil

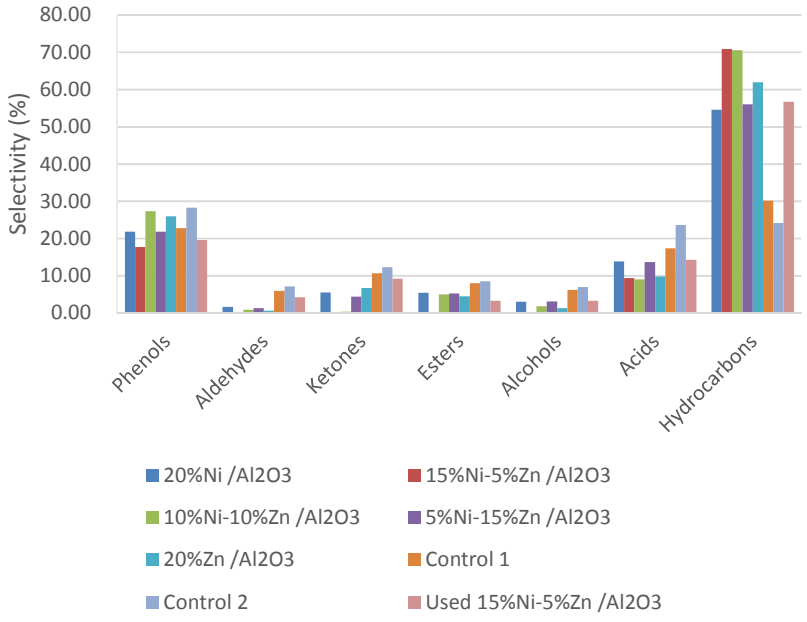

Figure 8.5 Selectivities of compounds present in upgraded bio-oil

CHAPTER 9

Conclusions

Biomass can be converted to transportation fuels through fast pyrolysis and bio-oil upgrading processes. Catalytic cracking and HDO are two promising chemical methods to upgrade bio-oils into liquid biofuels. However, efficient heterogeneous catalysts and hydrogen generation method still need to be exploited for bio-oil upgrading. Cheap and effective catalysts for bio-oil catalytic cracking and HDO were developed in this study. Hydrogen generation from cheap water using zinc metal hydrolysis was reported. Optimal metal loading ratio catalysts and operation parameters for improving biofuel yield and quality were determined. The specific conclusions of this study are the following:

1. Ni/HZSM-5 and Co-Mo/HZSM-5 catalysts for PCG bio-oil catalytic cracking were conducted in a two stage reactor system. 12%Ni/HZSM-5 catalyst yielded the highest amount of gasoline（C4-C12）hydrocarbons at 32.45%. 4%Mo-2%Co/HZSM-5 catalyst yielded the highest amount of hydrocarbons at 41.08 %.

2. HDO upgrading of PCG bio-oil over different Ni/AC catalysts under mild conditions was carried out. Ni/AC catalysts produced the highest light hydrocarbons content at 32.63% in biofuel product. Ni-Mo/AC generated the biofuel product with the highest content of alkyl-phenols at 38.41%.

3. In situ HDO upgrading of pine sawdust bio-oil over Pd/C catalyst using hydrogen generated from cheap water using zin hydrolysis reaction was performed. 250 ℃ yielded biofuel with the highest heating value at 30.17 MJ/kg and the highest hydrocarbons content at 24.09%.

4. The HDO upgrading of pine sawdust bio-oil over zinc metal with zero valency under different temperatures was conducted. 20 ℃ bio-oil upgrading process generated the highest biofuel yield at 14.07%, 400 ℃ bio-oil upgrading process produced biofuel product with the highest hydrocarbons content at 68.95%.

5. NiO/HZSM-5 catalysts were used to produce hydrocarbon biofuels from alkali lignin pyrolysis bio-oil. 1.27 %NiO/HZSM-5 generated highest biofuel yield (27.5 %) and produced biofuel with the highest amount of hydrocarbons (69.4%).

6. The HDO upgrading of pine sawdust bio-oil over non-sulfide Ni-Zn/Al_2O_3 catalysts was conducted. The highest upgraded bio-oil yield at 44.64 wt.% and the highest hydrocarbon content at 50.12% were produced by 15%Ni-5%Zn/Al_2O_3 catalyst.

CHAPTER 10

Recommendations for Future Research

Biomass has great potential for conversion to transportation fuels through fast pyrolysis and subsequent upgrading processes. Catalytic cracking and HDO are two of the most promising chemical methods to upgrade bio-oils into liquid biofuels. Progress has been made in applications of efficient heterogeneous catalysts during catalytic cracking and HDO in this study. However, catalyst deactivation due to coking created from polymerization and polycondensation reactions still remains a challenge for bio-oil catalytic cracking and HDO processes. Available catalysts need further development to have higher selective activity, long-term stability, and easier regeneration properties without significant loss of activity before testing can be completed in an industrial scale biofuel production plant. In order to exploit appropriate heterogeneous catalysts to produce gasoline or diesel grade biofuel at a commercial scale, some suggestions for future research include:

1. Improve understanding of catalyst deactivation and regeneration mechanisms during bio-oil upgrading processes.

2. Develop effective catalysts with higher stability and better regeneration properties.

3. Integrate upgrading approaches of bio-oil catalytic cracking and/or hydrodeoxygenation with petroleum refining technologies to improve bio-oil upgrading efficiency.

4. Explore new biomass resources or genetically engineered biomass to improve the yield and quality of bio-oils produced.

References

[1] S. Mohr, J. Wang, G. Ellem, J. Ward, D. Giurco. (2015). Projection of world fossil fuels by country. *Fuel, 141*, 120-135.

[2] H. Zhang, T.R. Carlson, R. Xiao, G.W. Huber. (2012). Catalytic fast pyrolysis of wood and alcohol mixtures in a fluidized bed reactor. *Green Chemistry, 14*(1), 98-110.

[3] M.I. Jahirul, M.G. Rasul, A.A. Chowdhury, N. Ashwath. (2012). Biofuels production through biomass pyrolysis—a technological review. *Energies, 5*(12), 4952-5001.

[4] M.S. Masnadi, J.R. Grace, X.T. Bi, C.J. Lim, N. Ellis. (2015). From fossil fuels towards renewables: Inhibitory and catalytic effects on carbon thermochemical conversion during co-gasification of biomass with fossil fuels. *Appl. Energy, 140*, 196-209.

[5] D. Mohan, C.U. Pittman, P.H. Steele. (2006). Pyrolysis of wood/biomass for bio-oil: a critical review. *Energy Fuels, 20*(3), 848-889.

[6] Y. Chhiti, M. Kemiha. (2013). Thermal Conversion of Biomass, Pyrolysis and Gasification. *International Journal of Engineering and Science (IJES), 2*(3), 75-85.

[7] H. Goyal, D. Seal, R. Saxena. (2008). Bio-fuels from thermochemical conversion of renewable resources: a review. *Renewable Sustainable Energy Rev., 12*(2), 504-517.

[8] D. Vamvuka. (2011). Bio□oil, solid and gaseous biofuels from biomass pyrolysis processes—An overview. *International Journal of Energy Research, 35*(10), 835-862.

[9] Q. Lu, W.-Z. Li, X.-F. Zhu. (2009). Overview of fuel properties of biomass fast pyrolysis oils. *Energy Convers. Manage., 50*(5), 1376-1383.

[10] H.S. Heo, H.J. Park, Y.-K. Park, C. Ryu, D.J. Suh, Y.-W. Suh, J.-H. Yim, S.-S. Kim. (2010). Bio-oil production from fast pyrolysis of waste furniture sawdust in a fluidized bed. *Bioresour. Technol., 101*(1), S91-S96.

[11] X. Junming, J. Jianchun, S. Yunjuan, L. Yanju. (2008). Bio-oil upgrading by means of ethyl ester production in reactive distillation to remove water and to improve storage and fuel characteristics. *Biomass Bioenergy, 32*(11), 1056-1061.

[12] A. Oasmaa, E. Kuoppala. (2003). Fast pyrolysis of forestry residue. 3. Storage stability of liquid fuel. *Energy Fuels, 17*(4), 1075-1084.

[13] Y. Elkasabi, C.A. Mullen, A.L. Pighinelli, A.A. Boateng. (2014). Hydrodeoxygenation of fast-pyrolysis bio-oils from various feedstocks using carbon-supported catalysts. *Fuel Process. Technol., 123*, 11-18.

[14] M. Zhou, G. Xiao, K. Wang, J. Jiang. (2016). Catalytic conversion of aqueous fraction of bio-oil to alcohols over CNT-supported catalysts. *Fuel, 180*, 749-758.

[15] S. Wang, Q. Cai, J. Chen, L. Zhang, L. Zhu, Z. Luo. (2015). Co-cracking of bio-oil model compound mixtures and ethanol over different metal oxide-modified HZSM-5 catalysts. *Fuel, 160*, 534-543.

[16] G. Luo, F.L. Resende. (2016). In-situ and ex-situ upgrading of pyrolysis vapors from beetle-killed trees. *Fuel, 166*, 367-375.

[17] Y. Fan, Y. Cai, X. Li, N. Yu, H. Yin. (2014). Catalytic upgrading of pyrolytic vapors from the vacuum pyrolysis of rape straw over nanocrystalline HZSM-5 zeolite in a two-stage fixed-bed reactor. *J. Anal. Appl. Pyrolysis, 108*, 185-195.

[18] K. Murata, Y. Liu, M. Inaba, I. Takahara. (2012). Catalytic fast pyrolysis of jatropha wastes. *J. Anal. Appl. Pyrolysis, 94*, 75-82.

[19] D.J. Mihalcik, C.A. Mullen, A.A. Boateng. (2011). Screening acidic zeolites for catalytic fast pyrolysis of biomass and its components. *J. Anal. Appl. Pyrolysis, 92*(1), 224-232.

[20] X. Zhao, L. Wei, S. Cheng, J. Julson, G. Anderson, K. Muthukumarappan, C. Qiu. (2016). Development of hydrocarbon biofuel from sunflower seed and sunflower meat oils over ZSM-5. *J. Renewable Sustainable Energy, 8*(1), 013109.

[21] S. Stefanidis, K. Kalogiannis, E. Iliopoulou, A. Lappas, P. Pilavachi. (2011). In-situ upgrading of biomass pyrolysis vapors: catalyst screening on a fixed bed reactor. *Bioresour. Technol., 102*(17), 8261-8267.

[22] X.Y. Lim, J.M. Andrésen. (2011). Pyro-catalytic deoxgenated bio-oil from palm oil empty fruit bunch and fronds with boric oxide in a fixed-bed reactor. *Fuel Process. Technol., 92*(9), 1796-1804.

[23] A. Veses, M. Aznar, J. López, M. Callén, R. Murillo, T. García. (2015). Production of upgraded bio-oils by biomass catalytic pyrolysis in an auger reactor using low cost materials. *Fuel, 141*, 17-22.

[24] A. Imran, E.A. Bramer, K. Seshan, G. Brem. (2014). High quality bio-oil from catalytic flash pyrolysis of lignocellulosic biomass over alumina-supported sodium carbonate. *Fuel Process. Technol., 127*, 72-79.

[25] Y. Zheng, D. Chen, X. Zhu. (2013). Aromatic hydrocarbon production by the online catalytic cracking of lignin fast pyrolysis vapors using Mo 2 N/γ-Al 2 O 3. *J. Anal. Appl. Pyrolysis, 104*, 514-520.

[26] S. Cheng, L. Wei, X. Zhao, E. Kadis, Y. Cao, J. Julson, Z. Gu. (2016). Hydrodeoxygenation of prairie cordgrass bio-oil over Ni based activated carbon synergistic catalysts combined with different metals. *New Biotechnol., 33*(4), 440-448.

[27] S. Oh, H. Hwang, H.S. Choi, J.W. Choi. (2014). Investigation of chemical modifications of micro-and macromolecules in bio-oil during hydrodeoxygenation with Pd/C catalyst in supercritical ethanol. *Chemosphere, 117*, 806-814.

[28] I. Gandarias, V. Barrio, J. Requies, P. Arias, J. Cambra, M. Güemez. (2008). From biomass to fuels: Hydrotreating of oxygenated compounds. *Int. J. Hydrogen Energy, 33*(13), 3485-3488.

[29] Z. He, X. Wang. (2012). Hydrodeoxygenation of model compounds and catalytic systems for pyrolysis bio-oils upgrading. *Catal. Sustainable Energy, 1*, 28-52.

[30] J. Wildschut, F.H. Mahfud, R.H. Venderbosch, H.J. Heeres. (2009). Hydrotreatment of fast pyrolysis oil using heterogeneous noble-metal catalysts. *Ind. Eng. Chem. Res., 48*(23), 10324-10334.

[31] A. Popov, E. Kondratieva, L. Mariey, J.M. Goupil, J. El Fallah, J.-P. Gilson, A. Travert, F. Maugé. (2013). Bio-oil hydrodeoxygenation: Adsorption of phenolic compounds on sulfided (Co) Mo catalysts. *J. Catal., 297*, 176-186.

[32] H. Shafaghat, P.S. Rezaei, W.M.A.W. Daud. (2016). Catalytic hydrodeoxygenation of simulated phenolic bio-oil to cycloalkanes and aromatic hydrocarbons over bifunctional metal/acid catalysts of Ni/HBeta, Fe/HBeta and NiFe/HBeta. *J. Ind. Eng. Chem., 35*, 268-276.

[33] A. Ardiyanti, A. Gutierrez, M. Honkela, A. Krause, H. Heeres. (2011). Hydrotreatment of wood-based pyrolysis oil using zirconia-supported mono-and bimetallic (Pt, Pd, Rh) catalysts. *Appl. Catal., A, 407*(1), 56-66.

[34] A. Ardiyanti, S. Khromova, R. Venderbosch, V. Yakovlev, H. Heeres. (2012). Catalytic hydrotreatment of fast-pyrolysis oil using non-sulfided bimetallic Ni-Cu catalysts on a δ-Al 2 O 3 support. *Appl. Catal., B, 117*, 105-117.

[35] E.H. Lee, R.-s. Park, H. Kim, S.H. Park, S.-C. Jung, J.-K. Jeon, S.C. Kim, Y.-K. Park. (2016). Hydrodeoxygenation of guaiacol over Pt loaded zeolitic materials. *J. Ind. Eng. Chem., 37*, 18-21.

[36] M. Hellinger, S. Baier, P.M. Mortensen, W. Kleist, A.D. Jensen, J.-D. Grunwaldt. (2015). Continuous Catalytic Hydrodeoxygenation of Guaiacol over Pt/SiO2 and Pt/H-MFI-90. *Catalysts, 5*(3), 1152-1166.

[37] Y. Wang, T. He, K. Liu, J. Wu, Y. Fang. (2012). From biomass to advanced bio-fuel by catalytic pyrolysis/hydro-processing: hydrodeoxygenation of bio-oil derived from biomass catalytic pyrolysis. *Bioresour. Technol., 108*, 280-284.

[38] Y. Yang, A. Gilbert, C.C. Xu. (2009). Hydrodeoxygenation of bio-crude in supercritical hexane with sulfided CoMo and CoMoP catalysts supported on MgO: a model compound study using phenol. *Appl. Catal., A, 360*(2), 242-249.

[39] S. Leng, X. Wang, X. He, L. Liu, Y.e. Liu, X. Zhong, G. Zhuang, J.-g. Wang. (2013). NiFe/γ-Al 2 O 3: a universal catalyst for the hydrodeoxygenation of bio-oil and its model compounds. *Catal. Commun., 41*, 34-37.

[40] R. Olcese, M. Bettahar, D. Petitjean, B. Malaman, F. Giovanella, A. Dufour. (2012). Gas-phase hydrodeoxygenation of guaiacol over Fe/SiO 2 catalyst. *Appl. Catal., B, 115*, 63-73.

[41] N. Martínez, R. García, J. Fierro, C. Wheeler, R. Austin, J. Gallagher, J. Miller, T. Krause, N. Escalona, C. Sepúlveda. (2016). Effect of Cu addition as a promoter on Re/SiO 2 catalysts in the hydrodeoxygenation of 2-methoxyphenol as a model bio oil compound. *Fuel, 186*, 112-121.

[42] W. Wang, Y. Yang, H. Luo, T. Hu, W. Liu. (2011). Amorphous Co–Mo–B catalyst with high activity for the hydrodeoxygenation of bio-oil. *Catal. Commun., 12*(6), 436-440.

[43] L. Wang, P. Ye, F. Yuan, S. Li, Z. Ye. (2015). Liquid phase in-situ hydrodeoxygenation of bio-derived phenol over Raney Ni and Nafion/SiO 2. *Int. J. Hydrogen Energy, 40*(43), 14790-14797.

[44] C. Greenhalf, D. Nowakowski, A. Harms, J. Titiloye, A. Bridgwater. (2013). A comparative study of straw, perennial grasses and hardwoods in terms of fast pyrolysis products. *Fuel, 108*, 216-230.

[45] H.S. Heo, H.J. Park, J.-I. Dong, S.H. Park, S. Kim, D.J. Suh, Y.-W. Suh, S.-S. Kim, Y.-K. Park. (2010). Fast pyrolysis of rice husk under different reaction conditions. *J. Ind. Eng. Chem., 16*(1), 27-31.

[46] S.-J. Kim, S.-H. Jung, J.-S. Kim. (2010). Fast pyrolysis of palm kernel shells: influence of operation parameters on the bio-oil yield and the yield of phenol and phenolic compounds. *Bioresour. Technol., 101*(23), 9294-9300.

[47] W.J. DeSisto, N. Hill, S.H. Beis, S. Mukkamala, J. Joseph, C. Baker, T.-H. Ong, E.A. Stemmler, M.C. Wheeler, B.G. Frederick. (2010). Fast pyrolysis of pine sawdust in a fluidized-bed reactor. *Energy Fuels, 24*(4), 2642-2651.

[48] J. Yanik, R. Stahl, N. Troeger, A. Sinag. (2013). Pyrolysis of algal biomass. *J. Anal. Appl. Pyrolysis, 103*, 134-141.

[49] C.A. Mullen, A.A. Boateng, N.M. Goldberg, I.M. Lima, D.A. Laird, K.B. Hicks. (2010). Bio-oil and bio-char production from corn cobs and stover by fast pyrolysis. *Biomass Bioenergy, 34*(1), 67-74.

[50] S. Ren, X.P. Ye, A.P. Borole, P. Kim, N. Labbé. (2016). Analysis of switchgrass-derived bio-oil and associated aqueous phase generated in a semi-pilot scale auger pyrolyzer. *J. Anal. Appl. Pyrolysis, 119*, 97-103.

[51] W. Obeid, E. Salmon, M.D. Lewan, P.G. Hatcher. (2015). Hydrous pyrolysis of Scenedesmus algae and algaenan-like residue. *Org. Geochem., 85*, 89-101.

[52] R. Venderbosch, W. Prins. (2010). Fast pyrolysis technology development. *Biofuels, bioproducts and biorefining, 4*(2), 178-208.

[53] A. Oasmaa, D. Meier. (2005). Norms and standards for fast pyrolysis liquids: 1. Round robin test. *J. Anal. Appl. Pyrolysis, 73*(2), 323-334.

[54] S. Thangalazhy-Gopakumar, S. Adhikari, R.B. Gupta, M. Tu, S. Taylor. (2011). Production of hydrocarbon fuels from biomass using catalytic pyrolysis under helium and hydrogen environments. *Bioresour. Technol., 102*(12), 6742-6749.

[55] G.W. Huber, S. Iborra, A. Corma. (2006). Synthesis of transportation fuels from biomass: chemistry, catalysts, and engineering. *Chem. Rev., 106*(9), 4044-4098.

[56] H.J. Park, H.S. Heo, J.-K. Jeon, J. Kim, R. Ryoo, K.-E. Jeong, Y.-K. Park. (2010). Highly valuable chemicals production from catalytic upgrading of radiata pine sawdust-derived pyrolytic vapors over mesoporous MFI zeolites. *Appl. Catal., B, 95*(3), 365-373.

[57] B. Valle, A.G. Gayubo, A.s.T. Aguayo, M. Olazar, J. Bilbao. (2010). Selective production of aromatics by crude bio-oil valorization with a nickel-modified HZSM-5 zeolite catalyst. *Energy Fuels, 24*(3), 2060-2070.

[58] X. Ding, C. Li, C. Yang. (2010). Study on the oligomerization of ethylene in fluidized catalytic cracking (FCC) dry gas over metal-loaded HZSM-5 catalysts. *Energy Fuels, 24*(7), 3760-3763.

[59] M. Mhamdi, S. Khaddar-Zine, A. Ghorbel. (2009). Influence of the cobalt salt precursors on the cobalt speciation and catalytic properties of H-ZSM-5 modified with cobalt by solid-state ion exchange reaction. *Appl. Catal., A, 357*(1), 42-50.

[60] C. Yin, R. Zhao, C. Liu. (2005). Transformation of olefin over Ni/HZSM-5 catalyst. *Fuel, 84*(6), 701-706.

[61] B. Valle, A. Alonso, A. Atutxa, A. Gayubo, J. Bilbao. (2005). Effect of nickel incorporation on the acidity and stability of HZSM-5 zeolite in the MTO process. *Catal. Today, 106*(1), 118-122.

[62] Y. Huang, L. Wei, Z. Crandall, J. Julson, Z. Gu. (2015). Combining Mo–Cu/HZSM-5 with a two-stage catalytic pyrolysis system for pine sawdust thermal conversion. *Fuel, 150*, 656-663.

[63] A. Alaswad, M. Dassisti, T. Prescott, A. Olabi. (2015). Technologies and developments of third generation biofuel production. *Renewable Sustainable Energy Rev., 51*, 1446-1460.

[64] P. Kumar, D.M. Barrett, M.J. Delwiche, P. Stroeve. (2009). Methods for pretreatment of lignocellulosic biomass for efficient hydrolysis and biofuel production. *Ind. Eng. Chem. Res., 48*(8), 3713-3729.

[65] A. Boe, V. Owens, J. GONZALEZ□HERNANDEZ, J. Stein, D. Lee, B. Koo. (2009). Morphology and biomass production of prairie cordgrass on marginal lands. *GCB Bioenergy, 1*(3), 240-250.

[66] Z. Zhang, P. Bi, P. Jiang, M. Fan, S. Deng, Q. Zhai, Q. Li. (2015). Production of gasoline fraction from bio-oil under atmospheric conditions by an integrated catalytic transformation process. *Energy, 90*, 1922-1930.

[67] J.D. Adjaye, N. Bakhshi. (1995). Production of hydrocarbons by catalytic upgrading of a fast pyrolysis bio-oil. Part I: Conversion over various catalysts. *Fuel Process. Technol., 45*(3), 161-183.

[68] A. Sites. (1995). Hydration Behavior of Dealuminated Zeolite HZSM-5: A High-Resolution Solid State NMR Study Deng, Feng; Du, Youru; Ye, Chaohui; Wang, Jingzhong; Ding, Tatong; Li. *J. Phys. Chem., 99*(41), 15208-15214.

[69] P.S. Rezaei, H. Shafaghat, W.M.A.W. Daud. (2014). Production of green aromatics and olefins by catalytic cracking of oxygenate compounds derived from biomass pyrolysis: A review. *Appl. Catal., A, 469*, 490-511.

[70] J. Shu, A. Adnot, B.P. Grandjean. (1999). Bifunctional behavior of Mo/HZSM-5 catalysts in methane aromatization. *Ind. Eng. Chem. Res., 38*(10), 3860-3867.

[71] S. Liu, Q. Dong. (1998). Unique promotion effect of CO and CO 2 on the catalytic stability for benzene and naphthalene production from methane on Mo/HZSM-5 catalysts. *Chem. Commun.*(11), 1217-1218.

[72] J. Shen, X.-S. Wang, M. Garcia-Perez, D. Mourant, M.J. Rhodes, C.-Z. Li. (2009). Effects of particle size on the fast pyrolysis of oil mallee woody biomass. *Fuel, 88*(10), 1810-1817.

[73] F. Bin, C. Song, G. Lv, J. Song, X. Cao, H. Pang, K. Wang. (2012). Structural characterization and selective catalytic reduction of nitrogen oxides with ammonia: a comparison between Co/ZSM-5 and Co/SBA-15. *The Journal of Physical Chemistry C, 116*(50), 26262-26274.

[74] Y. Xu, Y. Suzuki, Z.-G. Zhang. (2013). Comparison of the activity stabilities of nanosized and microsized zeolites based Fe–Mo/HZSM-5 catalysts in the non-oxidative CH 4 dehydroaromatization under periodic CH 4–H 2 switching operation at 1073K. *Appl. Catal., A, 452*, 105-116.

[75] H. Jiang, L. Wang, W. Cui, Y. Xu. (1999). Study on the induction period of methane aromatization over Mo/HZSM-5: partial reduction of Mo species and formation of carbonaceous deposit. *Catal. Lett., 57*(3), 95-102.

[76] J.-F. Liu, L. Jin, Y. Liu, Q. Yun-Shi. (2008). Methane aromatization over cobalt and gallium-impregnated HZSM-5 catalysts. *Catal. Lett., 125*(3-4), 352-358.

[77] L. Chen, J. Lin, H. Zeng, K. Tan. (2001). Non-oxidative methane conversion into aromatics on mechanically mixed Mo/HZSM-5 catalysts. *Catal. Commun., 2*(6), 201-206.

[78] X. Zhao, L. Wei, S. Cheng, Y. Huang, Y. Yu, J. Julson. (2015). Catalytic cracking of camelina oil for hydrocarbon biofuel over ZSM-5-Zn catalyst. *Fuel Process. Technol., 139*, 117-126.

[79] R. French, S. Czernik. (2010). Catalytic pyrolysis of biomass for biofuels production. *Fuel Process. Technol., 91*(1), 25-32.

[80] M.S.A. Bakar, J.O. Titiloye. (2013). Catalytic pyrolysis of rice husk for bio-oil production. *J. Anal. Appl. Pyrolysis, 103*, 362-368.

[81] S. Oh, H. Hwang, H.S. Choi, J.W. Choi. (2015). The effects of noble metal catalysts on the bio-oil quality during the hydrodeoxygenative upgrading process. *Fuel, 153*, 535-543.

[82] J. Peng, P. Chen, H. Lou, X. Zheng. (2009). Catalytic upgrading of bio-oil by HZSM-5 in sub-and super-critical ethanol. *Bioresour. Technol., 100*(13), 3415-3418.

[83] A. Holmen. (2009). Direct conversion of methane to fuels and chemicals. *Catal. Today, 142*(1), 2-8.

[84] A. Güngör, S. Önenc, S. Ucar, J. Yanik. (2012). Comparison between the "one-step" and "two-step" catalytic pyrolysis of pine bark. *J. Anal. Appl. Pyrolysis, 97*, 39-48.

[85] X. Zhang, T. Wang, L. Ma, Q. Zhang, T. Jiang. (2013). Hydrotreatment of bio-oil over Ni-based catalyst. *Bioresour. Technol., 127*, 306-311.

[86] C. Zhao, J. He, A.A. Lemonidou, X. Li, J.A. Lercher. (2011). Aqueous-phase hydrodeoxygenation of bio-derived phenols to cycloalkanes. *J. Catal., 280*(1), 8-16.

[87] V. Yakovlev, S. Khromova, O. Sherstyuk, V. Dundich, D.Y. Ermakov, V. Novopashina, M.Y. Lebedev, O. Bulavchenko, V. Parmon. (2009). Development of new catalytic systems for upgraded bio-fuels production from bio-crude-oil and biodiesel. *Catal. Today, 144*(3), 362-366.

[88] X. Zhang, T. Wang, L. Ma, Q. Zhang, Y. Yu, Q. Liu. (2013). Characterization and catalytic properties of Ni and NiCu catalysts supported on ZrO 2–SiO 2 for guaiacol hydrodeoxygenation. *Catal. Commun., 33*, 15-19.

[89] Y. Romero, F. Richard, S. Brunet. (2010). Hydrodeoxygenation of 2-ethylphenol as a model compound of bio-crude over sulfided Mo-based catalysts: Promoting effect and reaction mechanism. *Appl. Catal., B, 98*(3), 213-223.

[90] S. Echeandia, P. Arias, V. Barrio, B. Pawelec, J. Fierro. (2010). Synergy effect in the HDO of phenol over Ni–W catalysts supported on active carbon: Effect of tungsten precursors. *Appl. Catal., B, 101*(1), 1-12.

[91] M. Saidi, F. Samimi, D. Karimipourfard, T. Nimmanwudipong, B.C. Gates, M.R. Rahimpour. (2014). Upgrading of lignin-derived bio-oils by catalytic hydrodeoxygenation. *Energy Environ. Sci., 7*(1), 103-129.

[92] E. Liakakou, E. Heracleous, K. Triantafyllidis, A. Lemonidou. (2015). K-promoted NiMo catalysts supported on activated carbon for the hydrogenation reaction of CO to higher alcohols: Effect of support and active metal. *Appl. Catal., B, 165*, 296-305.

[93] F.A.L. Sy, L.C. Abella, T.G. Monroy. (2012). Hydrogen Production via Thermo Catalytic Decomposition of Methane over Bimetallic Ni-Cu/AC Catalysts: Effect of Copper Loading and Reaction Temperature. *International Journal of Chemical Engineering and Applications, 3*(2), 92.

[94] G.-J. Wang, J.-K. Zhang, Y. Liu. (2013). Catalytic oxidative desulfurization of benzothiophene with hydrogen peroxide over Fe/AC in a biphasic model diesel-acetonitrile system. *Korean J. Chem. Eng., 30*(8), 1559-1565.

[95] J.R. Anderson. (1975). Structure of metallic catalysts. *Academic Press, ix+ 469, 24 x 16 cm, illustrated(<-> 16. 50.*

[96] P.M. Mortensen, J.-D. Grunwaldt, P.A. Jensen, K. Knudsen, A.D. Jensen. (2011). A review of catalytic upgrading of bio-oil to engine fuels. *Appl. Catal., A, 407*(1), 1-19.

[97] R. Zhou, H. Lei, J. Julson. (2013). The effects of pyrolytic conditions on microwave pyrolysis of prairie cordgrass and kinetics. *J. Anal. Appl. Pyrolysis, 101*, 172-176.

[98] X. Xu, C. Zhang, Y. Liu, Y. Zhai, R. Zhang. (2013). Two-step catalytic hydrodeoxygenation of fast pyrolysis oil to hydrocarbon liquid fuels. *Chemosphere, 93*(4), 652-660.

[99] R.J. French, J. Stunkel, R.M. Baldwin. (2011). Mild hydrotreating of bio-oil: effect of reaction severity and fate of oxygenated species. *Energy Fuels, 25*(7), 3266-3274.

[100] M. Bykova, D.Y. Ermakov, V. Kaichev, O. Bulavchenko, A. Saraev, M.Y. Lebedev, V. Yakovlev. (2012). Ni-based sol–gel catalysts as promising systems for crude bio-oil upgrading: Guaiacol hydrodeoxygenation study. *Appl. Catal., B, 113*, 296-307.

[101] S. Sitthisa, W. An, D.E. Resasco. (2011). Selective conversion of furfural to methylfuran over silica-supported Ni Fe bimetallic catalysts. *J. Catal., 284*(1), 90-101.

[102] Y.-n. Yang, H.-k. Zhang, L. En-jing, C.-h. Zhang, J. Ren. (2011). Effect of Fe, Mo promoters on acetic acid hydrodeoxygenation performance of nickel-based catalyst. *Journal of Molecular Catalysis (China), 25*, 30-36.

[103] I. Vishnevetsky, M. Epstein. (2007). Production of hydrogen from solar zinc in steam atmosphere. *Int. J. Hydrogen Energy, 32*(14), 2791-2802.

[104] M. Lv, J. Zhou, W. Yang, K. Cen. (2010). Thermogravimetric analysis of the hydrolysis of zinc particles. *Int. J. Hydrogen Energy, 35*(7), 2617-2621.

[105] R. Nava, B. Pawelec, P. Castaño, M. Álvarez-Galván, C. Loricera, J. Fierro. (2009). Upgrading of bio-liquids on different mesoporous silica-supported CoMo catalysts. *Appl. Catal., B, 92*(1), 154-167.

[106] Y. Luo, V.K. Guda, P.H. Steele, B. Mitchell, F. Yu. (2016). Hydrodeoxygenation of oxidized distilled bio-oil for the production of gasoline fuel type. *Energy Convers. Manage., 112*, 319-327.

[107] R. Gunawan, X. Li, C. Lievens, M. Gholizadeh, W. Chaiwat, X. Hu, D. Mourant, J. Bromly, C.-Z. Li. (2013). Upgrading of bio-oil into advanced biofuels and chemicals. Part I. Transformation of GC-detectable light species during the hydrotreatment of bio-oil using Pd/C catalyst. *Fuel, 111*, 709-717.

[108] W.-M. Xiong, Y. Fu, F.-X. Zeng, Q.-X. Guo. (2011). An in situ reduction approach for bio-oil hydroprocessing. *Fuel Process. Technol., 92*(8), 1599-1605.

[109] S. Ahmadi, Z. Yuan, S. Rohani, C.C. Xu. (2016). Effects of nano-structured CoMo catalysts on hydrodeoxygenation of fast pyrolysis oil in supercritical ethanol. *Catal. Today, 269*, 182-194.

[110] W.-J. Liu, X.-S. Zhang, Y.-C. Qv, H. Jiang, H.-Q. Yu. (2012). Bio-oil upgrading at ambient pressure and temperature using zero valent metals. *Green Chemistry, 14*(8), 2226-2233.

[111] C. Hargus, R. Michalsky, A.A. Peterson. (2014). Looped-oxide catalysis: a solar thermal approach to bio-oil deoxygenation. *Energy Environ. Sci., 7*(10), 3122-3134.

[112] A. Weidenkaff, A. Reller, A. Wokaun, A. Steinfeld. (2000). Thermogravimetric analysis of the ZnO/Zn water splitting cycle. *Thermochim. Acta, 359*(1), 69-75.

[113] J. De Merchant, M. Cocivera. (1995). Preparation and doping of zinc oxide using spray pyrolysis. *Chem. Mater., 7*(9), 1742-1749.

[114] F. Fan, P. Tang, Y. Wang, Y. Feng, A. Chen, R. Luo, D. Li. (2015). Facile synthesis and gas sensing properties of tubular hierarchical ZnO self-assembled by porous nanosheets. *Sensors and Actuators B: Chemical, 215*, 231-240.

[115] P. Charvin, A. Stéphane, L. Florent, F. Gilles. (2008). Analysis of solar chemical processes for hydrogen production from water splitting thermochemical cycles. *Energy Convers. Manage., 49*(6), 1547-1556.

[116] F. Mueller-Langer, E. Tzimas, M. Kaltschmitt, S. Peteves. (2007). Techno-economic assessment of hydrogen production processes for the hydrogen economy for the short and medium term. *Int. J. Hydrogen Energy, 32*(16), 3797-3810.

[117] C. Liu, J.-j. Liang, S.-b. Wu, Y.-b. Deng. (2014). Effect of chemical structure on pyrolysis behavior of alcell mild acidolysis lignin. *BioResources, 10*(1), 1073-1084.

[118] Y. Weng, S. Qiu, L. Ma, Q. Liu, M. Ding, Q. Zhang, Q. Zhang, T. Wang. (2015). Jet-fuel range hydrocarbons from biomass-derived sorbitol over Ni-HZSM-5/SBA-15 catalyst. *Catalysts, 5*(4), 2147-2160.

[119] C. Zhao, J.A. Lercher. (2012). Upgrading Pyrolysis Oil over Ni/HZSM□5 by Cascade Reactions. *Angew. Chem., 124*(24), 6037-6042.

[120] T.M. Huynh, U. Armbruster, L.H. Nguyen, D.A. Nguyen, A. Martin. (2015). Hydrodeoxygenation of Bio-Oil on Bimetallic Catalysts: From Model Compound to Real Feed. *JSBS, 5*, 151-160.

[121] E. Kantarelis, W. Yang, W. Blasiak. (2013). Effects of silica-supported nickel and vanadium on liquid products of catalytic steam pyrolysis of biomass. *Energy Fuels, 28*(1), 591-599.

[122] S. Thangalazhy-Gopakumar, S. Adhikari, R.B. Gupta. (2012). Catalytic pyrolysis of biomass over H+ ZSM-5 under hydrogen pressure. *Energy Fuels, 26*(8), 5300-5306.

[123] Y. Xu, T. Wang, L. Ma, Q. Zhang, W. Liang. (2010). Upgrading of the liquid fuel from fast pyrolysis of biomass over MoNi/γ-Al 2 O 3 catalysts. *Appl. Energy, 87*(9), 2886-2891.

[124] X. Zhao, L. Wei, S. Cheng, E. Kadis, Y. Cao, E. Boakye, Z. Gu, J. Julson. (2016). Hydroprocessing of carinata oil for hydrocarbon biofuel over Mo-Zn/Al 2 O 3. *Appl. Catal., B, 196*, 41-49.

[125] R.O. Idem, S.P. Katikaneni, N.N. Bakhshi. (1996). Thermal cracking of canola oil: reaction products in the presence and absence of steam. *Energy Fuels, 10*(6), 1150-1162.

[126] Y. Qian, S. Liang, T. Wang, Z. Wang, W. Xie, X. Xu. (2011). Enhancement of pyrolysis gasoline hydrogenation over Zn-and Mo-promoted Ni/γ-Al 2 O 3 catalysts. *Catal. Commun., 12*(10), 851-853.

PUBLICATIONS

Peer-reviewed journal papers

1. **Cheng, S.,** Wei, L., Julson, J., Muthukum, K., Kharel, P., Boakye, E. (2017). Hydrocarbon bio-oil production from pyrolysis bio-oil using non-sulfide Ni-Zn/Al2O3 catalyst. Fuel Processing Technology,162,78-86.

2. **Cheng, S.,** Wei, L., Julson, J., Muthukum, K., Kharel, P., Cao, Y., Boakye, E., Raynie, D., Gu, Z. (2017). Hydrodeoxygenation upgrading of pine sawdust bio-oil using zinc metal with zero valency. Journal of the Taiwan Institute of Chemical Engineers, 74,146-153.

3. **Cheng, S.,** Wei, L., Zhao, X., Julson, J., Kadis, E. (2017). Converting Alkali Lignin to Biofuels over NiO/HZSM-5 Catalysts Using a Two-stage Reactor. Chemical Engineering & Technology. https://doi.org/10.1002/ceat.201600539.

4. **Cheng, S.,** Wei, L., Alsowij, M., Corbin, F., Julson, J., Boakye, E., Raynie, D. (2017). In-situ hydrodeoxygenation upgrading of pine sawdust bio-oil to hydrocarbon biofuel using Pd/C catalyst. Journal of the Energy Institute, http://dx.doi.org/10.1016/j.joei.2017.01.004.

5. **Cheng, S.**, Wei, L., Zhao, X., Julson, J.(2016). Application, deactivation and regeneration of heterogeneous catalysts in bio-oil upgrading. Catalysts, 6(12), 195.

6. **Cheng, S.**, Wei, L., Zhao, X., Kadis, E., Cao, Y., Julson, J., Gu, Z. (2016). Hydro-

deoxygenation of Prairie Cordgrass Bio-oil over Ni based activated carbon synergistic catalysts combined with different metals. New Biotechnology, 33(4), 440-448.

7. **Cheng, S.,** Wei, L., Zhao, X., Kadis, E., Julson, J. (2016). Conversion of Prairie Cordgrass to Hydrocarbon Biofuel over Co-Mo/HZSM-5 Using a Two-Stage Reactor System. Energy Technology **(Inside Cover)**, 4(6), 706-713.

8. **Cheng, S.,** Wei, L., Zhao, X. (2016). Develop Bifunctional Ni/HZSM-5 Catalyst for Converting Prairie Cordgrass to Hydrocarbon Biofuel. Energy Sources, Part A: Recovery, Utilization, and Environmental Effects, 38(16), 2433-2437.

9. **Cheng, S.,** Wei, L., Alsowij, M., Corbin, F., Boakye, E., Gu, Z., Raynie, D. (2017). Catalytic hydrothermal liquefaction (HTL) of biomass for bio-crude production using Ni/HZSM-5 catalysts.AIMS Environmental Science,4(3), 417-430.

10. **Cheng, S.,** Wei, L., Huang, Y., Raynie, D., Qiu, C., Kiratu, J., Yu, Y. (2015). Directly catalytic upgrading bio-oil vapor produced by prairie cordgrass pyrolysis over Ni/HZSM-5 using a two stage reactor. AIMS Energy, 3, 227-240.

11. Zhao, X., Wei, L., **Cheng, S.**, Julson, J. (2017). Review of heterogeneous catalysts for catalytically upgrading vegetable oils into hydrocarbon biofuels.Catalysts,7, 83.

12. Zhao, X., Wei, L., **Cheng, S.**, Kadis, E., Cao, Y., Boakye, E., Gu, Z., Julson, J. (2016). Hydroprocessing of carinata oil for hydrocarbon biofuel over Mo-Zn/Al_2O_3. Applied Catalysis B: Environmental, 196, 41–49.

13. Huang, Y., Wei, L., Zhao, X., **Cheng, S.**, Julson, J., Cao, Y., Gu, Z. (2016). Upgrading pine sawdust pyrolysis oil to green biofuels by HDO over zinc-assisted Pd/C catalyst. Energy Conversion and Management, 115, 8-16.

14. Zhao, X., Wei, L., **Cheng, S.**, Julson, J., Anderson, G., Muthukumarappan, K., Qiu, C. (2016). Development of hydrocarbon biofuel from sunflower seed and sunflower meat oils over ZSM-5. Journal of Renewable and Sustainable Energy, 8(1), 013109.

15. Wei, L., Gao, Y., Qu, W., Zhao, X., **Cheng, S.** (2016). Torrefaction of Raw and Blended Corn Stover, Switchgrass, and Prairie Grass. Transactions of the ASABE, 59(2), 717-726.

16. Zhao, X., Wei, L., **Cheng, S.**, Cao, Y., Julson, J., Gu, Z. (2015). Catalytic cracking of carinata oil for hydrocarbon biofuel over fresh and regenerated Zn/Na-ZSM-5. Applied Catalysis A: General, 507, 44-55.

17. Zhao, X., Wei, L., **Cheng, S**., Huang, Y., Yu, Y., Julson, J. (2015). Catalytic cracking of camelina oil for hydrocarbon biofuel over ZSM-5-Zn catalyst. Fuel Processing Technology, 139, 117-126.

18. Zhao, X., Wei, L., **Cheng, S.**, Julson, J. (2015). Optimization of catalytic cracking process for upgrading camelina oil to hydrocarbon biofuel. Industrial

Crops and Products, 77, 516-526.

Conference papers

1. **Cheng, S.**, Wei, L., Julson, J. (2016). Effect of Co-Mo/HZSM-5 on ex-situ catalytic fast pyrolysis of different biomass feedstocks. 2016 ASABE Annual International Meeting. American Society of Agricultural and Biological Engineers.

2. **Cheng, S.**, Wei, L., Julson, J. (2016). Ex-situ catalytic fast pyrolysis of pine sawdust over two different catalysts. 2016 ASABE Annual International Meeting. American Society of Agricultural and Biological Engineers.

3. **Cheng, S.**, Wei, L., Zhao, X., Shen, Y., Yu, Y., Jing, L. (2015). Isolate protein peptides from defatted camelina and canola

meals. 2015 ASABE Annual International Meeting. American Society of Agricultural and Biological Engineers.

4. Zhao, X., Wei, L., **Cheng, S.**, Yu, Y., Julson, J. (2015). Catalytic cracking of carinata oil for hydrocarbon biofuel over Zn/Na-ZSM-5. 2015 ASABE Annual International Meeting. American Society of Agricultural and Biological Engineers.

5. Wei, L., **Cheng, S.**, Zhao, X., Huang, Y., Yu, Y. (2015). Exploration of Lignocellulosic Biomass Precision Pyrolysis for Advanced Biofuel Production.

2015 ASABE Annual International Meeting. American Society of Agricultural and Biological Engineers.